8-2016

Second Law of Thermodynamics Analysis of an Internal Combustion Engine Fueled with Methane

Muataz Abotabik
Western Michigan University, moataza151@gmail.com

Recommended Citation

SECOND LAW OF THERMODYNAMICS ANALYSIS OF AN INTERNAL COMBUSTION
ENGINE FUELED WITH METHANE

by

Muataz Abotabik

A thesis submitted to the Graduate College
in partial fulfillment of the requirements
for the degree of Master of Science
Mechanical and Aerospace Engineering
Western Michigan University
August 2016

Thesis Committee:

Claudia Fajardo, Ph.D., Chair
Bade Shrestha, Ph.D.
Christopher Cho, Ph.D.

SECOND LAW OF THERMODYNAMICS ANALYSIS OF AN INTERNAL COMBUSTION
ENGINE FUELED WITH METHANE

Muataz Abotabik, M.S.

Western Michigan University, 2016

The second law of thermodynamics is a powerful tool for calculating the amount of energy that can be converted to work (i.e., the exergy or availability of a system), which cannot be predicted using the first law. The objectives of this research project are to quantify the availability during the compression, combustion and expansion processes of a spark-ignited engine fueled with methane; and to highlight differences in the thermo-mechanical availability of the ideal and spark-ignition (SI) engine cycles. A cooperative single-cylinder research engine was used to measure the data required for availability analysis at equivalence ratios ranging between 0.83 and 1.25. The thermo-mechanical availability, normalized by the energy content of the mixture, was found to increase as the equivalence ratio decreases. First and second-law of Thermodynamics efficiencies also increased for fuel-leaner mixtures, but remained within four percent of each other for methane in both the ideal and the SI engine cycles.

ACKNOWLEDGMENTS

TABLE OF CONTENTS

Table of Contents-Continued

LIST OF TABLES

LIST OF FIGURES

List of Figures-Continued

List of Figures-Continued

CHAPTER I

INTRODUCTION

1.1 Background

It is standard practice to use the first law of Thermodynamics to analyze energy conversion devices (e.g., heat engines). The first law is a statement of the conservation of energy principle; that is: energy cannot be created nor destroyed. Not all of the energy available in a particular source, however, can be converted to useful work. Ultimately, it is the work potential (exergy, or energy availability) of a source that should be considered [1]. The second law of Thermodynamics offers the means to determine the quality of energy and quantify the lost work potential during a process or a cycle [1]. As a result, a complete characterization of any thermodynamic system requires consideration of the second law. Work is a function of the initial and final states of a system, as well as of the process path. For a given initial state, work is maximized if the process is conducted reversibly until the system reaches equilibrium with the environment (i.e., the dead state). Under these conditions, the work extracted becomes the maximum amount of work that can be obtained from that particular system, without violating any thermodynamic laws. This is the availability of the system, which depends both on the system and the environment. In contrast to energy, which is a conserved property, availability can be destroyed due to irreversibilites, which arise due to processes such as friction, mixing, combustion and heat transfer, all of which are notably present in internal combustion engines. Further, during practical processes, the system may not reach the dead state (i.e., total equilibrium with its environment). For these reasons, there is always a difference between the work delivered by a system and the availability of a system [1]. The total availability of a system may include thermal, mechanical and chemical components. First,

the thermal aspect of the availability occurs when the temperature of the environment is below the system's temperature. Under this condition, the system is not in equilibrium with its surroundings, and has internal, thermal energy that can be converted into useful work. Second, the mechanical part of the availability arises when the environmental pressure is under the system's pressure. An ideal turbine, for example, provides the means to extract mechanical availability by expanding (reducing the pressure) of gases, thus bringing the system closer to the dead state. Chemical availability stems from differences in the concentrations of the species in a system relative to corresponding concentrations in the surroundings [2].

Due to limited energy resources, maximizing the amount of work that can be extracted from a particular device is of utmost importance [3]. For cyclic devices, such as reciprocating internal combustion engines, understanding which processes within the cycle contribute the most availability destruction can provide a foundation for design and optimization efforts. Entropy generation (and hence high exergy destruction) occurs during combustion processes. Since the first law of Thermodynamics does not deal with entropy generation and entropy changes, it cannot be used to quantify availability destruction during combustion-driven processes [1].

1.2 Theoretical Framework and Literature Review

1.2.1 A Review of Second Law Investigations Applied to Reciprocating Internal Combustion (IC) Engines

A four-stroke IC engine undergoing an ideal cycle can be treated as a closed system during compression and expansion and as an open system during the intake and exhaust strokes. The closed system formulation of the availability is shown in equation (1.1).

$$a = (u - u_o) + \left(P_o(v - v_o)\right) - T_o(s - s_o) \tag{1.1}$$

Here a represents the specific availability; v_o, u_o and s_o represent the specific volume, specific internal energy and specific entropy of the system at the conditions of the dead state. Also, P_o and T_o are the pressure and temperature at the dead state, respectively. Further, u, v and s represent the specific internal energy, volume and entropy of the system at a given state [2]. The work against the environment is represented by the term $P_o(v - v_o)$ which reduces the availability of the system if the gases work against the surroundings. For an open system, the availability equation can be formulated as in equation 1.2.

$$a_f = (h - h_o) - T_O(s - s_o) \tag{1.2}$$

Here h and h_o are the specific enthalpy of the system at a given state and the specific enthalpy of the system at the dead state, respectively. The total availability can be obtained from equation (1.3), where m is the system mass.

$$A = am \tag{1.3}$$

In an IC engine, the availability can be destroyed due to irreversible processes such as friction, combustion, and heat transfer. The change in availability can be related to a relevant process between any two states, as shown in equations 1.4 and 1.5.

3

$$\Delta A = A_{end} - A_{start} \qquad (1.4)$$

$$\Delta A = A_{in} - A_{out} + A_Q - A_W - A_{Destroyed} \qquad (1.5)$$

Where, the ΔA represents the total availability change of the system. A_{start} and A_{end} represent the availability at the start and end of the process, respectively; the difference of A_{in} and A_{out} represent the net transfer of availability into the system due to mass flow, A_W is the availability transferred due to work and, A_Q is the availability transferred due to the heat transfer [2]. Finally, the availability destruction, $A_{Destroyed}$, can be calculated by combining equations 1.4 and 1.5 as follows:

$$A_{Destroyed} = A_{start} - A_{end} + A_{in} - A_{out} + A_Q - A_W \qquad (1.6)$$

The availability due to work is equal to the amount of work (equation 1.7), whereas the availability due to heat transfer is given by equation 1.8, where δQ is the differential heat transferred at the system boundary.

$$A_W = W \qquad (1.7)$$

$$A_Q = \int \left| 1 - \frac{T_O}{T} \right| \delta Q \qquad (1.8)$$

The transfer of availability due to mass flow (A_{in} or A_{out}) is given by:

$$A_i = \int \left(\dot{m}_i \, a_{f,i} \right) dt \qquad (1.9)$$

where i and f indicate the intake or the exhaust flow, respectively [2].

Many researchers have used the second law of Thermodynamics to study internal combustion (I.C) engines. A review of these investigations in a variety of combustion

4

engines and different fuel types carried out by Caton [2] concluded that the majority of IC engine availability research has been conducted on diesel engines.

1.2.2 Diesel Engines

Zhang and Caton applied the second law of Thermodynamics to a diesel engine [4]. In this work, they used a GT-Power engine cycle simulation to quantify the energy transfers and availability destruction from different processes. The research focused on low temperature combustion, which can be achieved by late diesel injection (after or near top dead center), with high EGR levels. The simulation results were validated with experimental data at eight operating conditions and the model was used to estimate the effect of exhaust gas recirculation (EGR) and injection timing on first- and second-law of Thermodynamics parameters. According to figure (1), the rate of availability change of the system can be calculated according to equation (1.10).

$$\frac{dA_{sys}}{dt} = \dot{A}_{fuel} + \dot{A}_{in} - \dot{A}_{ex} + \dot{A}_Q - \dot{A}_W - \dot{A}_{dest} \qquad (1.10)$$
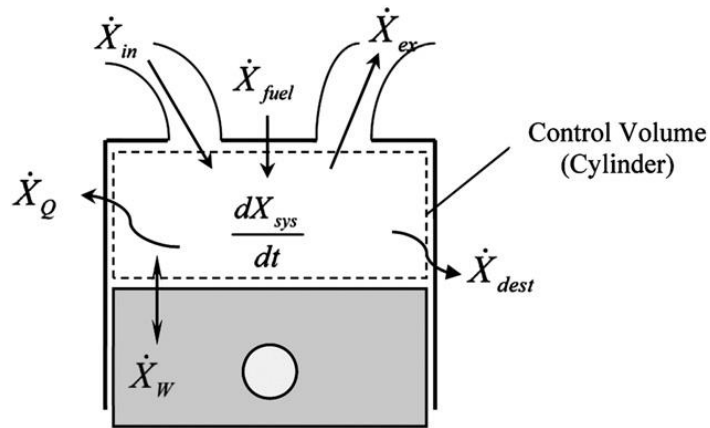
Figure 1. Availability balance of the engine *cylinder [4].*

With an assumption of no availability change with time over the entire cycle, integration of equation 1.10, for the entire engine cycle yields equation 1.11.

$$\int \frac{dA_{sys}}{dt} = 0 = A_{fuel} + A_{in} - A_{ex} + A_Q - A_W - A_{dest} \tag{1.11}$$

The terms A_{in} and A_{ex} represent the Availability transfer through mass flowing through the intake and exhaust ports, respectively, according to equation 1.12,

$$A_i = \int \dot{m}_\iota \left[(h_i - h_o) - T_o(s_i - s_o)\right]dt \tag{1.12}$$

where $\dot{m}_\iota$, s_i, h_i represent the mass flow rate, entropy and enthalpy of the intake or exhaust flows. The quantities T_o, s_o, h_o represent the temperature, entropy, and enthalpy at the dead state. In this work, the availability transfer through heat exchange, A_Q, was evaluated using equation 1.13,

$$A_Q = \int \left(1 - \frac{T_O}{T}\right) \delta Q \tag{1.13}$$

where δQ is the differential heat transfer at the system boundary temperature and T was assumed to be the bulk cylinder gas temperature. The term A_W in equation 1.11 is the availability due to the work interaction, equal to the net output work of the system. Lastly, the fuel availability was calculated using equation 1.14,

$$A_{fuel} = \left[\frac{-(\Delta G)_{T_O,P_O}}{-(\Delta H)_{T_O,P_O}}\right]Q_{lhv}.m_f \tag{1.14}$$

where the term in parenthesis is the Gibbs -to-enthalpy ratio, Q_{lhv} is the lower heating value of the fuel ($C_{13.6} H_{23.6}$ with Q_{LHV} of 43,250 kJ/kg), and m_f represents the fuel mass entering the engine during each cycle [4].

Consistent with the experimental data, the model showed that, by simultaneously increasing the amount of exhaust gas recirculation, intake temperature, and the equivalence ratio, the availability destruction decreased. Findings also suggests that higher net flow

availability and lower availability loss with heat transfer can be obtained with late injection timing. These findings were attributed to the retarded combustion process and longer ignition delay caused by the late injection.

1.2.3 Alcohol-Fueled Spark- Ignition Engines

Alcohol fuels are used in reciprocating engines due to their high octane number, fast flame speeds and high enthalpy of vaporization. They can yield high engine performance and efficiency when engines work with high levels of EGR, high compression ratios, and close to stoichiometric combustion [5]. Many studies have been conducted using alcohol as a fuel in spark ignition engines, but few using the second law of Thermodynamics [3].

A second-law performance comparison of a reciprocating engine fueled with alcohol fuels (ethanol and methanol) versus isooctane has been investigated [6]. In this work, Caton simulated the operation of in an eight-cylinder; four-stroke, spark ignition engine fueled with ethanol and methanol with the goal of quantifying overall engine performance in comparison to the isooctane-fueled baseline. The simulation was performed at a fixed equivalence ratio of 1, MBT timing, and 2000 RPM. The research presents a comparison between the alcohol fuels and isooctane in terms of the air/fuel ratio, lower heating value, fuel availability, and enthalpy of vaporization (table 1).

Table 1. Isooctane, methanol, and ethanol fuels property comparison [6]

Fuel Vapor	Formula	A/F Stoich.	Q $_{lhv}$ (MJ/kg_{Fuel})	Fuel Availability (MJ/kg fuel)	h_{fg} (kJ/kg)
Isooctane	C_8H_{18}	15.07	44.4	45.5	308
Methanol	CH_4O	6.45	20.0	21.1	1103
Ethanol	C_2H_6O	8.97	26.9	28.4	840

According to table 1, isooctane has the highest values of A/F, Q_{lhv}, and fuel availability; its Q_{lhv} and fuel availability are approximately double those of alcohol fuels. It was found that isooctane has the highest availability destruction during the cycle, which was attributed to its complex chemical composition. Changing the load or engine speed had no significant effect on the availability destruction during combustion for all the fuels [6].

1.2.4 Gasoline-Fueled Spark- Ignition and Compression Ignition Engines

A comparative availability and energy study of a four-stroke, four-cylinder, and spark- ignition engine fueled with gasoline at different octane numbers (91, 93 and 95.3) was conducted by Sayin [7]. For each fuel, the engine was tested at variable speeds with torques of 20 Nm and 40 Nm. Fuel availability calculations with respect to the environment at T_o=298.15 and $P_o = 1\ atm$ were conducted. The specific flow availability of the mixture was calculated using equation (1.17), which is the summation of the chemical and thermo-mechanical components.

$$\bar{a}=\bar{a}_t + \bar{a}_c \qquad (1.17)$$

In equation (1.17), a_t is the specific thermo-mechanical availability term, whereas $\bar{a}_c$ is

$$\bar{a}_t = \bar{h} - \overline{h_o} - T_o(\bar{s} - \overline{s_o}) \tag{1.18}$$

the specific chemical availability of the fuel per unit mass, calculated via equation (1.19).

$$a_c = [1.0401 + 0.1728\frac{h}{c} + 0.0432\frac{o}{c} + 0.2169\frac{s}{c}\left(1 - 2.0628\frac{h}{c}\right)]|Q_{lhv}| \tag{1.19}$$

h, c, o and s are the H, C, O and S mass fractions respectively. The exhaust gases were assumed ideal and the thermo-mechanical availability at T and P with n components was evaluated using equation (1.20)

$$\bar{a}_t = \sum_{i=1}^{n} a_i \{\bar{h}_\iota(T) - \bar{h}_\iota(T_o) - T_o\left(\bar{s}^o{}_i(T) - \bar{s}_o{}^o{}_i - \bar{R}\ln\frac{p}{p_o}\right)\} \tag{1.20}$$

Where a_i is the molar value of component i and $\bar{R}$ is the universal gas constant. The chemical availability of the exhaust gases was calculated via equation (1.21), where

$$a_{ce} = \bar{R}T_o \sum_{i=1}^{n} a_i \ln\frac{y_i}{y_i{}^e} \tag{1.21}$$

y_i and $y_i{}^e$ are the molar fraction of component i and the molar fraction of component i in the reference environment, respectively. The balance of the availability rate for the engine operating at steady state conditions is represented by equation (1.22) [7].

$$0 = \sum_j(1 - \frac{T_o}{T_j})\dot{Q}_{cv} - \dot{W}_{cv} + \dot{n}_F\overline{a_F} - \dot{n}_F\overline{a_{ex}} - \dot{E}_d \tag{1.22}$$

Here T_j is the boundary absolute temperature at which the heat is rejected. The first term on the right-hand-side of the equation represents the rate of availability transfer by heat; $\dot{n}_F\overline{a_F}$ and $\dot{n}_F\overline{a_{ex}}$ are the rate of specific availability of the exhaust gases and of the fuel, respectively; and the term $\dot{E}_d$ represents the availability destroyed. The second law efficiency was calculated using equation (1.23).

$$\eta_{II} = \frac{\dot{W}_{cv}}{\dot{n}_F \overline{a_F}} \tag{1.23}$$

Results suggests that higher-octane number fuels yield lower second law efficiency and higher exhaust availability. Heat availability losses also decreased the second law efficiency, but results are not conclusive due to the experimental uncertainty associated with the measurements. The second law efficiency increases with engine speed because of the higher turbulence, which improves mixture homogeneity and the combustion process. The main contributors to availability loss were the combustion process, exhaust gases flow availability, and heat transfer [7].

1.2.5 Natural Gas-Fueled Spark-Ignition Engines

Sobiesiak and Zhang applied the first and the second law of Thermodynamics to an engine model working with compressed natural gas (CNG) [8]. The objective of this study was to analyze the potential advantages of compressed natural gas if used as fuel in a spark-ignition engine. Two simulations were used in this study, one with a single-zone heat release model with constant properties, and the other using a two-zone combustion model with crank-angle dependent burning rate.

Simulation results were validated with experimental data measured in a 4.7-liter, V8 engine fueled with compressed natural gas at wide-open throttle (WOT) and 4000 RPM. The availability destruction due to heat transfer and combustion were calculated. Most of the availability destruction was attributed to the combustion process. According to the second law analysis performed in this study, the availability destruction caused by the combustion process for both gasoline and compressed natural gas are comparable, but the availability destruction due to heat transfer is higher for gasoline (i.e., about 23 % of the

total availability in comparison to 15 % for CNG). Further, it is suggested that a CNG-fueled engine with high octane number and high compression ratio would outperform a gasoline-fueled engine based on second law efficiency and indicated-mean-effective pressure (IMEP) metrics. Higher availability transfer with work was found for CNG (43% compared to 37% for gasoline), which led to a second-law efficiency increase [8].

A comparative study was conducted by Gharehghani et al. on the effect of fuel type on the energy and energy balances of a four-cylinder, naturally-aspirated, spark-ignition engine fueled with gasoline and CNG [9]. The engine was operated at wide-open throttle and variable speeds. A control-volume, first law of thermodynamic analysis was performed on the engine, according to equation 1.24,

$$\dot{Q}_f + \dot{Q}_a = \dot{W}_{sh} + \dot{Q}_e + \dot{Q}_c + \dot{Q}_u \tag{1.24}$$

where $\dot{Q}_f$ is the energy rate of the fuel, $\dot{Q}_a$ is the rate of air energy intake, $\dot{W}_{sh}$ is the shaft power output, $\dot{Q}_e$ is the exhaust energy rate, $\dot{Q}_c$ is the heat transfer rate to the coolant, and $\dot{Q}_u$ is the unaccounted energy rate losses. The $\dot{Q}_f$ term can be calculated from equation 1.25, where

$$\dot{Q}_f = \dot{Q}_{lhv,f} * \dot{m}_f \tag{1.25}$$

$\dot{Q}_{LHV,f}$ is the lower heating value of the fuel. The rate of energy change for the air $\dot{Q}_a$ was evaluated through equation 1.26,

$$\dot{Q}_a = \dot{m}_a(\Delta h_a + w_a \Delta h_{H2O}) \tag{1.26}$$

where, $\dot{m}_a$ is the mass flow rate of air, and the term in parenthesis is the enthalpy change of atmospheric air (i.e, w_a is the absolute humidity). The term $\dot{Q}_c$ was estimated from equation 1.27, where

$$\dot{Q}_c = C_c * \dot{m}_c * \Delta T_{engine} \tag{1.27}$$

$\dot{m}_c$ is the cooling fluid mass flow rate and C_c is the cooling fluid heat capacity. The energy of the exhaust gases was calculated using the set of empirical relations in 1.28, with A, B_1, and B_2 calculated via equations 1.28 a, b, and c [9].

$$\dot{Q}_e = \dot{m}_e(A + B_1 + B_2 T^2) \tag{1.28}$$

$$A = 8279.5 - 13744.4\lambda + 5160.9\lambda^2 \tag{1.28 a}$$

$$B_1 = 1.35 - 0.6\lambda + 0.22\lambda^2 \tag{1.28 b}$$

$$B_2 = 0.00002 - 0.00007\,\lambda + 0.00005\lambda^2 \tag{1.28 c}$$

Here the parameter λ represents the (air/fuel) equivalence ratio and T is the exhaust gas temperature. The uncounted energy term was calculated from the difference between the input and the output engine power. For the second-law analysis, a steady state condition was assumed, such that the availability rate balance was represented by equation 1.29.

$$\dot{A}_{fuel} + \dot{A}_{in} - \dot{A}_{ex} + \dot{A}_Q - \dot{A}_W - \dot{A}_{dest} = 0 \tag{1.29}$$

Where $\dot{A}_{fuel}$, $\dot{A}_{ex}$, and $\dot{A}_W$ are the availabilities of the fuel, the exhaust gas, and the brake power, respectively. The $\dot{A}_Q$ term was evaluated using equation 1.30, where

$$\dot{A}_Q = \sum (1 - \frac{T_O}{T_J}) * \dot{Q}_C \tag{1.30}$$

$\dot{A}_Q$ is the rate of availability transfer by heat and T_J is the absolute boundary temperature at the section where heat was rejected. The terms $\dot{A}_{in}$ and $\dot{A}_{ex}$, which represent the availability transfer via intake and exhaust processes, were evaluated using equation 1.31.

$$\dot{A}_{in \, or \, ex} = \sum \dot{m}_{in \, or \, ex} * (h_{in \, or \, ex} - h_o) - T_O(s_{in \, or \, ex} - s_o) \qquad (1.31)$$

The o subscript in equation 1.31 represents the dead state, and *s*, and *h* are the specific entropy and enthalpy, respectively.

The second law efficiency was quantified as the ratio of the brake power to the fuel availability (equation 1.32).

$$\eta_{II} = \frac{\dot{W}}{\dot{A}_{fuel}} \qquad (1.32)$$

This research suggests that higher total availability is associated with CNG in comparison to gasoline. That is because of the higher combustion temperature when using CNG as fuel, which decreases the availability destruction during combustion compared to gasoline. CNG also yielded higher second-law efficiency [9].

1.3 Thesis Objective

The energy crisis has motivated researchers to increase the efficiency of energy conversion devices [3]. While multiple second-law studies have been conducted on spark-ignition and compression-ignition internal combustion engines fueled with gasoline and diesel, respectively, fewer availability investigations have been conducted on methane fueled engines. Therefore, in this work the second law of thermodynamics will be used to analyze the availability of a methane-fueled, spark-ignition engine during the compression, combustion and expansion processes in both the ideal and spark-ignition engine cycles

First, the effect of equivalence ratio on the availability will be quantified. First and second-law efficiencies will be calculated and compared for each equivalence ratio. Finally, the availability of the ideal spark-ignition engine cycle (i.e., Otto cycle) will be compared to that of a spark-ignition engine cycle. The term "spark-ignition engine cycle" will be used throughout this thesis to refer to the thermodynamic processes taking place in a practical, reciprocating, spark-ignited, internal combustion engine.

CHAPTER II

EXPERIMENTAL SETUP

2.1 Overview

The current work was carried out using a collaborative fuel research (CFR) engine. The engine was equipped with metered air and fuel systems to control the equivalence ratio, as well as additional pressure and temperature sensors to monitor operating conditions. Triggering, monitoring and data acquisition was achieved using a LabVIEW graphical user interface (GUI) upgraded for this research project. In addition, an exhaust gas analyzer was used to measure species concentrations and confirm the prescribed air-to-fuel (AF) ratio. A layout schematic for the experimental equipment is shown in figure 2, with a detailed explanation provided in the following sections.
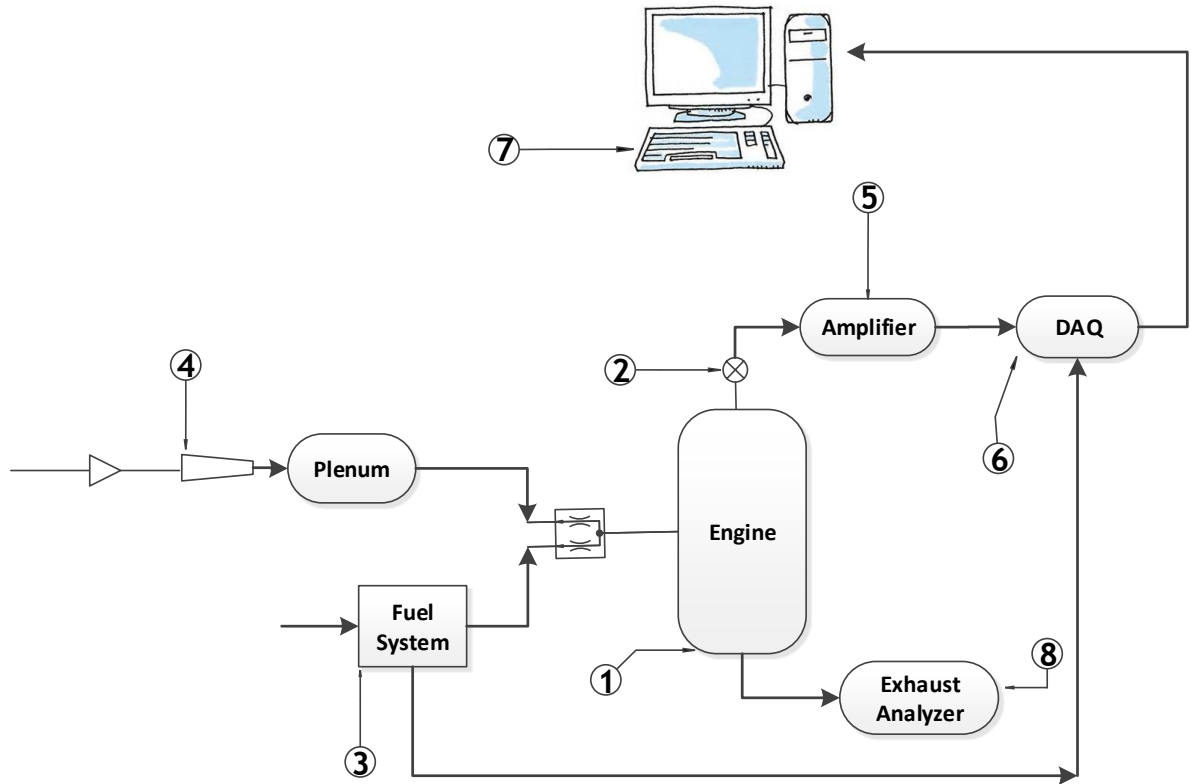
Figure 2. Schematic of the experiment setup showing 1: engine, 2: pressure sensor, 3: fuel system, 4: air flow meter, 5: amplifier, 6: data acquisition hardware, 7: LabVIEW interface, 8: exhaust gas analyzer.

2.1.1 Engine

The current study was conducted on a Waukesha collaborative fuel research (CFR) engine (figure 3), retrofitted to work with natural gas instead of liquid fuels. Originally conceived to study fuel quality, CFR engines are still being used to conduct internal combustion studies. The single-cylinder CFR engine used in the current experiments has variable compression ratio, 3.25-inch bore and 4.5-inch stroke combustion chamber. It is spark-ignited, water-cooled and operates at a constant speed of 600 RPM [10]. Intake and exhaust valve timings, as well as operating conditions for the current experiments are summarized in table 2.

16

Table 2. CFR engine operating conditions

Compression Ratio	10
Intake valve Opening	10° ATDC
Intake valve Closing	34° ABDC
Exhaust valve Opening	40° BBDC
Exhaust valve Closing	15° ATDC
Load	WOT
Engine speed (RPM)	600
Fuel Type	Methane
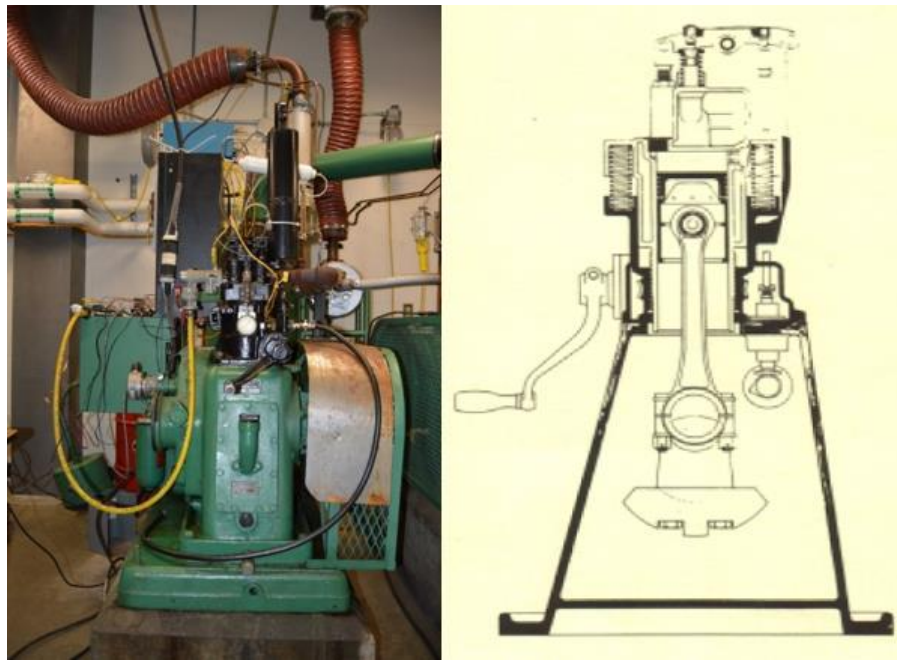
Figure 3. Picture of the engine in the laboratory (left) and diagram of the cooperative fuel research engine (right) [10].

2.1.2 Air Flow Meter

Air metering was accomplished using a critical orifice nozzle (Flow Systems Inc. model ES-16-AN-0.870-SS). Critical flow nozzles, also known as "critical flow venturi" or "sonic" nozzles provide a constant mass flow rate as a function of upstream pressure. They are commonly used in flow metering applications that require high accuracy and repeatability. Most importantly for the current experiment, they are fairly insensitive to downstream disturbances, caused for example, by pressure fluctuations due to valvetrain actuation. [11]. Figure (4) shows the sonic flow meter used in the experiment.
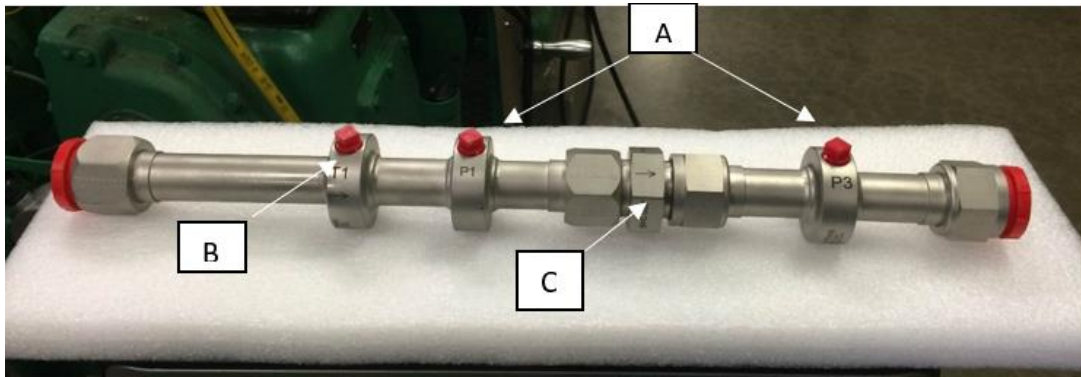
Figure 4. A critical nozzle flow meter. (A) taps for pressure gages. (B) tap for thermocouples. (C) Critical nozzle position.

The critical flow venturi was sized by first estimating the maximum air mass flow rate assuming a 100% volumetric efficiency at 600 RPM (equation 2.1).

$$\xi_v = \frac{\dot{m}_{air}}{\rho_{air} \, \forall_d \left(\frac{N}{n}\right)} \tag{2.1}$$

The quantity ρ_{air} is the density of the intake air, which was calculated at 1 bar and 25 C^o; N represents the number of revolutions per minute; n is the number of revolutions per cycle (2 for a four-stroke engine), and $\forall_d$ is the displacement volume, calculated using equation 2.2, where B and S are the engine bore and stroke, respectively.

18

$$\forall_d = \frac{\pi\, B^2 * S}{4} * NC \tag{2.2}$$

The air mass flow rate was calculated as 0.0034 $\frac{kg}{s}$, with a corresponding nozzle diameter of 0.088 inches. A NIST traceable calibration (Appendix II) supplied with the instrument provided the mass flow rate of air as a function of upstream absolute pressure. A pressure regulator and a pressure gauge were installed immediately upstream of the nozzle. The air flow meter just described was connected to a 57-liter plenum located upstream of the intake port.

2.1.3 Fuel System

Since the current investigation focuses on the effect of equivalence ratio on the availability of system, accurately fuel metering to minimize variations in the fuel supply received considerable attention. As shown in figure 5, methane was supplied to the engine from a 125 cubic feet tank, and the fuel pressure was regulated down to 12 psig. The fuel temperature and pressure were measured upstream a 5-gallon secondary fuel accumulator. A solenoid valve, pressure gauge and fuel flow meter were installed after the fuel accumulator. Finally, a fuel check valve was installed before the intake port to prevent fuel backflow during the experiments.
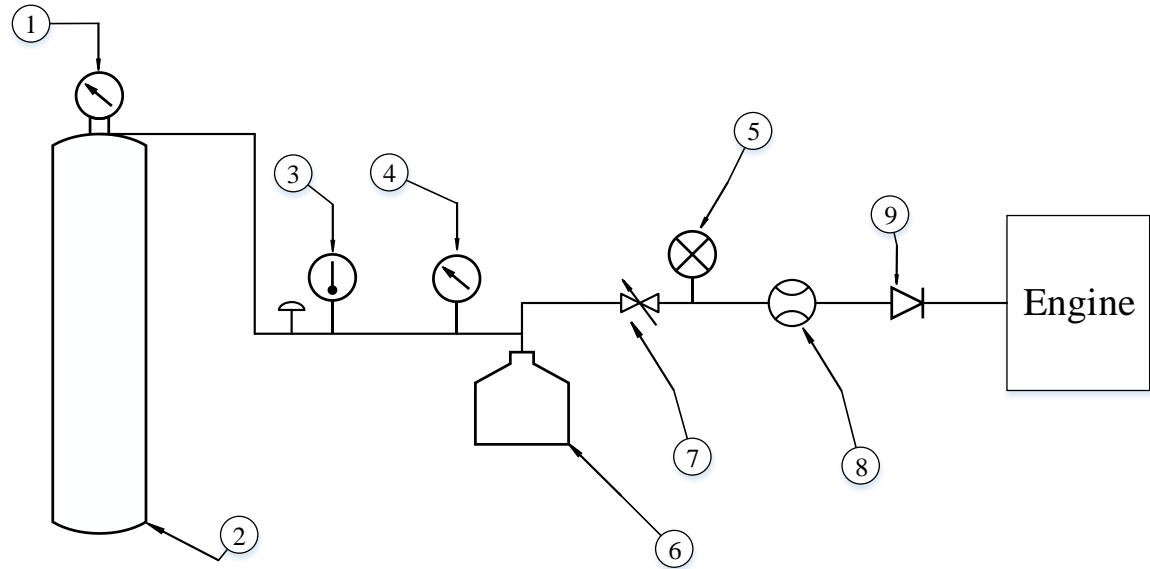
Figure 5. Layout of the fuel system 1: pressure regulator, 2: fuel tank, 3: thermocouple, 4: pressure gauge, 5: digital pressure gauge, 6: accumulator, 7: solenoid, 8: fuel flow meter, 9: check valve.

2.1.3.1 Fuel Flow Meter

A digital flow meter (Honeywell Zephyr model HAFUHT0100L4AXT 300 SLPM) was used to measure the fuel flow rate (figure 6). The sensor works on the principle of a temperature-volume flow rate relation. The sensor was selected based on its $\pm$ 3.5% accuracy of the flow rate reading, fast response time of 1 ms, (i.e., to capture changes in fuel supply rate) and its capability to operate at very low voltages (3.3 VDC) [12]. The fuel flow was controlled via a solenoid-actuated valve (AFC-121) operated on 24V. Figure 6 shows the flow meter and the solenoid valve.
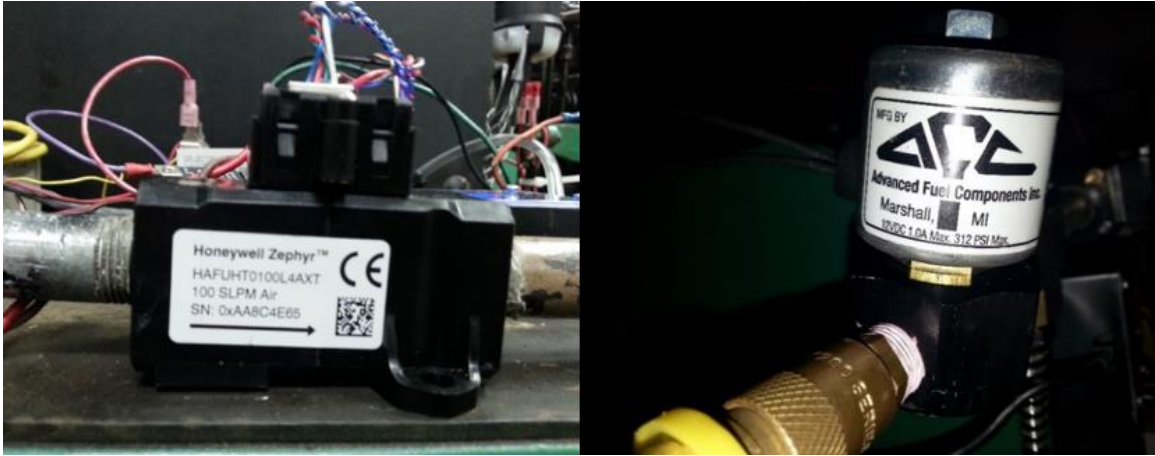
Figure 6. Fuel flow meter (left) and solenoid valve (right) used in the current experiment.

The fuel pressure was measured upstream and downstream of the solenoid valve using pressure transducers (Omega Px139-030D4V and Honeywell model 26PCCFA3G, respectively), to provide feedback for fuel flow metering and control.

2.1.3.2 Temperature Measurements

K-type thermocouples were used to measure the temperature of the gaseous fuel in order to account for density variations during engine steady-state operation, as well as intake and exhaust port temperatures (figure 7). The analog (voltage) signal was processed by the data acquisition system and converted to a temperature reading using the standard calibration curve supplied by the manufacturer.
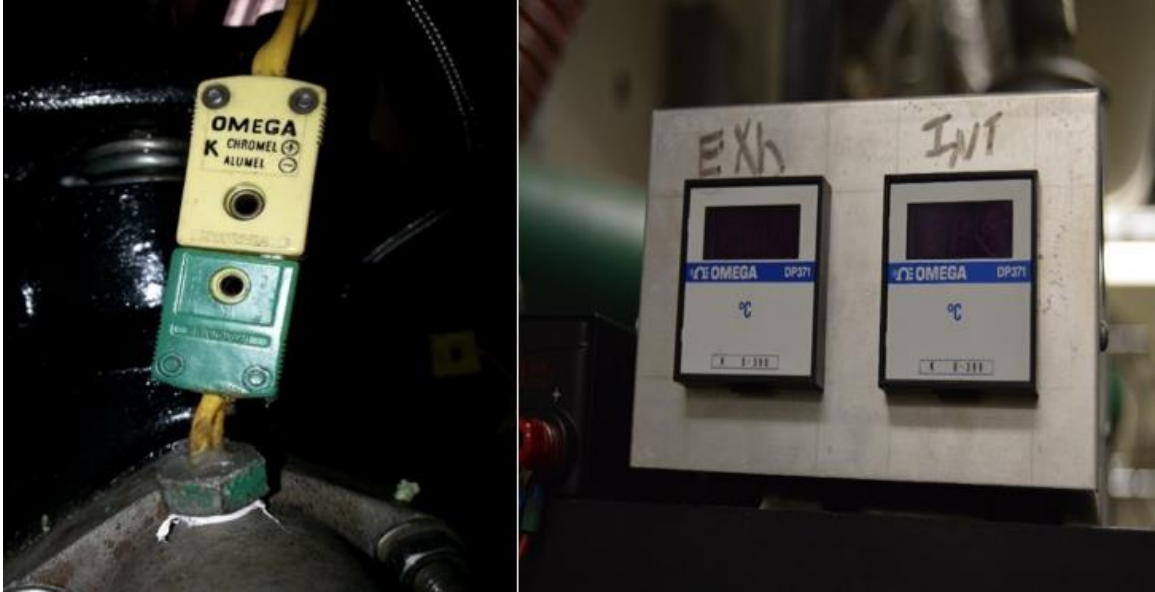
Figure 7. Intake thermocouple (left) and a display module (right) used in the current experiment.

2.1.4 In-cylinder Pressure

A water-cooled piezoelectric transducer (Kistler model 7061B), was used to measure the pressure inside the combustion chamber (figure 8). In this device, a piezoelectric bridge (inside the transducer) bends due to the gas pressure and generates a charge that was subsequently converted to a low-voltage signal using a charge amplifier (PCB model 462A). Water-cooling enables high thermal stability and precise readings. The sensor was re-calibrated prior to the experiments. A copy of the calibration data sheet can be found in Appendix III.

Figure 8. The in-cylinder water-cooled pressure transducer (Kistler model 7061B).

2.1.5 Crankshaft Rotational Speed

A rotary encoder (BEI model HS25) was used to synchronize spark timing events with piston position (crank angle). The crankshaft-mounted rotary optical encoder provides the instantaneous piston position. The encoder generates a single square cycle at each increment, producing 360 square cycles per crankshaft revolution. In the current work, the reference point was set at -180º BTDC (beginning of the compression stroke). The device was set to restart counting every 720º to cover the four strokes of the engine cycle.

2.1.6 User Interface

The experiment was controlled and engine parameters were monitored through a graphical user interface (GUI) developed in LabVIEW version 15.0 (see Appendix IV). Signals from the crank angle encoder, piezoelectric transducer amplifier, digital pressure sensors, and thermocouples were routed through a data acquisition card (NI model SCB-68), as shown in figure (9). An Arduino Nano (V 2.3) unit was used to control the fuel flow

sensor signal. The spark timing, solenoid duty cycle, gas flow meter correction factor[1], and

spark dwell were controlled directly through the GUI. The in-cylinder pressure and crank

angle data were processed to generate pressure-volume and pressure-crank angle graphs

for quick feedback to the user. The GUI also enabled data writing to a file for further

processing. A screen shot of the GUI can be seen in appendix IV.
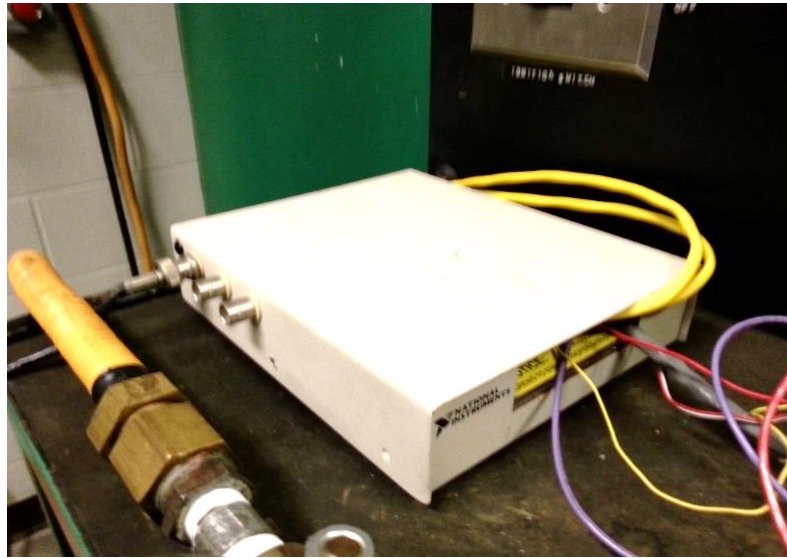
Figure 9. Data acquisition system (NI SCB-68) used in the current research.

2.1.7 Exhaust Gas Analyzer

An exhaust gas analyzer (Horiba model MEXA-584L) was used to measure the

concentration of gases in the exhaust stream (needed for the second-law analysis) and to

validate the prescribed air-to-fuel ratio. Specifically, volumetric concentrations of

$HC, CO_2, CO, O_2, and\ NO_X$ were measured. The analyzer also displays the air-to-fuel ratio

---

[1] The fuel flow meter can work with multiple types of fuel, but it needs a calibration correction factor
specified for each fuel (i.e. methane has a correction factor of 0.9)

and air-to-fuel equivalence ratio λ, which were used as feedback to optimize the fuel solenoid valve ON time.

Figure 10. Exhaust gas analyzer (model MEXA-584L) used in the current experiment.

2.2 Experimental Procedure

Before running the CFR engine, lubricant, coolant level, fuel system connections and valves were checked. The micrometer reading, used in the compression ratio calculation, was verified to match the value specified in the LabVIEW GUI. The water valves were opened to supply cooling to the engine and to the water-cooled pressure transducer. The amplifier settings (8 for pC/unit sensitivity and 5k unit/volt range) were verified prior to each test. These values correspond to a LabVIEW calibration of 5 MPa per volt.

After these preliminary checks, the main air pressure valve was opened and the pressure regulator was set at 40 psig, corresponding to an airflow rate of 0.00336 kg/s (see

Appendix II). The engine was motored by holding the start switch until the oil pressure reached 35 psig, to ensure adequate oil flow. The user (LabVIEW) interface was started and the input parameters were supplied, as shown in table 3.

Table 3. Settings specified through the user interface

Parameter	Set Value
Micrometer setting	0.2
Compression ratio	10
Solenoid trigger angle (ATDC)	350
Dwell (CA degrees)	10

Next, the manual fuel valves (main and secondary) were opened. As a safety precaution, the user interface is configured such that fuel is not delivered to the engine until the ignition is triggered. Once the spark timing is set at the desired value, the ignition is triggered to initiate combustion. Before recording data, the engine was allowed to reach steady state, as quantified by stable exhaust gas temperature readings. Table 4 shows the exhaust temperature (averaged for three tests) as a function of equivalence ratio.

Table 4. The exhaust temperature (averaged for three tests) as a function of equivalence ratio for a 0.6 L CFR fueled with methane run at 600 and WOT load

Equivalence ratio	Averaged Exhaust Temperature (C°)	Standard deviation (C°)
0.830	408	6.9
0.903	426	1.0
0.991	433	4.9
1.131	407	2.5
1.250	395	3.0

The next sections will discuss instrument mounting and calibration as well as the optimization of the engine operating conditions to ensure a high quality experiment output.

2.3 Instrument Calibration

2.3.1 Combustion Chamber Pressure Transducer Calibration

The combustion chamber pressure sensor (Kistler model 7061B) was calibrated by its manufacturer. The calibration sensitivity was -80.5 pC/bar. The voltage-amplifier sensitivity scale (figure 11a) was updated to 8.55 Pc/unit.
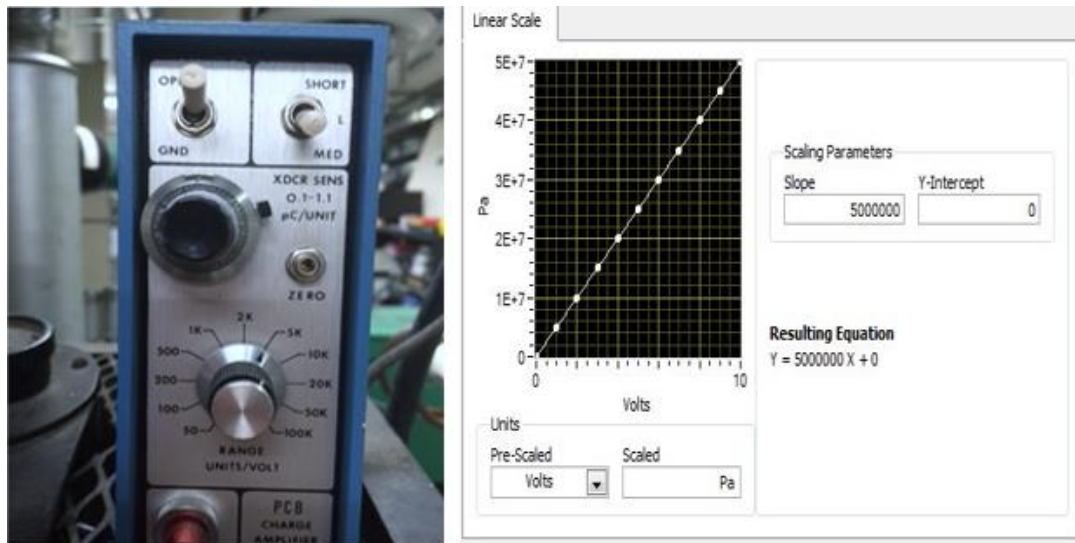
Figure 11. (a) Voltage amplifier unit PCB model 462A (b) LabVIEW calibration settings.

Figure 11.b shows the linear calibration function supplied to the LabVIEW GUI. specified. Each volt represents a 1 kPa pressure with a maximum pressure value of 5 MPa.

2.3.2 Intake Fuel Pressure Transducer

A pressure transducer (OMEGA PX139-030D4V) was used to measure the fuel pressure. The sensor was calibrated in-house using a dead-weight tester (figure 12). The

sensor was connected to a port on the tester. As known loads were applied, the corresponding voltage output was measured with a voltmeter.

Figure 12. Dead-weight-tester used for static calibration of the fuel pressure sensor.

The calibration experiment was conducted three times, and a linear equation of pressure versus voltage was generated, as shown in figure 13. The function was supplied to LabVIEW to automate future fuel pressure measurements (figure 14).
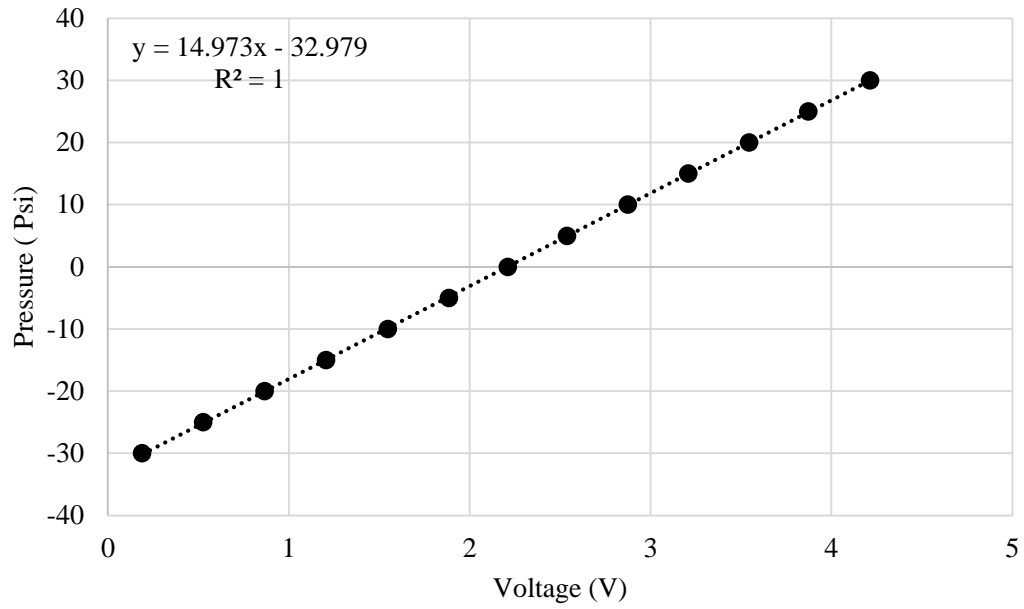
Figure 13. Fuel pressure sensor calibration curve.
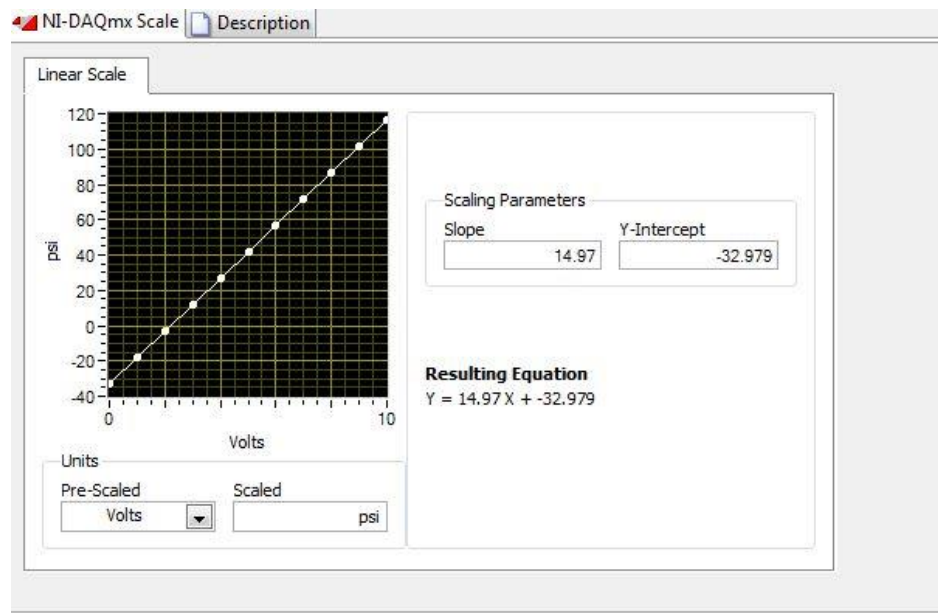
Figure 14. Fuel pressure sensor calibration curve supplied to the LabVIEW GUI.

2.3.3 Intake Air Pressure Sensor

A differential pressure transducer (Honeywell model 26PCCFA3G) was used to measure the intake air pressure. The device was calibrated using the same procedure as for the fuel pressure transducer. The calibration curve and corresponding LabVIEW GUI interface are shown in Figures 15 and 16, respectively.
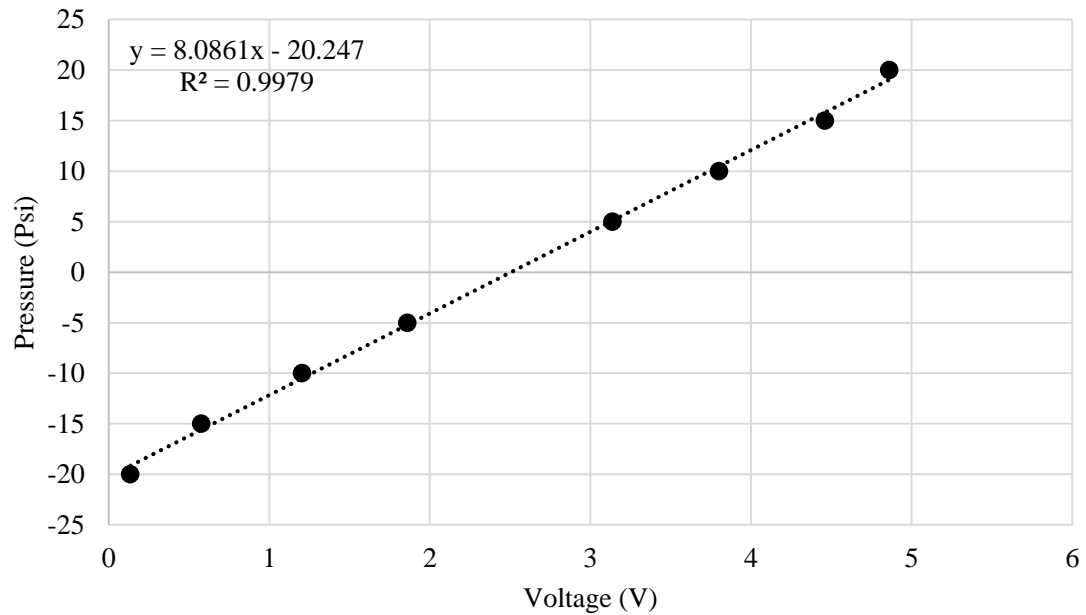
Figure 15. Calibration curve for the intake air pressure transducer.
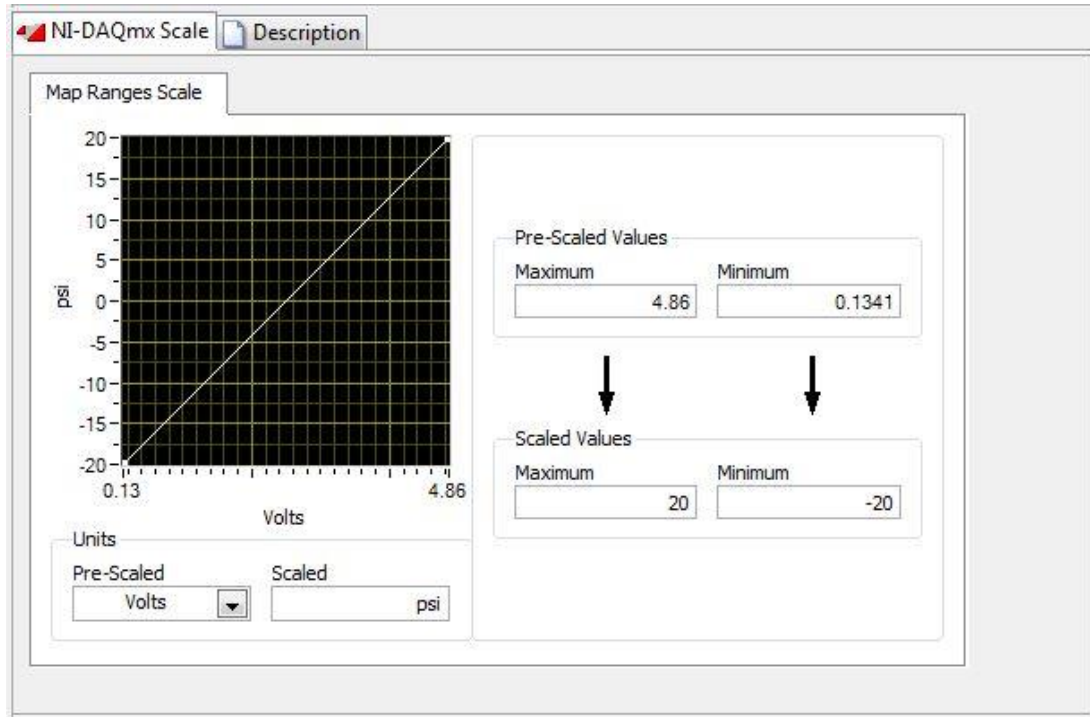
Figure 16. LabVIEW updated calibration data for the Intake air pressure transducer.

The remaining instruments had either been recently calibrated or are brand new (e.g. Exhaust gas analyzer, mechanical pressure (air and fuel) gauges, and fuel flow meter).

2.4 Optimization of Experimental Parameters

Before collecting the data required for the second-law analysis, the fuel delivery and spark timing were optimized.

2.4.1 Optimization of the Fuel Arc-Length and Solenoid Trigger Angle

The amount of fuel delivered to the engine (and thus the equivalence ratio) was controlled via the solenoid fuel valve duty cycle. In this thesis, we define the arc length as the time (in crank angles) the solenoid valve remains open, and the solenoid trigger angle as the crank angle at which the solenoid valve opens. The amount of fuel delivered to the

engine was extracted directly from the LabVIEW program, which was set to numerically integrate the fuel volumetric flow rate (LPM) versus time (s) and display the total fuel volume (mL) for each cycle. Figure 17 illustrates the arc length and solenoid trigger angle relative to the CFR engine intake and exhaust valve-timing events. The intake valve opens relatively late at 10° degrees after top-dead-center (TDC intake) and closes at 34° degrees after bottom-dead-center (BDC) compression. The exhaust valve opens at 40° degrees before BDC (expansion) and closes 15° degrees after TDC intake. This built-in configuration yields a five-degree valve overlap.
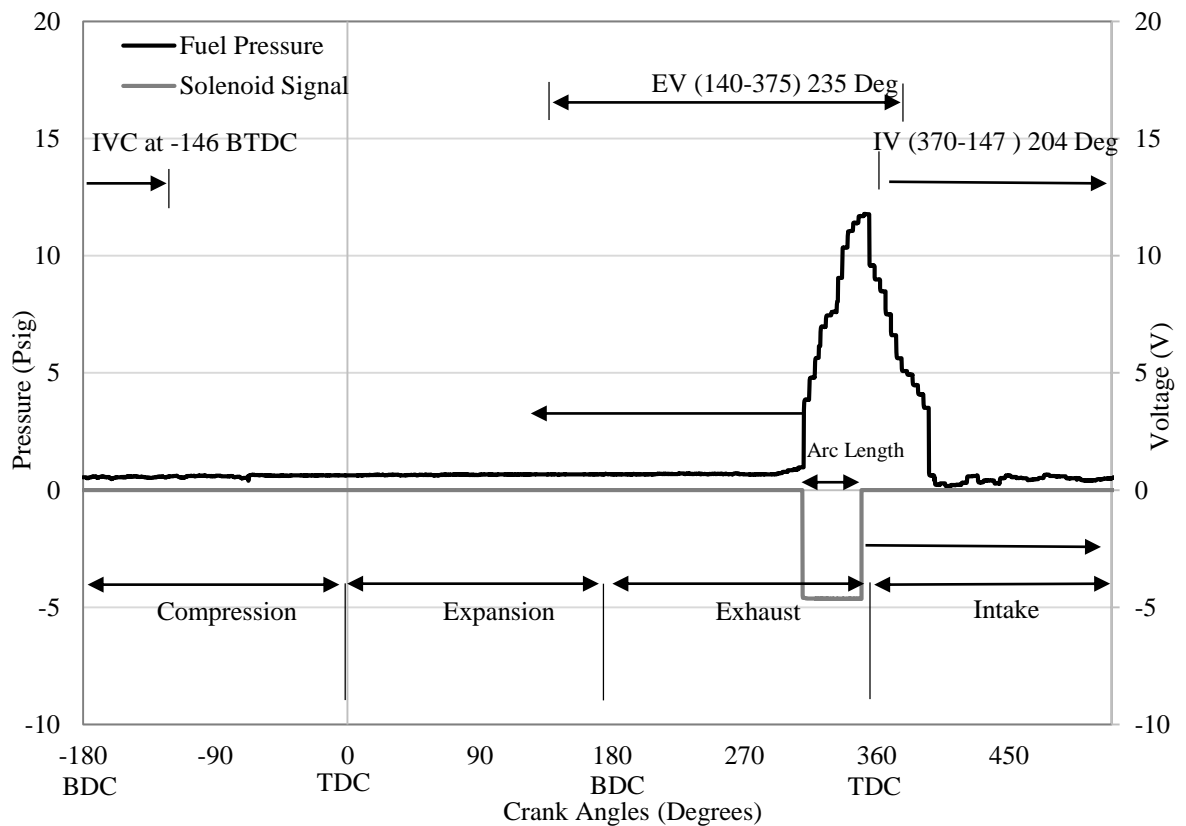
Figure 17. Valve timing and arc length relative to the Otto cycle strokes for a single cylinder, 0.6 L internal combustion engine.

In figure 17, the solenoid trigger angle was set at 350° degrees. A digital pressure sensor was installed after the solenoid valve for two reasons: first to check if the solenoid opens in time and second to measure the pressure of the fuel after the solenoid for fuel density calculations.

The fuel volume (in mL) delivered to the engine was evaluated based on the LabVIEW output integration, which was confirmed analytically. Table 5 shows the corresponding fuel volume (L) (averaged over 35 random cycles) relative to the fuel arc length (in CAD). The mass flow rate of fuel was calculated by multiplying the measured volumetric flow rate by the fuel density. Since the fuel enters in gaseous phase, the pressure and temperature affect its density, which in turn directly affects the air-to-fuel ratio for a fixed air mass flow rate. For this reason, the fuel pressure was regulated at the main fuel tank and measured at three points along the main fuel line (i.e., before the fuel accumulator and before and after the solenoid valve).

Table 5. Arc length optimization for a methane-fueled CFR engine at 600 RPM and WOT

Solenoid trigger angle (ATDC)	Arc Length (Degrees)	IVC (BTDC)	Fuel Volume (L)	Standard deviation
350	30	-146	0.0233	0.0028
350	35	-146	0.0270	0.0020
350	40	-146	0.0322	0.0015
350	55	-146	0.0422	0.0016
350	65	-146	0.0468	0.0016

The fuel volume at each arc length was used to calculate the air-fuel ratio via equation 2.3.

$$A/F_{actual} = \frac{m_{air}}{V_f * \rho} \qquad (2.3)$$

where A/F_{actual} is the actual air to fuel ratio, V_f is the delivered fuel volume, and ρ is the fuel density. The air mass (m_{air}) was calculated by multiplying the air mass flow rate (0.00337 kg/s) by the time duration of one cycle (0.2 s).

By knowing the actual air-fuel ratio, and the stoichiometric air-fuel ratio (17.2 for methane), the air-to-fuel equivalence ratio was calculated according to equation 2.4.

$$\lambda = \frac{A/F_{Actual}}{A/F_{stoich}} \qquad (2.4)$$

The equivalence ratio was calculated using equation 2.5.

$$\Phi = \frac{1}{\lambda} \qquad (2.5)$$

Table 6 displays the arc length, fuel volume, as well as the calculated and measured lambda and equivalence ratios.

Table 6. Fuel settings for a methane-fueled CFR engine at 600 RPM and WOT

Arc (Degrees)	Fuel Volume (L)	A/F actual ratio	Lambda calculated	Lambda measured	Equivalence ratio calculated	Equivalence ratio measured	Error %
30	0.023	23.62	1.37	1.20	0.73	0.83	14.01
35	0.027	20.35	1.18	1.11	0.85	0.90	6.91
40	0.032	17.07	0.99	1.01	1.01	0.99	1.60
55	0.042	13.01	0.76	0.88	1.32	1.13	14.45
65	0.047	11.74	0.68	0.80	1.46	1.25	14.69

Although the agreement between calculated and measured equivalence ratio values was acceptable, the error is significant. Each of the fuel flow measurement instruments (fuel flow meter, solenoid valve, fuel pressure and temperature gauges, and the pressure regulator) have a limited measurement accuracy, which in total cause this significant error. The direct equivalence ratio measured via the exhaust gas analyzer was used for analysis in the following sections, under the assumption that the error from this device was less than the cumulative error just described.

After completing the air-to-fuel ratio mapping, the maximum brake torque (MBT) timing was determined for each equivalence ratio. Details of this process will be described in the next section.

2.3 Spark Timing Optimization

At any predetermined engine operating condition, the optimum spark timing (i.e., MBT timing) yields the highest output torque [13], [14]. The MBT timing varies with engine speed, load and mixture stoichiometry. Since the load and speed remained constant in all experiments, the spark timing was optimized for each equivalence ratio. For the current experiments, the MBT timing was determined based on the gross indicated work obtained from the pressure-volume diagram at each spark timing [15]. To evaluate the MBT first, the spark timing was swept over a wide range of crank angles, between 60° and 16° BTDC compression in ten-degree increments. Through this preliminary sweep, it was found that advancing the spark timings from 40° to 60° increased the peak pressure and advanced its location relative to TDC (compression). In addition, it was observed that the compression work increased. This phenomenon can be attributed to the combined effects

of charge compression by the piston and expanding combustion gases due to combustion. Retarding the spark timing from 30° to 16° BTDC decreased the peak pressure magnitude and shifted its location after top dead center compression. A decrease in compression work was also noticeable in this range, with misfiring occurring at very retarded spark timings. Figure 18 displays the peak pressure location as a function of spark timing for an equivalence ratio of 0.991. The abscissa starts at -180° BDC, which is the beginning of the compression stroke, and ends at 180° TDC, which is the end of the expansion stroke.
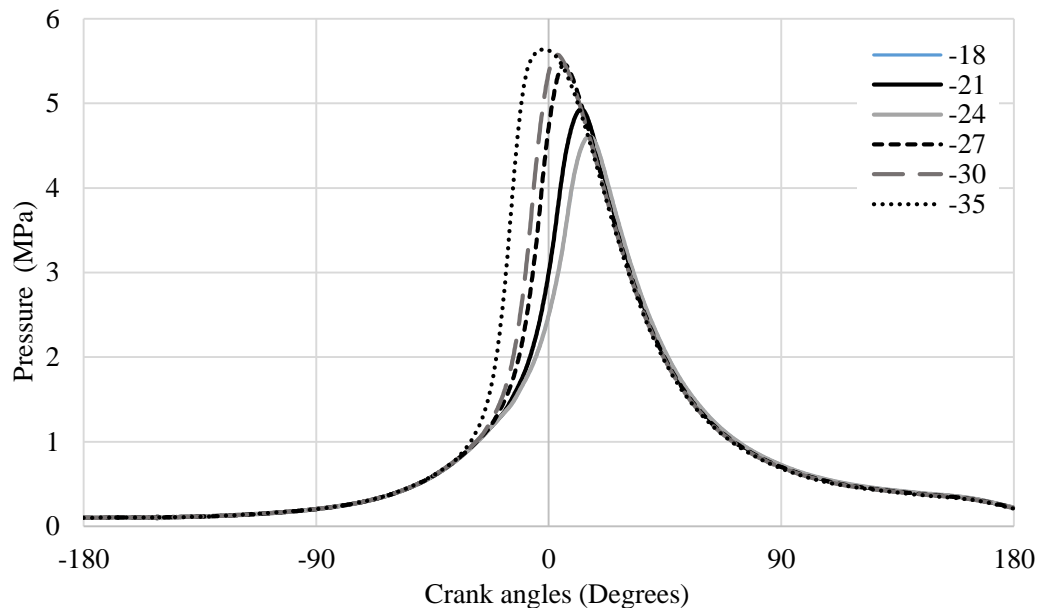
Figure 18. Pressure profiles versus crank angle as a function of spark timing for a methane-fueled CFR engine at 600 RPM, WOT, and 0.991 equivalence ratio.

The spark timing window was progressively narrowed while calculating the gross-indicated work, until the optimum spark timings was found at 24° BTDC for equivalence ratios of 0.83, 0.903, and 0.991 and 21° BTDC for equivalence ratios of 1.131, and 1.25. The gross indicated mean effective pressure (IMEP), defined as the gross work divided by

the displacement volume of the engine (equation 2.6) was used to determine the optimum spark timing location [14].

$$IMEP = \frac{W_{g,i}}{\forall d} \tag{2.6}$$

Figures 19, 20 and 21 show the $IMEP_{i,g}$ versus spark timing at 0.83, 0.90 and 1.13 respectively, where the maximum $IMEP_{i,g}$ occurs at approximately 24 BTDC. The error bars indicate the standard deviation calculated from three trials at each spark timing.
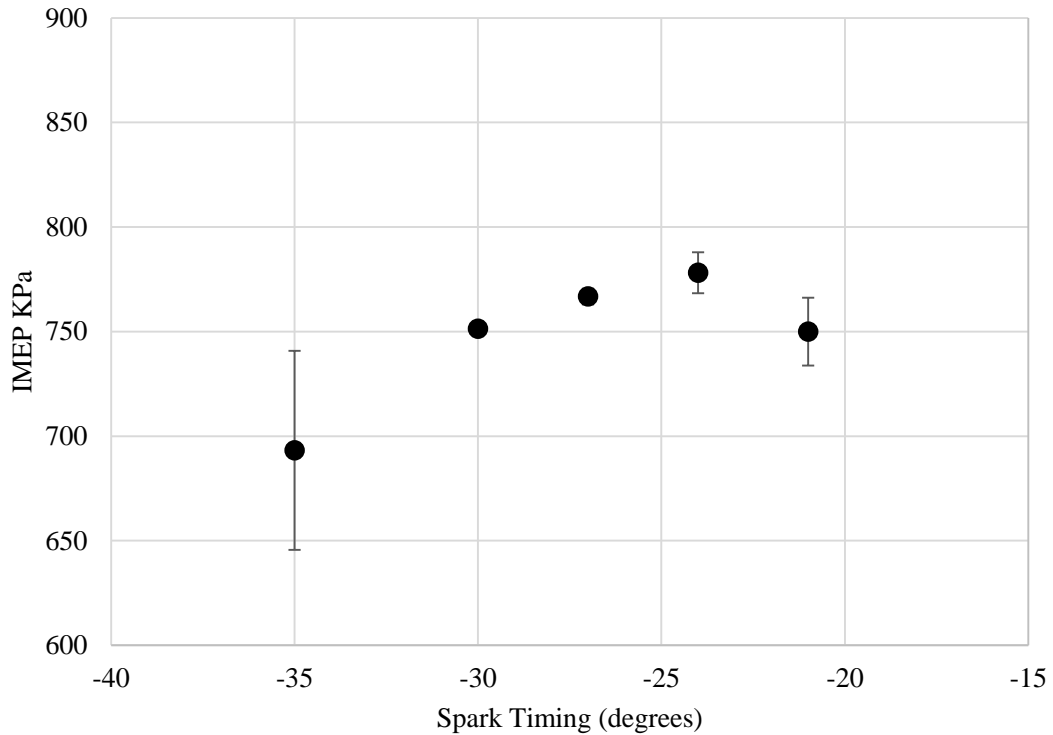
Figure 19. Gross $IMEP_{i,g}$ versus spark timing at 0.83 equivalence ratio for a methane-fueled CFR engine at WOT and 600 RPM.
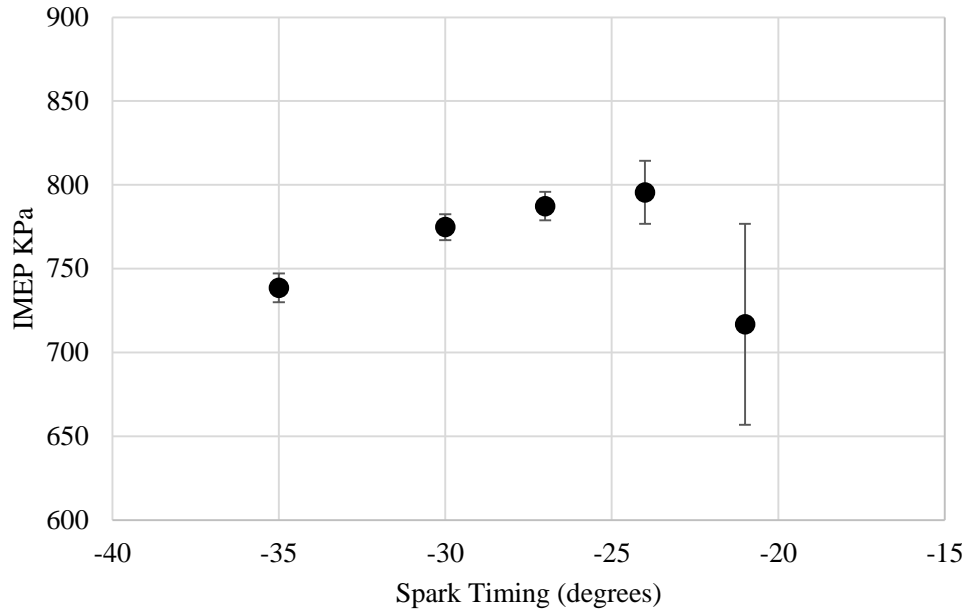
Figure 20. Gross $IMEP_{i,g}$ versus spark timing at 0.903 equivalence ratio for a methane-fueled CFR engine at WOT and 600 RPM.
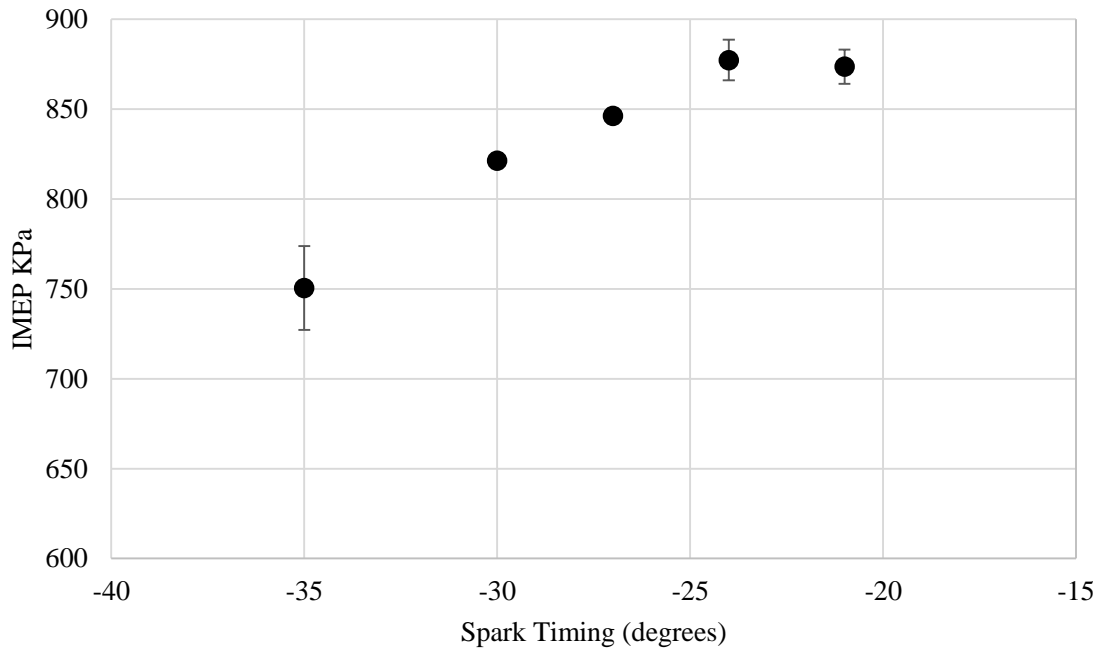
Figure 21. Gross $IMEP_{i,g}$ versus spark timings at 0.991 equivalence ratio for a methane-fueled CFR engine at WOT and 600 RPM.

At equivalence ratios of 1.131 and 1.25, the optimum spark timing was determined to be 21 BTDC, as shown in Figures 22 and 23. Table 7 shows spark timing optimization data, including the gross indicated work, IMEP, optimum spark timing, and coefficient of variation of $IMEP_{i,g}$ at each tested equivalence ratio. For lean equivalence ratios, there was misfiring at a spark timing of -18 BTDC; therefore, the data at that point were not considered due to the high uncertainty, and the high standard deviation in the $IMEP_{i,g}$. At rich equivalence ratios, the engine was able to fire normally at -18 BTDC, but misfiring happened at spark timings retarded beyond this point.
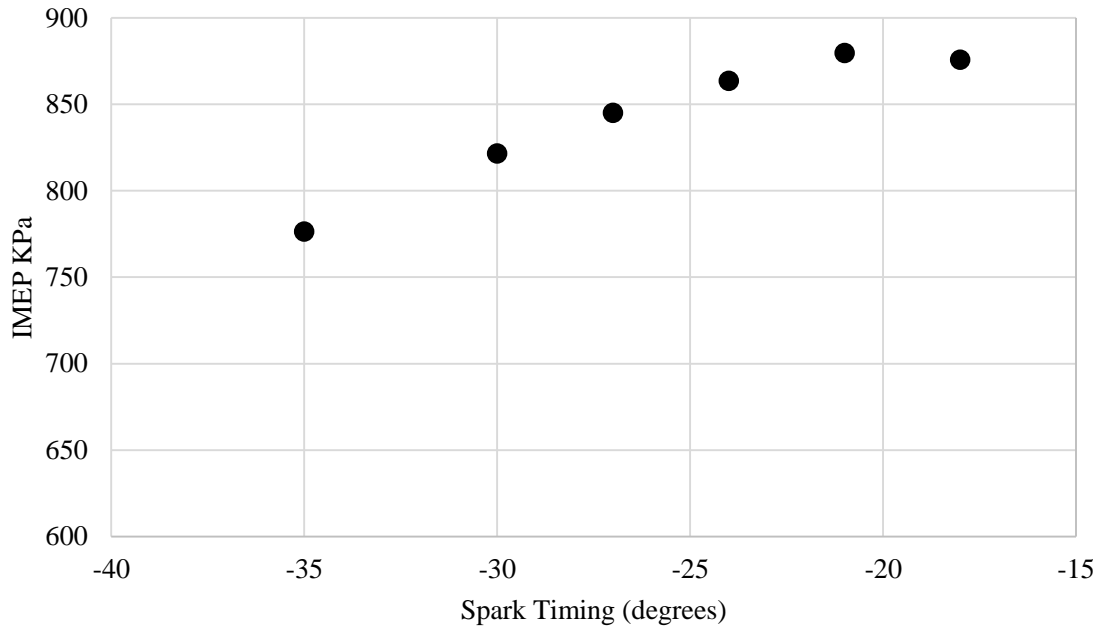
Figure 22. Gross $IMEP_{i,g}$ versus spark timing at 1.131 equivalence ratio a methane-fueled CFR engine at WOT and 600 RPM.
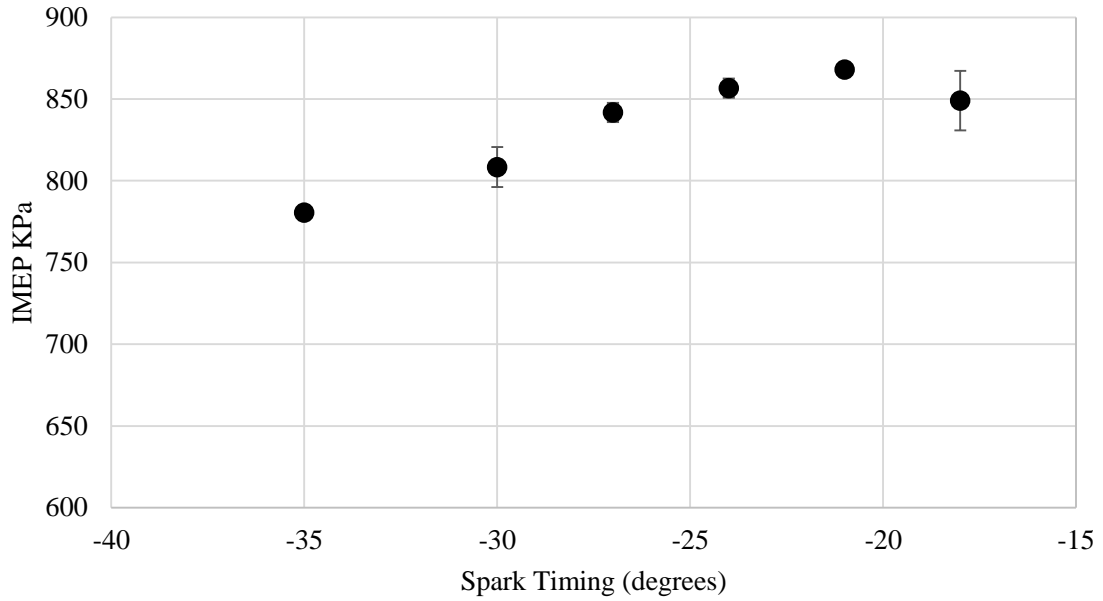
Figure 23. Gross $IMEP_{i,g}$ versus spark timing at 1.25 equivalence ratio for a methane-fueled CFR engine at WOT and 600 RPM.

From table 7, the coefficient variation (COV) in indicated mean effective pressure $IMEP_{i,g}$ was calculated using equation 2.7 to quantify the cycle-to-cycle variability in IMEP and provide a measure of combustion stability.

$$COV_{IMEP}(\%) = \frac{STD_{IMEP}*100}{IMEP} \qquad (2.7)$$

Table 7. Spark timing optimization data for a CFR engine 600 RPM and WOT at different equivalence ratios.

S.T[2] (BTDC)	Φ = 0.830			Φ = 0.903			Φ = 0.991			Φ = 1.131			Φ = 1.250		
	IMEP (kPa)	S.D[3]	COV in IMEP	IMEP (kPa)	S.D	COV in IMEP	IMEP (kPa)	S.D	COV in IMEP	IMEP (kPa)	S.D	COV in IMEP	IMEP (kPa)	S.D	COV in IMEP
-18	-	-	-	-	-	-	-	-	-	875.73	2.05	0.23	848.95	18.21	2.15
-21	749.98	16.17	2.16	716.86	59.96	8.36	873.58	9.47	1.08	879.75	3.34	0.38	868.01	0.77	0.09
-24	778.11	9.84	1.26	795.56	18.81	2.36	877.27	11.28	1.29	863.56	0.72	0.08	856.69	5.80	0.68
-27	766.79	3.75	0.49	787.31	8.48	1.08	846.25	2.03	0.24	845.02	1.52	0.18	841.86	5.88	0.70
-30	751.32	3.19	0.42	774.80	7.70	0.99	821.30	0.76	0.09	821.63	1.20	0.15	808.39	12.28	1.52
-35	693.21	47.55	6.86	738.54	8.57	1.16	750.49	23.33	3.11	776.32	2.09	0.27	780.53	2.79	0.36

[2] Spark timing
[3] Standard deviation

41

Given the minimal variation of spark timing with equivalence ratio observed in the baseline experiments, an additional test was conducted to check spark timing accuracy relative to the input spark timing value specified through the LabVIEW GUI. The test was based on the operation of the ignition system coil, which consists of primary and secondary windings. By suppling a voltage from an external source (typically 12V), a current flow through the primary winding and creates a magnetic field around it. At the time of spark, the external voltage source is shut off, causing the magnetic field to collapse. This action generates high voltage (approximately 220 kV) in the secondary winding. The high voltage transfers and arcs across the spark plug gap and ignites the air-fuel mixture [16].

The ignition timing voltage signal, specified by the user through the LabVIEW (GUI), was extracted from the DAQ and displayed on an oscilloscope. The actual spark timing voltage signal was measured by wrapping a wire around the primary coil and connecting it to a 100 Ω resistor. The magnetic field induces a current in the wire, which flows through the resistor to produce a voltage. This voltage was displayed on the oscilloscope and compared to the user-specified voltage (figure 24). For the test, The LabVIEW spark timing was set at 30° BTDC (compression) (150° ABDC). The black line in figure 24 represents the crank angle encoder index, and the reference point (i.e. the small tick on the black line) equals 180° BTDC (compression). The dark grey line represents the actual spark voltage, while the light grey line represents the voltage signal from the data acquisition. The time difference between the encoder index and the spark timing was measured as 42.2 ms, which is equivalent to 151.9^o degrees BTDC, according to equation (2.8)

$$t = N \left(\frac{rev}{min}\right) * \left(\frac{min}{60 \ sec}\right) * \left(\frac{720 \ \theta}{rev}\right)$$
(2.8)

Where t is the time in seconds, N is the engine speed (600 RPM), and θ is the crank angle in degrees. For this work, equation 2.8 was rearranged to be a general relation (equation 2.9) between time and crank angles.

$$t = \frac{\theta}{3600} \qquad (2.9)$$

Therefore, the actual spark timing was triggered at 28.1^o degrees BTDC. This suggests that the offset between the user-specified and actual spark timings is 1.9^o degrees.
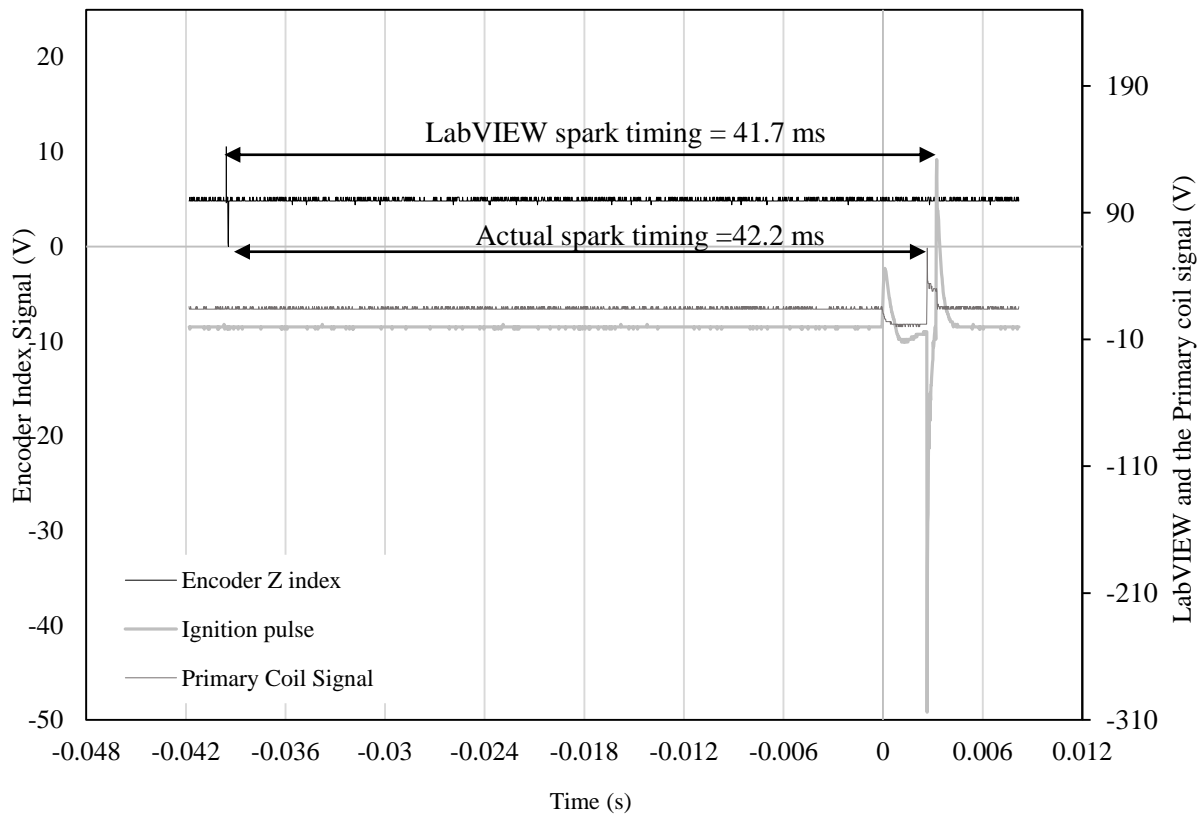
Figure 24. Results from the spark timing experiment performed to validate the LabVIEW spark timing signal for a methane-fueled CFR engine at 600 RPM and WOT load.

After completing the instrument calibration and parameter optimization, an experimental matrix was developed to organize the data collection and ensure consistency in the process.

2.4 Experimental Plan

       This section will include only the experimental inputs, whereas the outputs (results) will be discussed in chapter 4 (results and discussion). Table 8 shows the inputs of the experiment at the selected equivalence ratios. The experiment was conducted three times for each equivalence ratio to account for cycle-to-cycle variability.

Table 8. Experimental inputs for the methane-fueled CFR engine tests.

Inputs	$\Phi = 0.830$	$\Phi = 0.903$	$\Phi = 0.991$	$\Phi = 1.131$	$\Phi = 1.250$
Load	WOT	WOT	WOT	WOT	WOT
Speed RPM	600	600	600	600	600
Micrometer reading	0.2	0.2	0.2	0.2	0.2
Compression ratio	10	10	10	10	10
Ambient Temperature (K)	300	300	300	300	300
Ambient Pressure (kPa)	99	99	99	99	99
Inlet air mass flow rate (kg/s)	0.003365	0.003365	0.003365	0.003365	0.003365
Arc Setting (degrees)	30	35	40	55	65
Stoich. A/F ratio	17.2	17.2	17.2	17.2	17.2
Actual A/F	23.62	20.35	17.07	13.01	11.74
Lambda	1.39	1.20	1.004	0.77	0.69
Equivalence ratio (Calculated)	0.72	0.84	0.996	1.32	1.45

       The experimental inputs were categorized based on the measured equivalence ratio, since it was assumed to carry less uncertainty than the calculated values, as discussed in section 2.4.1. Before discussing the experimental results and corresponding analysis, the set of equations used in current work are presented next.

CHAPTER III

EQUATIONS AND FORMULATIONS

3.1 Equations

This chapter introduces the equations used in the ideal and spark-ignition (SI) engine cycle availability analyses. The latter term is used throughout this thesis to refer to the thermodynamic processes in a practical spark-ignition engine.

3.1.1 Air Mass Flow Rate

The air mass flow rate was measured experimentally and the corresponding volumetric efficiency was calculated using equation 3.1 [14], where $\frac{N}{n}$ is the ratio of engine speed to the number of revolutions per cycle, ξ_v is the volumetric efficiency, and $\dot{m}_{air}$ is the air mass flow rate. All experiments were conducted at 95% volumetric efficiency

$$\xi_v = \frac{\dot{m}_{air}}{\rho_{air}\, \forall_d \left(\frac{N}{n}\right)} \qquad (3.1)$$

3.1.2 Specific Heats

Values of the specific heat ratio (γ) and the specific heat at constant volume (Cv) were needed for the second law of Thermodynamics analysis. Under the ideal gas assumption, the specific heats are only functions of temperature. For the ideal Otto cycle analysis, Cv and Cp of air were assumed constant at 298 K. In the spark-ignition cycle analysis, the temperature dependence was accounted for through the empirical polynomial relation shown in equation 3.2 [1], where a, b, c, and d are the air constants and equal to 28.11, $0.1967*10^{-2}$, $0.4802*10^{-5}$, and $1.966*10^{-9}$, respectively.

$$\overline{Cp} = a + bT + cT^2 + dT^3 \qquad \text{(kJ / kmol. K)} \qquad (3.2)$$

The results from equation 3.2 were divided by the molar mass of air to calculate the Cp on a per unit mass basis. After evaluating Cp from equation 3.2, the Cv was calculated using the relation ($Cv = Cp - R$), where R is the ideal gas constant of air. The ratio of specific heats γ, was computed as the ratio of Cp and Cv.

3.1.3 Instantaneous Cylinder Volume

The LabVIEW GUI was programed to compute the instantaneous cylinder volume via equation 3.3.

$$\frac{V(\theta)}{Vc} = 1 + \frac{1}{2}\,(r-1) * \left(\frac{l}{a} + 1 - cos(\theta) - \left(\left(\frac{l}{a}\right)^2 - sin(\theta)^2 \right)^{\frac{1}{2}} \right) \qquad (3.3)$$

Where:

$V(\theta)$: Instantaneous volume at any crank angle

Vc: Clearance volume

r: Compression ratio

$\frac{l}{a}$:   Connecting rod to crank offset ratio

3.1.4 Polytropic Exponent

The polytropic relation ($Pv^n = c$) was used to evaluate the polytropic exponent for the compression and expansion strokes. This relation was expanded by taking the logarithm of the pressure and the volume between two states, according to equation 3.4 [13], where n is the

46

polytropic exponent and the pressure was experimentally measured using the piezoelectric transducer (section 2.1.4).

$$n = \frac{\log P2 - \log P1}{\log v2 - \log v1} \qquad (3.4)$$

3.1.5 Second Law Equations for a Closed System.

In this section, the generalized availability change for a closed system is presented [17], starting with the general formulation for the thermo-mechanical availability (equation 3.5). The closed-system formulation was used for the compression and expansion strokes. This project did not consider the intake and exhaust strokes.

$$(A_2 - A_1)_{tm} = \int_1^2 \left(1 - \frac{T_O}{T}\right) \delta Q - W + P_O(V_2 - V_1) - T_O \sigma \qquad (3.5)$$

where $(A_2 - A_1)_{tm}$ is the thermo-mechanical availability change. The term $\int_1^2 \left(1 - \frac{T_O}{T}\right) \delta Q$ represents the availability transfer accompanying heat transfer; $W + P_O(V_2 - V_1)$ quantifies the availability transfer accompanying work, and the last term represents the irreversibility, I. In addition, σ represents the entropy generation. Equation 3.5 can be written in a rate form as in equation 3.6 [17].

$$\left(\frac{dA}{dt}\right)_{tm} = \left(1 - \frac{T_O}{T}\right) \delta \dot{Q} - \dot{W} + P_O \frac{dV}{dt} - T_O \dot{\sigma} \qquad (3.6)$$

Dividing equations (3.5) and (3.6) by the system mass, the specific thermo-mechanical availability can be calculated, as shown in equations 3.7 and 3.8.

$$(a_2 - a_1)_{tm} = \int_1^2 \left(1 - \frac{T_O}{T}\right) \delta q - w + P_O(v_2 - v_1) - T_O \sigma_m \qquad (3.7)$$

$$\frac{da}{dt} = \left(1 - \frac{T_O}{T}\right) \delta \dot{q} - \dot{w} + P_O \frac{dv}{dt} - T_O \dot{\sigma}_m \qquad (3.8)$$

Equations 3.5 and 3.6 can be used to evaluate the thermo-mechanical availability change of a closed system with variable volume. The total availability can be calculated by using equation 3.9,

$$\Delta A_t = \Delta A_{tm} + \Delta A_{ch} \tag{3.9}$$

where ΔA_{tm} is the thermo-mechanical availability change and ΔA_{ch} is the change in chemical availability. For the ideal Otto cycle, the ΔA_{ch} term represents the availability of the reaction, ΔA_R, defined in equation 3.10,

$$\Delta A_{ch} = \Delta A_R = U_P(T_S) - U_R(T_S) - T_O(S_R(T_S) - S_P(T_S)) \tag{3.10}$$

where T_S (the standardized temperature = 298 K) is the temperature at which the reaction energy and entropy are calculated; U_R is the internal energy of the reaction, equal to the caloric value of the fuel (since no work is produced during constant-volume combustion, $(\Delta U_R = Q - W)$). With the assumption of 100% combustion efficiency at constant volume (i.e. W=0) for the ideal Otto cycle, $Q=Q_{lhv}$. Based on this, equation (3.10) can be written as:

$$\Delta A_R = \Delta U_R - T_O(S_R(T_S) - S_P(T_S))$$

$$\Delta A_R = Q_{lhv} - T_O(S_R(T_S) - S_P(T_S)) \tag{3.11}$$

Now adding the chemical availability (ΔA_R) to equation (3.5) yields the total availability, represented in equation 3.12

$$(A_2 - A_1)_t = \Delta A_R + \int_1^2 \left(1 - \frac{T_O}{T}\right)\delta Q - W + P_O(V_2 - V_1) - T_O\sigma \tag{3.12}$$

Then, from the first law of Thermodynamics:

$$U_2 - U_1 = \int_1^2 (\delta Q - \delta W) = \int_1^2 \delta Q - W \tag{3.13}$$

And from the second law of Thermodynamics:

$$S_2 - S_1 = \int_1^2 \frac{\delta Q}{T} + \sigma \tag{3.14}$$

Substituting equations 3.13 and 3.14 into equation 3.12 yields:

$$(A_2 - A_1)_t = \Delta A_R + (U_2 - U_1) + P_O(V_2 - V_1) - T_O(S_2 - S_1) \tag{3.15}$$

Equation (3.15) is used to evaluate the change in the total availability between two states of the ideal Otto cycle. It can also be generalized to calculate the change in the total availability between a given state i relative to the dead state, as shown in equation 3.16.

$$(A_i - A_o)_t = \Delta A_R + (U_i - U_o) + P_O(V_i - V_o) - T_O(S_i - S_o)$$

$$(a_i - a_o)_t = m_f \Delta a_R + m[(u_i - u_o) + P_O(v_i - v_o) - T_O(s_i - s_o)] \tag{3.16}$$

Where the total mass of the mixture, m, is evaluated with assumption of no residual gases, such that:

$$m = m_f + m_{air} \tag{3.17}$$

Dividing equation 3.16 by the total mass yields:

$$(a_i - a_o)_t = \frac{A_i - A_o}{m} = \frac{m_f}{m} \Delta a_R + [(u_i - u_o) + P_O(v_i - v_o) - T_O(s_i - s_o)] \tag{3.18}$$

Defining the air-to-fuel ratio, A/F as $(\frac{m_{air}}{m_f})$, equation (3.18) becomes:

$$(a_i - a_o)_t = \frac{A_i - A_o}{m} = \frac{1}{A/F + 1} \Delta a_R + [(u_i - u_o) + P_O(v_i - v_o) - T_O(s_i - s_o)] \tag{3.19}$$

The availability of reaction Δa_R is related to the internal energy of reaction through equation 3.20.

$$\Delta a_R = Q_{lhv} \left(1 - \frac{T_O(S_R(P_o,T_O) - S_P(P_o,T_O))}{Q_{lhv}}\right) = x_a Q_{lhv} \tag{3.20}$$

Substituting equation 3.20 into 3.19 yields:

$$(a_i - a_o)_t = \frac{x_a Q_{lhv}}{A/F+1} + [(u_i - u_o) + P_O(v_i - v_o) - T_O(s_i - s_o)] \tag{3.21}$$

where the energy of reaction can be evaluated from $q^* = \frac{Q_{lhv}}{A/F+1}$. Dividing both sides of equation

3.21 by q^* produces the generalized equation for calculating the availability change of a closed

system [17]:

$$\frac{(a_i - a_o)_t}{q^*} = \frac{1}{q^*}[\frac{x_a Q_{lhv}}{A/F+1} + ((u_i - u_o) + P_O(v_i - v_o) - T_O(s_i - s_o))]$$

$$\frac{(a_i - a_o)_t}{q^*} = \frac{1}{q^*}[x_a q^* + ((u_i - u_o) + P_O(v_i - v_o) - T_O(s_i - s_o))] \tag{3.22}$$

Under the perfect gas assumption (i.e., ideal gas with constant specific heats), equations

3.22 a, b, and c can be used to calculate the change in the internal energy, the work against the

surroundings and the change in the entropy, as follows:

$$u_i - u_o = c_v(T_i - T_o) = c_v T_o \left(\frac{T_i}{T_o} - 1\right) \tag{3.22a}$$

$$P_O(v_i - v_o) = P_O v_o \left(\frac{v_i}{v_o} - 1\right) = RT_o \left(\frac{v_i}{v_o} - 1\right) = (k-1)\, c_v T_o \left(\frac{v_i}{v_o} - 1\right) \tag{3.22b}$$

$$T_O(s_i - s_o) = T_o \left\{c_p \ln\frac{T_i}{T_o} - R \ln\frac{P_i}{P_o}\right\} = c_v T_o\{k \ln\frac{T_i}{T_o} - (k-1) \ln\frac{P_i}{P_o}\} \tag{3.22c}$$

Subject to the aforementioned assumptions, the total availability equation becomes

$$\frac{(a_i - a_o)_t}{q^*} = \frac{c_v T_o}{q^*}[\frac{x_a q^*}{c_v T_o} + \left(\frac{T_i}{T_o} - 1\right) + ((\gamma - 1)\left(\frac{v_i}{v_o} - 1\right)) - \{\gamma \ln\frac{T_i}{T_o} - (\gamma - 1) \ln\frac{P_i}{P_o}\}] \tag{3.23}$$

Equation 3.23 can be applied around the ideal Otto cycle to calculate the total availability of the

system at any given state, relative to the dead state. A spreadsheet was developed as part of this

50

work to evaluate equation 3.23. The change in availability between two states was calculated using equation 3.24.

$$\left(\frac{a_{i+1}-a_o}{q^*} - \frac{a_i-a_o}{q^*}\right) = \left[\frac{c_v T_o}{q^*}\left[\left(\frac{T_{i+1}}{T_o}-1\right) - \left(\frac{T_i}{T_o}-1\right) + ((\gamma-1)\left(\frac{v_{i+1}}{v_o}-1\right) - (\gamma-1)\left(\frac{v_i}{v_o}-1\right)\right)\right] \tag{3.24}$$

In [17], equation 3.24 was applied to an ideal Otto cycle engine, in which the combustion process is assumed to occur instantaneously and the availability change during constant-volume combustion was calculated using equation 3.25.

$$\frac{a_3-a_o}{q^*} = \frac{a_2-a_o}{q^*} + \frac{c_v T_o}{q^*}\left[-\left\{\gamma\ln\frac{T_3}{T_2} - (\gamma-1)\ln\frac{P_3}{P_2}\right\}\right] \tag{3.25}$$

In equation 3.25, the indices 2 and 3 refers to the start and the end of the adiabatic combustion process, respectively.

In this work, equations 3.23, 3.24, and 3.25 were used only for the ideal Otto cycle code validation. The ideal Otto cycle and spark-ignition cycle were then compared on the basis of thermo-mechanical availability (equation 3.26), since in the latter combustion is not instantaneous and consideration of combustion rates was beyond the scope of the current work.

$$\frac{(a_i-a_o)_{tm}}{q^*} = \frac{c_v T_o}{q^*}\left[\left(\frac{T_i}{T_o}-1\right) + ((\gamma-1)\left(\frac{v_i}{v_o}-1\right)) - \left\{\gamma\ln\frac{T_i}{T_o} - (\gamma-1)\ln\frac{P_i}{P_o}\right\}\right] \tag{3.26}$$

3.1.6 Temperature Analysis

The temperature analysis for the ideal Otto cycle was conducted in three stages (compression, combustion and expansion). The compression and expansion strokes were considered as isentropic processes with a specific heat ratio of 1.3. The maximum temperature (i.e., the adiabatic flame temperature) was assumed during combustion (full analysis details will be shown in the next chapter). For the SI engine cycle temperature analysis, the compression and

expansion strokes were considered as polytropic processes. The polytropic exponents were evaluated from equation 3.4, as demonstrated in section 3.1.4. Equation 3.27 shows the polytropic relation between the pressure and the temperature at two states, where n is the polytropic exponent during the compression or the expansion stroke.

$$\left(\frac{T_{i+1}}{T_i}\right) = \left(\frac{P_{i+1}}{P_i}\right)^{\left(\frac{n-1}{n}\right)}$$

(3.27)

The pressure was known experimentally and the initial temperature was calculated using the ideal gas law (equation 3.28), where P, V, R_t, and T are the pressure, volume, ideal gas constant and temperature of the mixture, respectively; m_t is the mixture total mass (a known value at each equivalence ratio).

$$PV = m_t R_t T$$

(3.28)

Equation 3.27 cannot be applied during combustion since this process is not polytropic. Therefore, a theoretical temperature calculation was carried out by first determining the incremental temperature change, according to equations 3.29 and 3.30. Results from the temperature analysis will presented in chapter 4.

$$T = \frac{PV}{m_t R_t}$$

(3.29)

$$dT = \frac{1}{m_t R_t} \, (PdV + VdP)$$

(3.30)

3.1.7 Second-Law Efficiency

The second law efficiency was quantified at each equivalence ratio through equation 3.31,

$$\eta_{II} = \frac{W_{i,g}}{W_{rev}}$$

(3.31)

where $W_{i,g}$ is the gross indicated work, which can be extracted from the pressure-volume

analysis of the cycle and W_{rev} is the maximum possible work that can be achieved from a system

between two thermodynamic states. A complete analysis is presented in chapter 4.

CHAPTER IV

RESULTS AND DISCUSSION

4.1 Results and Discussion

In this section, theoretical and experimental results will be presented regarding the effect of equivalence ratio on the thermo-mechanical availability of the spark-ignition (Otto) cycle. The discussion will focus on compression, combustion and expansion processes for the ideal spark-ignition (Otto) cycle and for the cycle a typical spark-ignition engine undergoes, which will be referred to as the spark-ignition (SI) cycle. First, a code developed in-house to calculate the cycle availability based on thermodynamics principles was validated with isooctane using results from the technical literature [17] and [13]. Once validated, the code was used to evaluate the availability of the ideal Otto cycle using methane as a fuel. Experimental data were then used to calculate the thermo-mechanical availability of the SI engine cycle at MBT timing for five equivalence ratios: 0.830, 0.903, 0.991, 1.131, and 1.25. Results were compared from a second-law perspective.

4.2 Second-Law Analysis of the Ideal Spark-Ignition (Otto) Cycle

4.2.1 Background, Analysis Procedure and Code Validation

The Otto cycle, which is the ideal cycle for spark-ignited, reciprocating, internal combustion engines, consists of four processes. As shown in figure 25, these are: isentropic compression (1-2), constant volume heat addition (2-3), isentropic expansion (3-4), and constant volume heat rejection (4-1). Processes (5-6) and (6-5) represents the pumping loop for the intake and the exhaust processes. Further assumptions include treating the mixture as air, ideal gas

54

behavior, 100% combustion efficiency, and simulating the combustion process as heat addition from an external source.
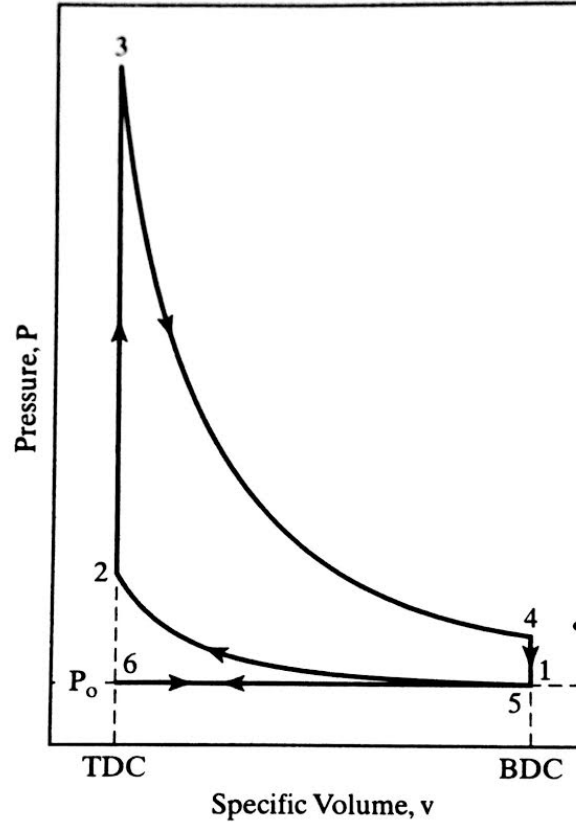
Figure 25. Pressure-volume (P-V) diagram of the ideal Otto cycle [14].

A numerical code was developed to evaluate the total availability during the compression, combustion and expansion processes using equations 3.23, 3.24, and 3.25. As a first step and to validate the code, the analysis was conducted on the ideal Otto cycle and compared with existing results [17]. The non-dimensional total availability during the compression was evaluated based on equation (3.23), repeated next for convenience.

$$\frac{a_i - a_o}{q^*} = \frac{c_v T_o}{q^*} \left[\frac{x_a q^*}{c_v T_o} + \left(\frac{T_i}{T_o} - 1 \right) + \left((\gamma - 1) \left(\frac{v_i}{v_o} - 1 \right) \right) - \left\{ \gamma \ln \frac{T_i}{T_o} - (\gamma - 1) \ln \frac{P_i}{P_o} \right\} \right]$$

Equation (3.25) was used to calculate the availability during combustion,

$$\frac{a_3 - a_o}{q^*} = \frac{a_2 - a_o}{q^*} + \frac{c_v T_o}{q^*} \left[-\left\{ \gamma \ln \frac{T_3}{T_2} - (\gamma - 1) \ln \frac{P_3}{P_2} \right\} \right]$$

Equation 3.24 was used for the expansion stroke.

$$\left(\frac{a_{i+1} - a_o}{q^*} - \frac{a_i - a_o}{q^*} \right) = \left[\frac{c_v T_o}{q^*} \left[\left(\frac{T_{i+1}}{T_o} - 1 \right) - \left(\frac{T_i}{T_o} - 1 \right) + ((\gamma - 1) \left(\frac{v_{i+1}}{v_o} - 1 \right) - (\gamma - 1) \left(\frac{v_i}{v_o} - 1 \right) \right)$$

In contrast to equation (3.23) it allows for calculating the availability change between two states. Either equation can be used for the compression and expansion strokes; the choice made in this project is consistent with [17], since the objective of this step is to validate the code.

Residual gasses were neglected in the analysis, a constant specific heat ratio of 1.3 was assumed and, consistent with the ideal Otto cycle, combustion was assumed to occur instantaneously (i.e., at constant volume). As discussed in Chapter 3, the term x_a is related to the availability as follows (equation 3.20):

$$\Delta A_R = Q_{lhv} \left(1 - \frac{T_o \left(S_R (P_o, T_o) - S_P (P_o, T_o) \right)}{(Q_v)_s} \right) = x_a Q_{lhv}$$

where x_a represents the ratio of the availability of the reaction to the lower heating value ($x_a = \frac{\Delta A_R}{Q_{lhv}}$). The entropy of each mixture constituent was calculated using equation 4.1.

$$\bar{s}_i(T, P_i) = \bar{s}^o{}_i(T, P_o) - Ru \ln \frac{y_i P_m}{P_o} \qquad \text{(kJ /kmol K)} \qquad (4.1)$$

Where $\bar{s}^o{}_i(T, P_o)$ is the absolute entropy for reactants and products, y_i is the mole fraction for each species and P_m is the mixture pressure (bar). Ambient conditions are assumed to be $P_o = 1\ bar, T_o = 300\ K$.

For lean and stoichiometric conditions, equation 4.2 [17] was used to calculate the number of moles of reactants and products for methane-air combustion.

56

$$CH_4 + \frac{2}{\Phi}(O_2 + 3.76\, N_2) = CO_2 + 2H_2O + 2\left(\frac{1-\Phi}{\Phi}\right)O_2 + \frac{7.52}{\Phi}N_2 \qquad (4.2)$$
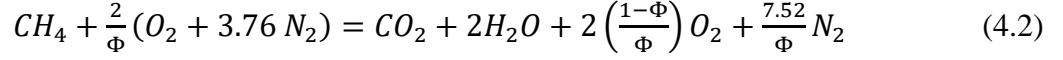
Here Φ is the equivalence ratio, as defined in equation 2.5. The second equation (4.3) [17] was

used for rich fuel-air mixtures, under the assumption of no oxygen in the products.

$$CH_4 + \frac{2}{\Phi}(O_2 + 3.76\, N_2) = \left(\frac{4-3\Phi}{\Phi}\right)CO_2 + 2H_2O + 4\left(\frac{\Phi-1}{\Phi}\right)CO + \frac{7.52}{\Phi}N_2 \qquad (4.3)$$
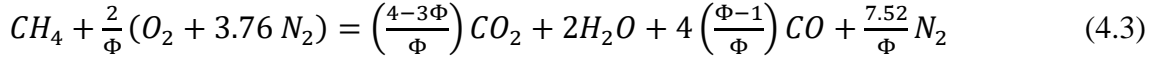
Equation 4.3 is limited to $\Phi \le 4/3$ to avoid negative CO_2 values [17]. For cases of $\Phi \ge 4/3$, a

more complicated calculation process by using the water-gas shift reaction relation can be used

to obtain the chemical balance.

For the ideal Otto cycle, the temperature after combustion was assumed to be the adiabatic

flame temperature. Which is the maximum temperature for a given combustion process, under the

assumptions of no heat transfer, negligible changes in kinetic and potential energies, and no work

interactions, based on the first law for combusting systems. For closed systems, the adiabatic flame

temperature is calculated according to equation 4.4-a [1].

$$Q - W = \sum N_P(\overline{h^o}_f + \overline{h} - \overline{h^o} - R_uT)_P - \sum N_r(\overline{h^o}_f + \overline{h} - \overline{h^o} - R_uT)_r \qquad (4.4)$$

$$\sum N_P(\overline{h^o}_f + \overline{h} - \overline{h^o} - R_uT)_P = \sum N_r(\overline{h^o}_f + \overline{h} - \overline{h^o} - R_uT)_r \qquad (4.4\text{-a})$$

where N_P and N_r are the total number of moles of the products and the reactants, respectively; $\overline{h^o}_f$

represents the enthalpy of formation (kJ/kmol), $\overline{h}$ is the enthalpy at a given thermodynamic state

(kJ/kmol), and $\overline{h^o}$ is the enthalpy at the reference state (T=298 K, P=1 atm) (kJ/kmol). Since the

temperature of the reactants is known, the enthalpy of the products can be calculated using an

iterative approach. A spreadsheet of thermodynamic properties was incorporated into the code to

automate the iterative process and evaluate the adiabatic flame temperature for different air-to-fuel

ratios. Table 9 shows the inputs needed in equations 3.23, 3.24, and 3.25 for the ideal Otto cycle-availability analysis.

Table 9. Otto cycle parameters for code validation

Property / Inputs	value
Initial temperature (K)	333
Specific heat ratio, γ	1.3
Compression ratio, r	12
Caloric heat value (kJ/kg)	44,437
Specific heat ratio of air at constant volume, Cv (kJ/kg. K)	0.946
Initial Pressure (bar)	1
Air-to-Fuel ratio	15.12
Surrounding temperature (K)	300
Surrounding pressure (bar)	1
Fuel Composition (isooctane)	C_8H_{18}
$\frac{l}{a}$ ratio	4.5
Displacement volume (L)	0.612

The term q^* in equation 3.23 was calculated via the relation $q^* = \frac{Q_{lhv}}{A/F+1}$ (Chapter 3). The lower heating value Q_{lhv} was calculated by using equation 4.5 [1],

$$Q_{hhv} = Q_{lhv} + (mh_{fg})_{H_2O} \quad \text{(kJ/kg fuel)} \tag{4.5}$$

where Q_{hhv} is the absolute value of the enthalpy of combustion, computed from equation 4.6.

$$|hc| = \sum N_P(\overline{h^o}_f)_P - \sum N_r(\overline{h^o}_f)_r \tag{4.6}$$

The instantaneous cylinder volume $V(\theta)$ was evaluated via equation 3.3.

$$\frac{V(\theta)}{Vc} = 1 + \frac{1}{2}\,(r-1) * \left(\frac{l}{a} + 1 - \cos(\theta) - \left(\left(\frac{l}{a}\right)^2 - \sin(\theta)^2 \right)^{\frac{1}{2}} \right)$$

Where Vc is the clearance volume calculated from the compression ratio according to equation

4.7; Vd is the displacement volume and $\dfrac{l}{a}$ is the connecting rod-to-crank offset ratio, as defined

in chapter 3.

$$r = \frac{Vc + Vd}{Vc} \qquad (4.7)$$

The instantaneous pressure was calculated using the isentropic relation (equation 4.8).

$$\left(\frac{P_i}{P_{i+1}}\right) = \left(\frac{V_{i+1}}{V_i}\right)^{n=\gamma} \qquad (4.8)$$

Also, the mixture temperature was evaluated via equation 3.27 (Chapter 3) where $n = \gamma$ for

isentropic processes.

$$\left(\frac{T_{i+1}}{T_i}\right) = \left(\frac{P_{i+1}}{P_i}\right)^{\left(\frac{\gamma-1}{\gamma}\right)}$$

A comparison between the current work and [17] for the analysis of the ideal Otto cycle is shown

in table 10 and figure 26.

Table 10. Comparison between the current ideal Otto cycle analysis and results from [17]

Parameter	Current work data (input/output)	Previous work data (input/output)
Caloric heat value (kJ/kg)	44,437	44,000
x_a	1.031	1.029
Air/Fuel ratio	15.12	15.39
Fuel Type	Isooctane C_8H_{18}	Gasoline $C_nH_{1.87n}$
The start of the combustion Temp K	701.6	701.6
Start of Combustion Pressure bar	25	25
Adiabatic Flame temp (K)	3217	3397
$\frac{(a_i-a_o)_t}{q^*}$ initial state	1.032	1.029
$\frac{(a_i-a_o)_t}{q^*}$ at the start of comb.	1.127	1.127
$\frac{(a_i-a_o)_t}{q^*}$ at the end of comb	0.967	0.955
$\frac{(a_i-a_o)_t}{q^*}$ at the final state	0.384	0.330

As can be seen from figure 26 and table 10, very good agreement is found at the beginning of compression, end of compression and end of the combustion process. The 16 % discrepancy at the end of expansion may be attributed to fuel type uncertainty. In the baseline study [17] gasoline was used as fuel in the ideal Otto cycle calculation; however, the fuel chemical formula was not specified. Isooctane was selected for the current work as a representative gasoline component. The unknown fuel composition had a tangible effect on the adiabatic flame temperature and the enthalpy analysis, since the enthalpy of formation and caloric heat values are specific to each fuel. Since the mixture stoichiometry was no specified in [17], a stoichiometric mixture was assumed in the calculations. This directly impacts the term $q^* = \frac{Q_{lhv}}{A/F+1}$ because it is a function of the air-to-fuel ratio. Based on these results, the code developed as part of this research was confirmed to be

a valid tool for the ideal Otto cycle availability calculation. For the comparison between the ideal

Otto cycle and the spark-ignition engine cycle, only the thermo-mechanical availability portion of

the code was used.
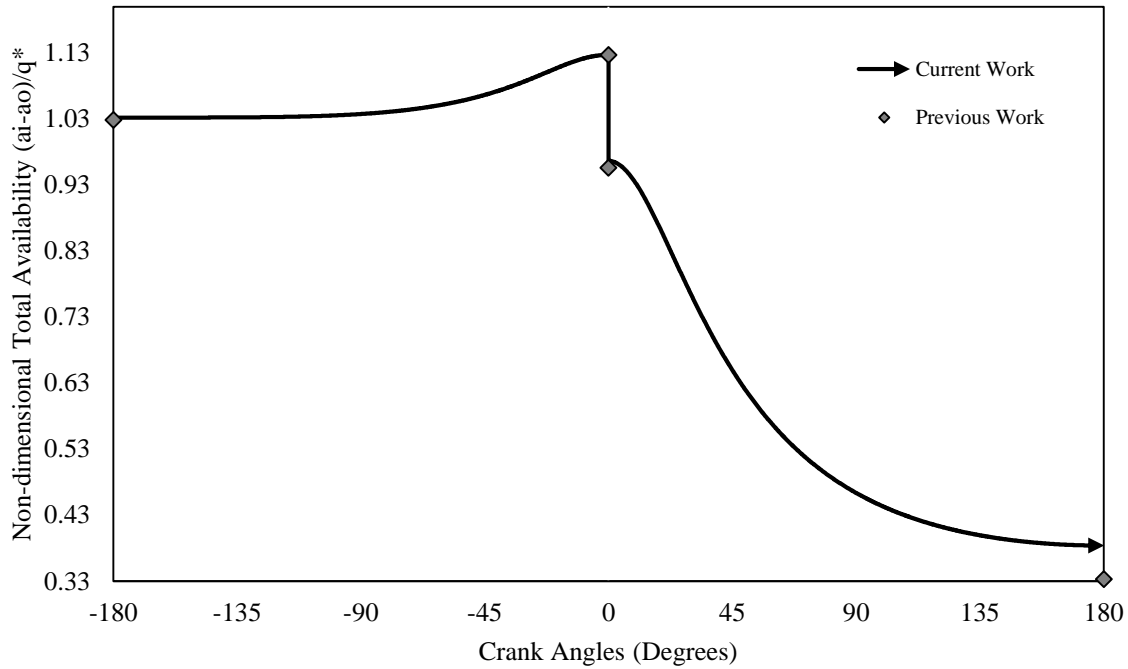
Figure 26. Non-dimensional total availability versus crank angle (compression, combustion and expansion strokes) for the ideal Otto cycle. The discrete data points [17] were used to validate the code developed as part of this research project.

Once validated, the code was used to calculate the availability during the compression,

combustion and expansion strokes of a methane-fueled spark-ignition engine operating on the ideal

Otto cycle for a range of equivalence ratios. Figure 27 shows the non-dimensional total availability

versus crank angle (compression, combustion and expansion strokes) for the ideal Otto cycle

obtained in [17]. Here the mixture's chemical availability is considered from the beginning of the

closed portion of the cycle. The thermo-mechanical availability increases during compression.

Since constant-volume combustion is assumed, and the combustion process itself is modeled as

heat transfer from an external source, only the availability destruction is shown during the

61

combustion process (see [17], [13]) for equation derivation. For an effective comparison between the ideal Otto and SI cycles within the scope of the current work, only the thermo-mechanical availability component is compared.
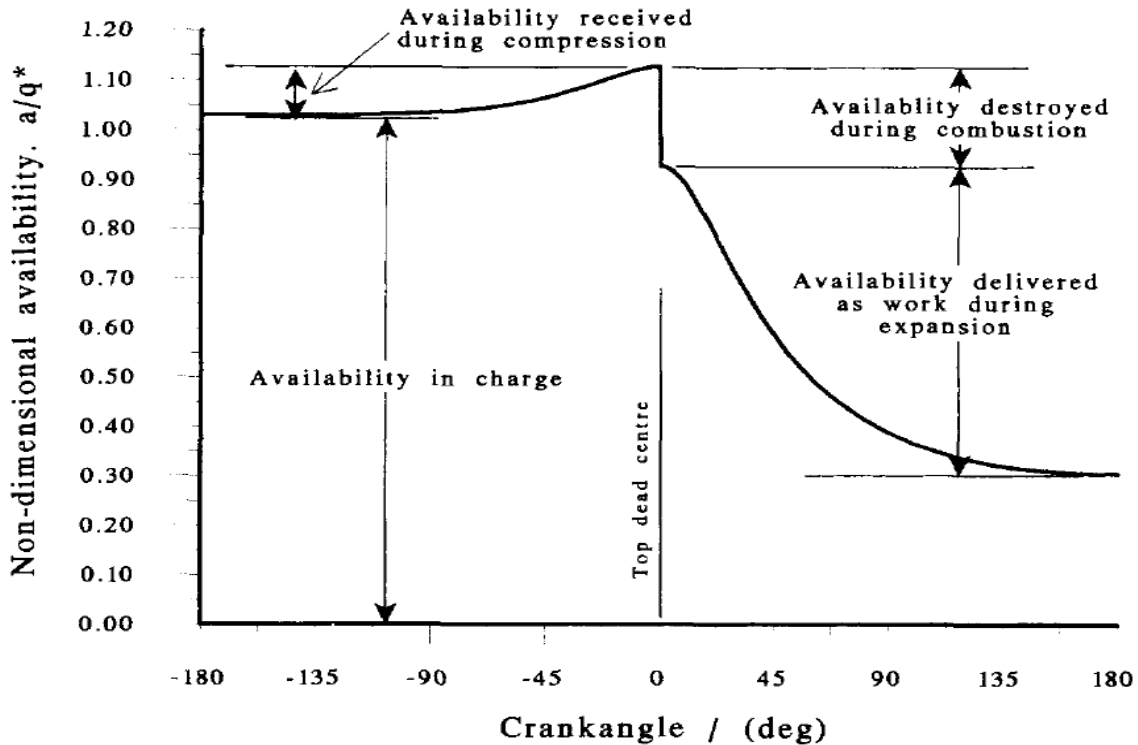
Figure 27. Non-dimensional availability versus crank angles (compression, combustion and expansion strokes) for the ideal Otto cycle using gasoline as fuel [17].

4.2.2 Availability Analysis of the Ideal Otto Cycle for a Stoichiometric Methane-Air Mixture

Figures 28 and 29 show the non-dimensional total availability versus crank angle and instantaneous, in-cylinder volume, respectively, when using a stoichiometric methane-air mixture in an ideal Otto cycle. The purpose of these graphs is to illustrate the ability of the current code to reproduce results from the technical literature [17], [13].

The availability of the intake mixture increases due to the work done by piston on the charge during the compression stroke (-180°BDC 0° TDC) as shown in (B). The fuel availability

62

in the form of chemical bonds is converted into thermal energy during the constant volume (instantaneous at 0° TDC) combustion. This process generates entropy, causing irreversibility and, therefore, availability destruction (C). Since in [17] the combustion process was simulated as heat transfer from an external source, the availability increase due to combustion energy release was not considered. Part (D) represents a reduction in the mixture availability during the expansion stroke [17]. The trend observed in figure 28 may also be explained by applying the thermo-mechanical availability balance equation (4.9) from [2] to the closed portion of the ideal Otto cycle, as follows:

$$A_{in} - A_{out} - A_{dest} = A_{final} - A_{initial} \tag{4.9}$$

Or equivalently equation 4.10:

$$\Sigma\left(1 - \frac{To}{T}\right)Q - [W - P_o(V_{final} - V_{initial})] - A_{dest} = A_{final} - A_{initial} \tag{4.10}$$

For the compression process, which is assumed to be reversible and adiabatic for the ideal Otto cycle equation 4.10 becomes:

$$W_{rev,in} = A_2 - A_1 \tag{4.11}$$

For the expansion process, under the same assumptions, equation 4.11 becomes:

$$W_{rev,out} = A_3 - A_4 \tag{4.12}$$

And for the constant volume combustion process, modeled as heat transfer from an external source at a boundary temperature equal to T_O, equation 4.12 becomes:

$$A_{dest} = A_{initial} - A_{final} \tag{4.13}$$

Since the entropy is generated during combustion, the availability destruction must be positive, hence the decreasing trend during combustion for the ideal Otto cycle. Notice, however, that this is merely a consequence of modeling the process as heat transfer from an external source. In a SI engine cycle the heat is released internally, as a result of combustion, causing pressure and temperature to increase, hence increasing the thermo-mechanical availability of the system. In [17], the chemical availability was added a priori, and carried through the cycle availability calculation, since the energy is assumed to be released instantaneously and with 100% efficiency during combustion.
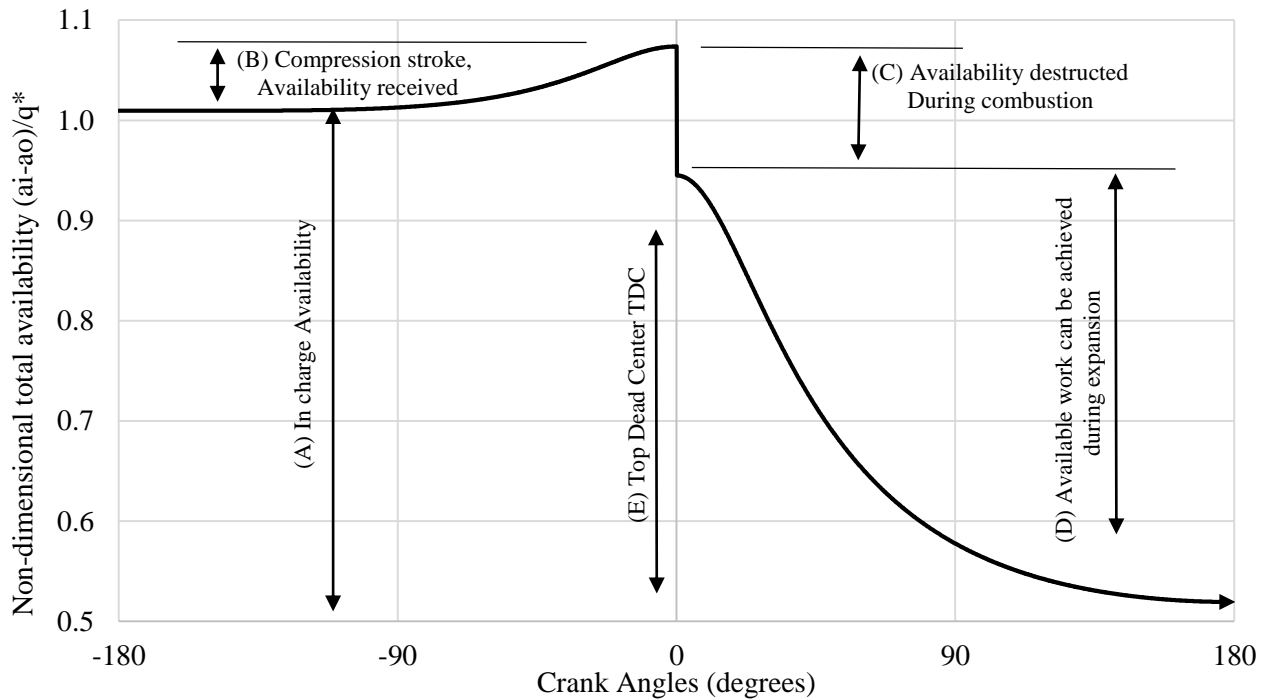
Figure 28. The non-dimensional total availability versus crank angle for the ideal Otto cycle using methane at an equivalence ratio of 1.
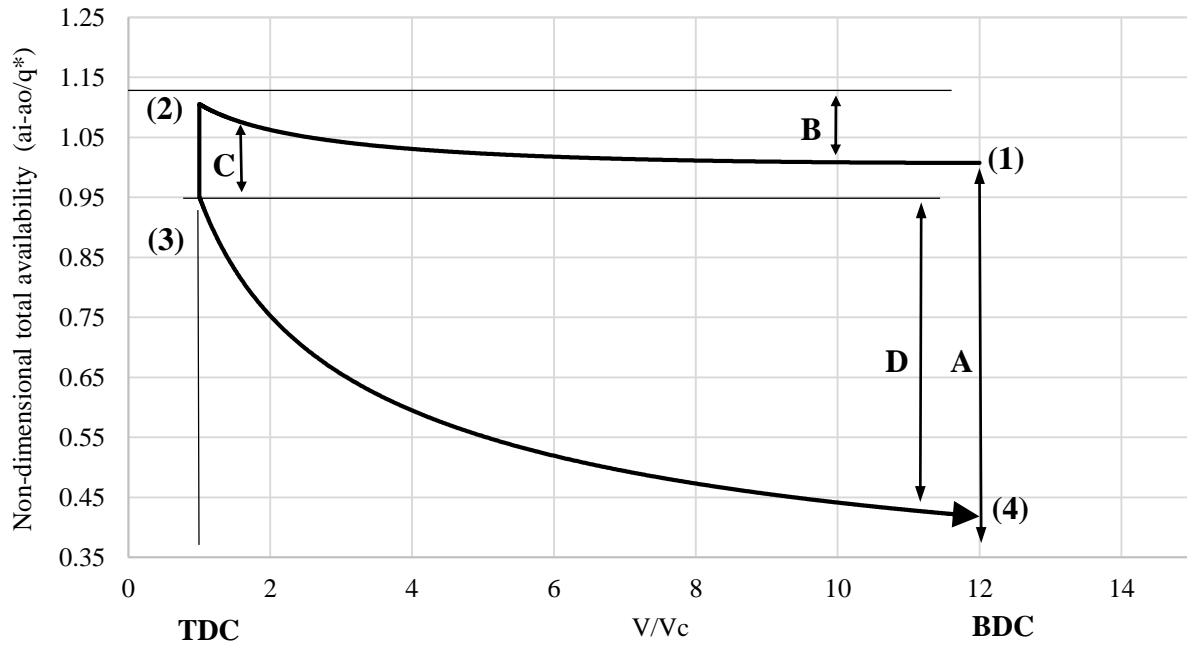
Figure 29. Non-dimensional total availability versus the instantaneous in-cylinder volume for an ideal Otto cycle using methane as a fuel at equivalence ratio of 1.

To better visualize what happens during the combustion process, Figure 30 shows the fuel chemical availability ΔA_R added after the compression stroke. Here the total non-dimensional availability is presented as a function of crank angle for an ideal Otto cycle fueled with methane at stoichiometric conditions. During combustion, the net availability is shown as the algebraic sum of the fuel availability and the availability destroyed due to entropy generation.
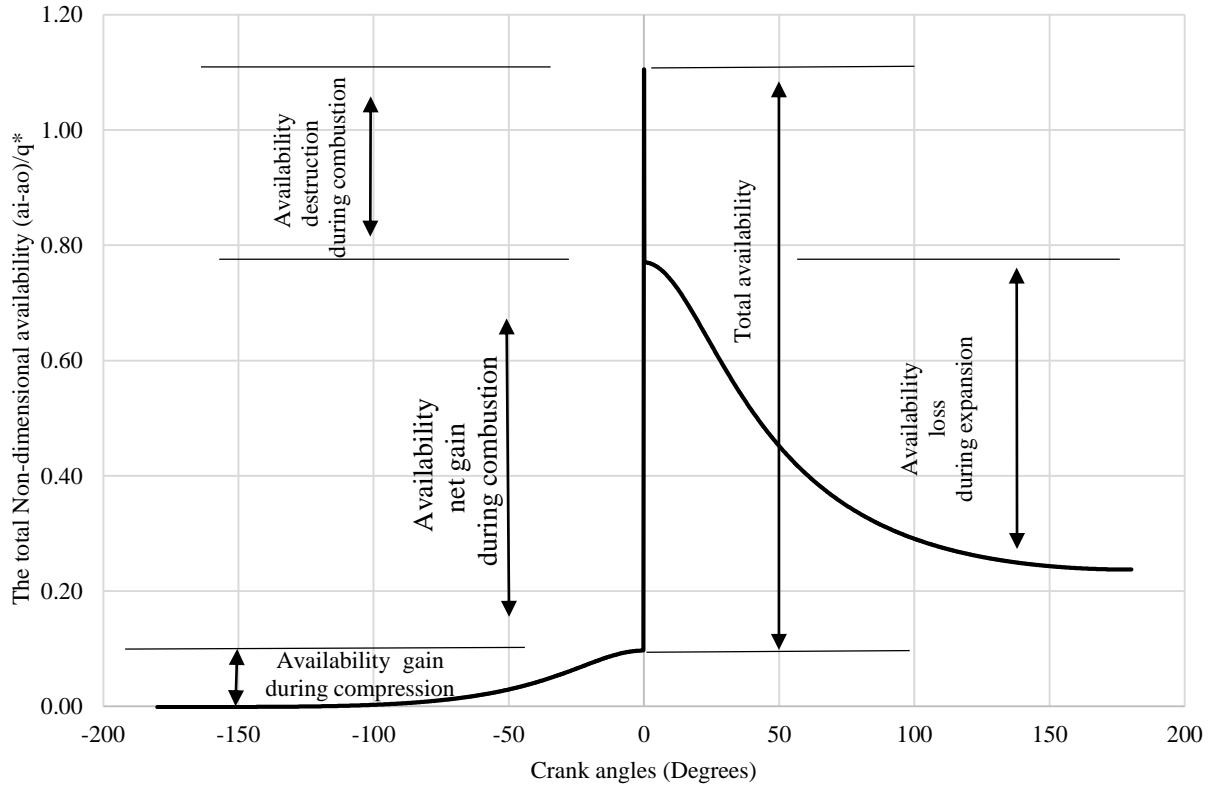
Figure 30. The total Non-dimensional availability versus crank angle for an ideal Otto cycle fueled with methane and runs at stoichiometric equivalence ratio of 1.

In spark-ignition engine cycles, combustion is not instantaneous and occurs with significant heat loss. Quantifying the change in the chemical availability of the mixture as a function of crank angle was beyond the scope of the current work. Therefore, only the thermo-mechanical availability, quantified through equation 3.26, is compared.

$$\frac{a_i - a_o}{q^*} = \frac{c_v T_o}{q^*} [\left(\frac{T_i}{T_o} - 1\right) + ((\gamma - 1)\left(\frac{v_i}{v_o} - 1\right)) - \{\gamma \ln \frac{T_i}{T_o} - (\gamma - 1) \ln \frac{P_i}{P_o}]$$

Figure 31 shows the non-dimensional thermo-mechanical availability as a function of crank angle for an ideal Otto cycle using methane as a fuel at an equivalence ratio of 1. Figure 31 is different than figure 30 because it represents the thermo-mechanical availability only, while figure 30 represents the total availability of the ideal Otto cycle. Since only the closed portion of the

66

cycle is considered and the mixture is approximately at the dead state at the beginning of compression, the thermo-mechanical availability starts at the zero baseline and increases during compression. When the energy release is considered, the thermo-mechanical availability is seen to increase during combustion, and then decrease during expansion as work is extracted from the cycle.

Figure 31. The non-dimensional thermo-mechanical availability versus crank angle for the ideal Otto cycle using methane at an equivalence ratio of 1.

4.2.3 Availability Analysis of the Ideal Otto Cycle at Non-Stoichiometric Equivalence Ratios

The effect of equivalence ratio on the thermo-mechanical availability is shown in figure 32. A methane-air mixture was used in the ideal Otto cycle at the equivalence ratios of 0.83, 0.991, and 1.25 to illustrate trends. During compression (1-2), higher availability is associated with the lean mixture (equivalence ratio of 0.83).
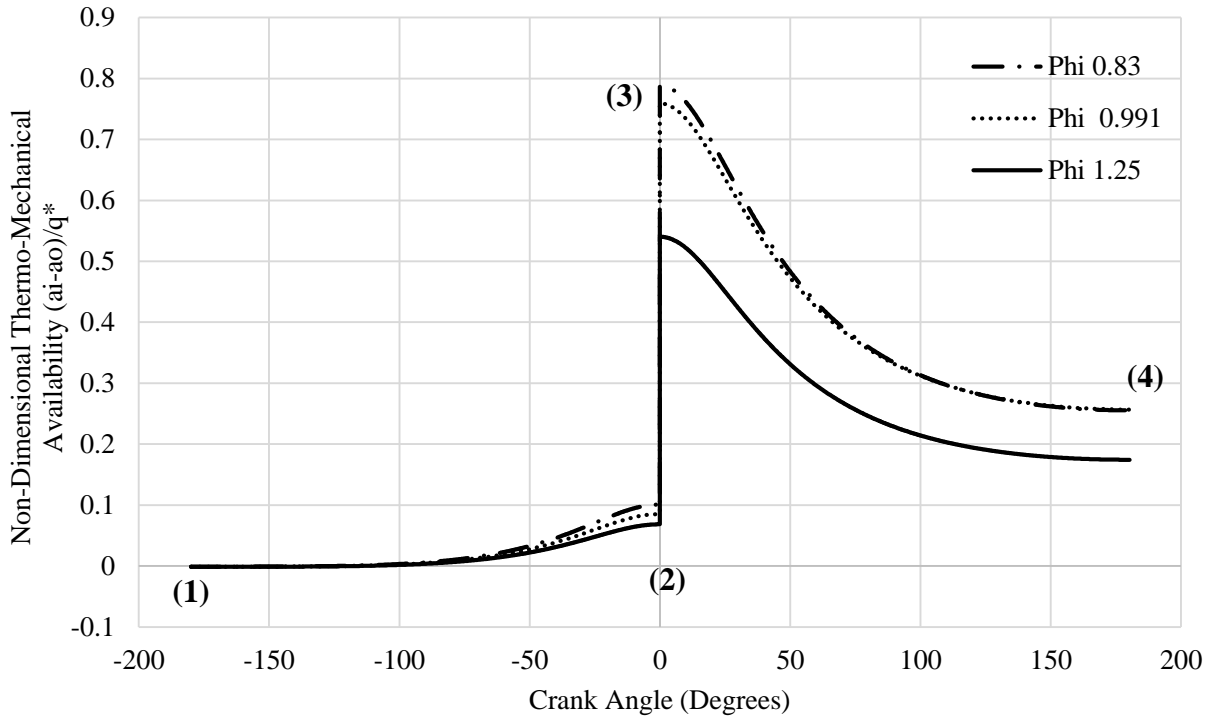
Figure 32. The non-dimensional thermo-mechanical availability versus crank angle. Conditions: methane-air mixture, ideal Otto cycle, three equivalence ratios (0.83, 0. 99, and 1.25).

During combustion (2-3 in figure 32) and according equation 3.26,

$$\frac{a_i - a_o}{q^*} = \frac{c_v T_o}{q^*} [\left(\frac{T_i}{T_o} - 1\right) + \left((\gamma - 1)\left(\frac{v_i}{v_o} - 1\right)\right) - \{\gamma \ln \frac{T_i}{T_o} - (\gamma - 1) \ln \frac{P_i}{P_o}\}]$$

the lean mixture also has higher availability gain since it has lower energy of reaction. Since the curves are normalized, this indicates higher availability for fuel-lean mixtures relative to the energy content in the mixture. Both curves decrease as the availability is delivered as an expansion work during the power stroke (3-4). However, the decrease in the expansion curves is different because of the different assumptions for the chemical balance between the lean and the rich regions.

The non-normalized thermo-mechanical availability can be seen in figure 33 as a function of crank angle at different equivalence ratios. Equation 3.26 was used to generate figure 33 after multiplying it by the energy of the reaction (q^*) term and the mixture mass. When visualized in this manner, the thermo-mechanical availability peaks at stoichiometric conditions. This may be attributed to the maximum energy released at around stoichiometric ($\Phi = 0.99$). The normalized approach is typically preferred because it quantifies availability relative to the energy content of the mixture.
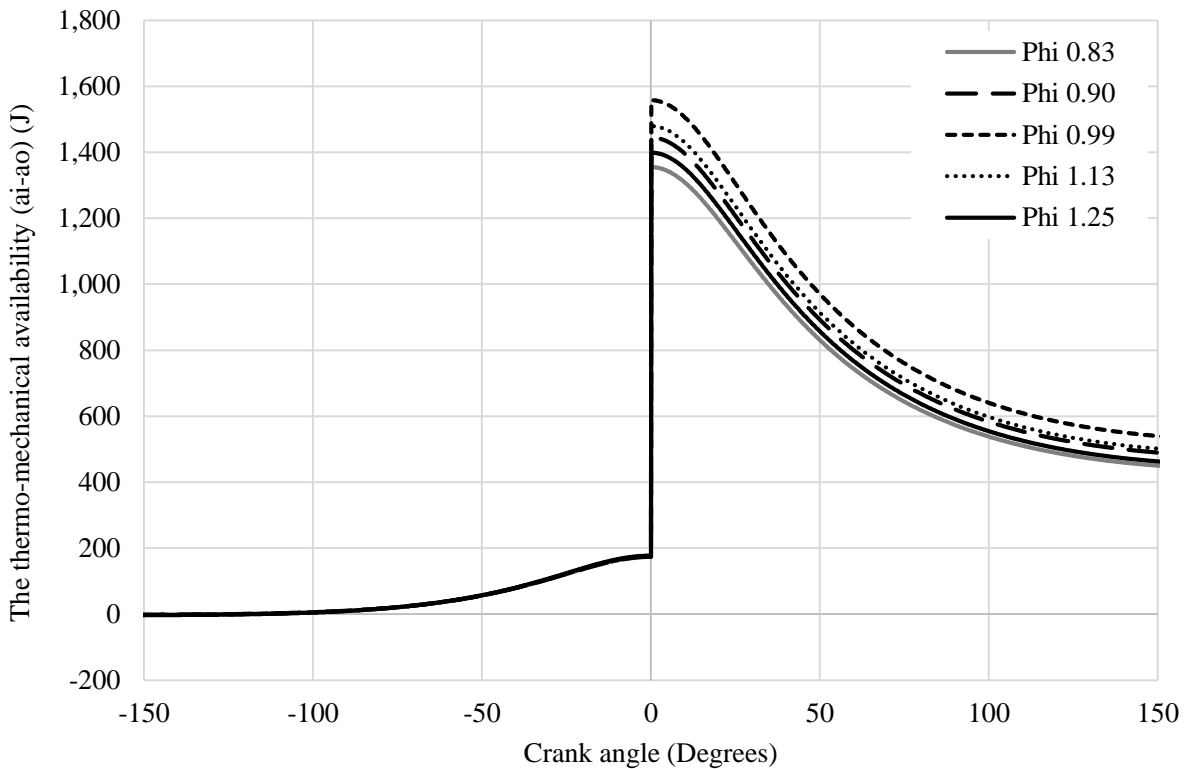
Figure 33. The non-normalized thermo-mechanical availability versus crank angle at different equivalence ratios. Conditions: methane-air mixture, ideal Otto cycle.

The first and second law of thermodynamic efficiencies were computed using equations 4.14 and 4.15, respectively, to demonstrate the effect of equivalence ratio on these parameters.

$$\eta_I = \frac{W_{g,i}}{Q_{lhv}\ m_f} \tag{4.14}$$

$$\eta_{II} = \frac{W_{g,i}}{\Delta A_R\ m_f} \tag{4.15}$$

In these equations, $W_{g,i}$ is the gross indicated work, evaluated through numerical (trapezoidal) integration of the ideal Otto cycle pressure-volume (P-V) diagram. Q_{lhv}, and ΔA_R are the lower heating value of methane and the availability of the reaction (i.e., the change in the Gibbs free energy), respectively. As figure 34 shows, the first and second law efficiencies increase as the equivalence ratio decreases. As the equivalence ratio increases (i.e., the mixture becomes fuel-richer), the denominator in equations 4.14 and 4.15 increases. Since the gross indicated work does not increase proportionally, the overall effect is a decrease in the first and second-law efficiencies. It can be noticed that the first and the second law efficiencies follow similar trends. This can be attributed to the ratio of Q_{lhv} to ΔA_R for methane being approximately one (1.01) at any equivalence ratio [18].
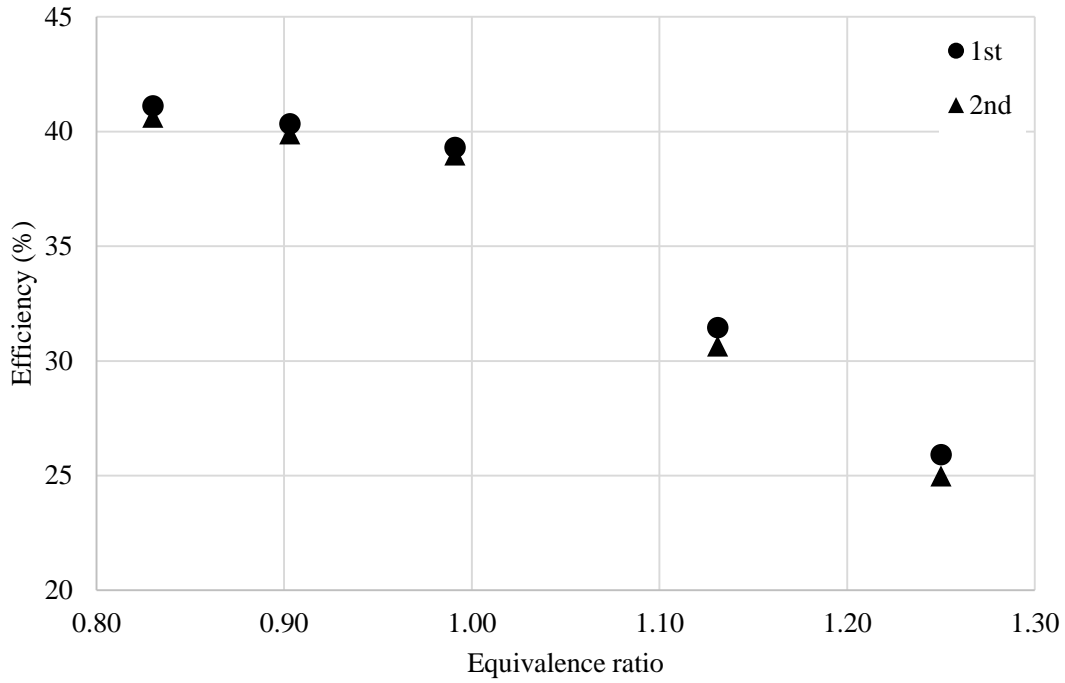
Figure 34. First and second law efficiencies for the ideal Otto cycle using a methane-air mixture.

The maximum available work that can be achieved from the thermo-mechanical availability was computed for the ideal Otto cycle, following the process illustrated in section 4.2.2. By using equation 4.10:

$$\sum \left(1 - \frac{To}{T}\right)Q - \left[W - P_o\left(V_{final} - V_{initial}\right)\right] - A_{dest} = A_{final} - A_{initial}$$

the term $\left[W - P_o\left(V_{final} - V_{initial}\right)\right]$ can be expressed as the normalized maximum available work ($(\frac{a}{q^*})_w$). $A_{initial}$ and A_{final} represent the beginning of the compression $(\frac{a}{q^*})_{Comp}$ and the end of expansion $(\frac{a}{q^*})_{Exp}$ strokes. The term $(\sum \left(1 - \frac{To}{T}\right)Q - A_{dest})$ represents as the net availability during combustion $(\frac{\Delta a}{q^*})_{Comb}$, which it can be obtained by computing the availability difference between the end and the start of combustion $(\frac{\Delta a}{q^*})_{Comb} = (\frac{a}{q^*})_3 - (\frac{a}{q^*})_2$. Rearranging equation 4.10 yields equation 4.16.

71

$$\left(\frac{a}{q^*}\right)_w = \left(\frac{a}{q^*}\right)_{Comp} - \left(\frac{a}{q^*}\right)_{Exp} + \left(\frac{\Delta a}{q^*}\right)_{Comb} \qquad (4.16)$$

Table 11 and figure 35 shows results as a function of equivalence ratio. It can be seen that the maximum work that can be obtained from the ideal cycle increases as the equivalence ratio decreases, in agreement with first and second law efficiencies trends. These findings suggest that, for the ideal Otto cycle, higher first-law and second-law efficiencies can be achieved for fuel-lean mixtures (i.e. with decreasing equivalence ratio).

Table 11. The non-dimensional maximum available work of the ideal Otto cycle for methane-air mixtures at various equivalence ratios

Equivalence ratio	The non-dimensional maximum available work $\left(\frac{a}{q^*}\right)_w$
0.830	0.431
0.903	0.424
0.991	0.416
1.131	0.346
1.250	0.296
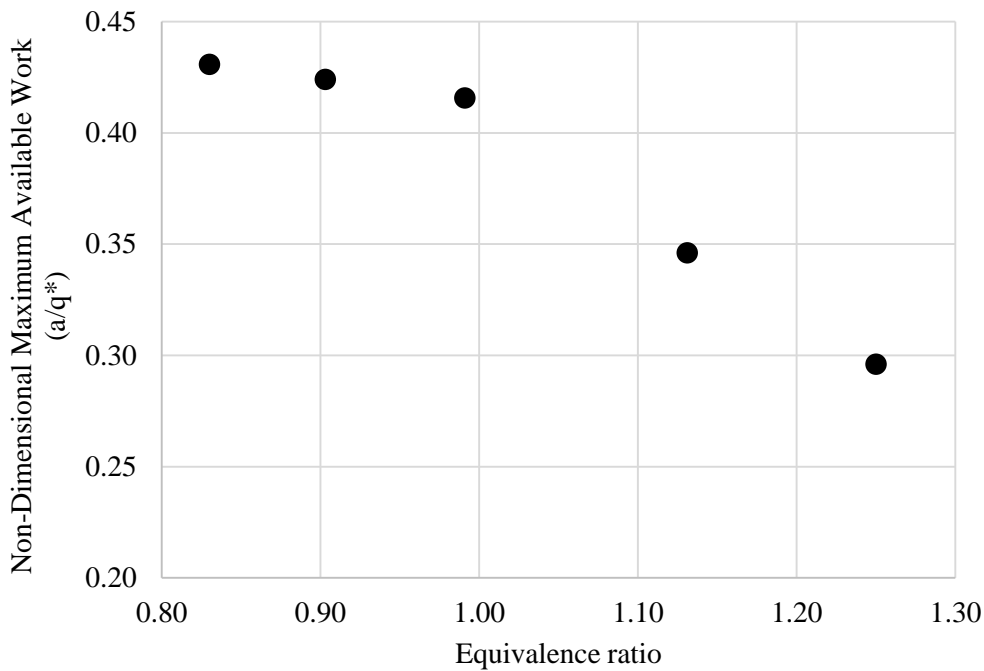
Figure 35. The non-dimensional maximum available work of the ideal Otto cycle for methane-air mixtures at various equivalence ratios.

4.3 Second-Law of Thermodynamic Analysis of the Spark-Ignition (SI) Engine Cycle

Experimental data at equivalence ratios of 0.803, 0.903, 0.991, 1.131, and 1.25 were collected from a single-cylinder, spark-ignition engine to conduct an availability analysis during the compression, combustion and expansions processes of a practical SI engine cycle. In contrast to the ideal Otto cycle, the combustion process is not instantaneous and the compression and expansion processes are not isentropic, but rather treated as polytropic. Further, combustion efficiencies are equivalence-ratio dependent and not 100%. In this work, the variation of the specific heat with temperature was taken into account. Results are presented next.

4.3.1 Analysis Procedure and Experimental Data Validation

For the SI engine cycle, equation 3.26 (shown below for convenience) was used to compute the thermo-mechanical availability during the compression, combustion, and the expansion strokes (section 3.1.5).

$$\frac{a_i - a_o}{q^*} = \frac{c_v T_o}{q^*}[(\frac{T_i}{T_o} - 1) + ((\gamma - 1)(\frac{v_i}{v_o} - 1)) - \{\gamma \ln\frac{T_i}{T_o} - (\gamma - 1)\ln\frac{P_i}{P_o}\}]$$

The pressure was experimentally measured and averaged over 100 cycles at each equivalence ratio. The measured pressure and the calculated in-cylinder instantaneous volume were used to evaluate the temperature profiles to be used in equation 3.26 for the availability calculations. As described in section 3.1.6, the temperature was calculated in four stages. At the start of compression, the ideal gas law (equation 3.28) was used, where P, V, R_t and T are the pressure, volume, ideal gas constant and temperature of the mixture, m_t is the mixture mass (mass of air and fuel), known at each equivalence ratio from the experiments.

$$PV = m_t R_t T$$

The variation in the temperature at the start of compression (i.e., at intake-valve-closing) and the mixture gas constant are shown in the table 12. The temperature decreases as the equivalence ratio increases. According to the ideal gas equation, the temperature is a function of the pressure, volume, mixture mass, and the ideal gas constant of the mixture. The pressure and the volume remain constant as the equivalence ratio increases, but the total mass of the mixture will increase as the equivalence ratio increases due to the added fuel. Also, the mixture gas constant, increases (albeit not significantly) because of the increasing fuel mole fraction with increasing equivalence ratio. Both effects tend to decrease the initial temperature.

Table 12. Temperature at the start of compression as a function of equivalence ratio for a single cylinder, 0.6L, methane-fueled, CFR engine operated at wide-open-throttle and 600 RPM.

Equivalence ratio	Volume (L)	Pressure kPa	Temperature (K)	R_{mix} kJ/(kg K)	$m_{mixture}$ (g)
0.830	0.64	107	310	0.306	0.706
0.903	0.64	107	308	0.307	0.709
0.991	0.64	108	306	0.309	0.712
1.131	0.64	107	296	0.312	0.718
1.250	0.64	107	290	0.314	0.723

Figure 36 shows the temperature profile for the SI engine cycle analysis at wide-open-throttle, 600 RPM and at 0.991 equivalence ratio. Part (A) represents the compression temperature profile, starting at intake-valve-closing and ending at the spark timing (i.e., $146\,^O$BTDC to -24^OBTDC). The temperature during compression was calculated via equation 3.27.

$$\left(\frac{T_{i+1}}{T_i}\right) = \left(\frac{P_{i+1}}{P_i}\right)^{\left(\frac{n-1}{n}\right)}$$

The temperature increases as the pressure increases and the volume decreases due compression work by the piston on the charge. Section (B) is the combustion temperature profile; it starts at the spark timing of -24° BTDC and ends at 23.9^O ATDC (more details about the calculation of combustion duration and the polytropic exponents numerical calculation will be discussed later in this section). The temperature during the combustion process was evaluated incrementally through equation (3.30) (already discussed but presented here again for clarity).

$$dT = \frac{1}{m_t\,R_t}\ (PdV + VdP)$$
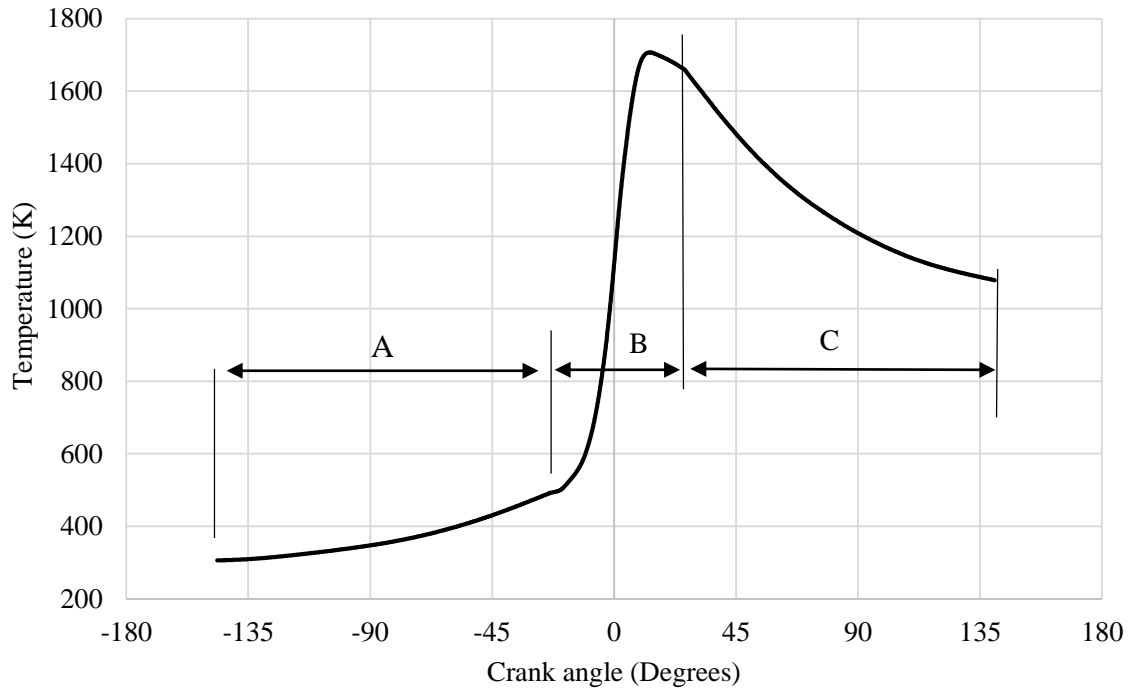
Figure 36. Temperature profile for a SI engine cycle for a methane-fueled CFR engine.
Conditions: wide-open-throttle, 600 RPM, 0.991equivalence ratio.

Table 13 shows a sample of numerical data for the equation 3.30 parameters (dP, dV, P, V) to

calculate the incremental temperature change with crank angle (dT).

Table 13. A sample of the numerical data for temperature calculation during the combustion
process for a single cylinder, 0.6L, methane-fueled CFR engine operated at wide-open-throttle
and 600 RPM at an equivalence ratio of 0.83.

Crank angles (Degrees)	Volume (L)	Pressure (MPa)	Temperature (K)	ΔV (m^3) * 10^{-7}	ΔP (KPa)	ΔT (K)
-23.73	0.099	1.084	499.1	-4.573	9.5	2.095
-23.55	0.099	1.090	499.4	-4.542	5.5	0.244
-23.38	0.099	1.096	499.6	-4.511	5.6	0.244
-23.20	0.098	1.101	499.9	-4.480	5.6	0.262
-23.03	0.098	1.107	500.1	-4.450	5.5	0.207

76

The temperature increases during the combustion because of the conversion of chemical energy into internal energy of the mixture. Section (C) represents the temperature profile decreasing due to the reduction in the in-cylinder pressure as a result of gas expansion during the expansion (power) stroke. The expansion stroke temperature profile was evaluated as for the compression process. The same approach was followed for the remaining equivalence ratios.

In addition to the temperature profiles, it was necessary to determine the polytropic exponent for the compression and the expansion strokes, and the combustion duration.

4.3.1.1 Combustion Duration and Polytropic Exponent

Identifying the start and the end of combustion was needed to correctly apply the temperature equation in the availability calculation. The combustion duration was determined at each equivalence ratio using the log P- log V graph [13]. To explain the method, figure 37 shows the averaged absolute pressure versus in-cylinder volume (in logarithmic scale). It should be noted that, at each equivalence ratio, each data point represents an average of three experiments, each consisting of approximately 100 engine cycles. The start of combustion was assumed to coincide with the spark timing $(-24^O$ BTDC or$-21^O)^4$, approximated by the onset of the curvature in the Log P– Log V graph [13]. The end of combustion was predicted from the end of the curvature. Three points were averaged at the end of combustion to reduce uncertainty. The standard deviation was also computed. This method was used for all the equivalence ratios.

---

[4] Typically, the start of combustion is tied to the 5% mass fraction burned. However, in this current work mass fraction burned calculations were not conducted.
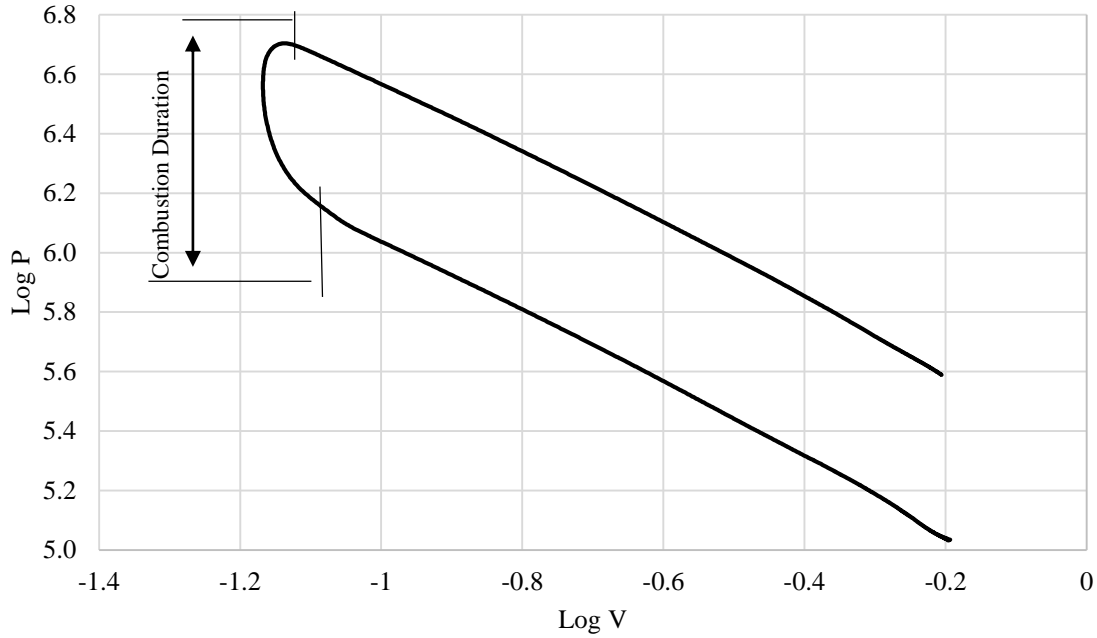
Figure 37. Logarithmic plot of in-cylinder pressure versus volume during the compression, combustion, and expansion processes of a 0.6 L CFR engine. Conditions: methane fuel, 600 RPM and WOT.

Table 14 shows the combustion duration at each equivalence ratio. It is clear that the combustion duration increases as the equivalence ratio deviates from stoichiometry toward to the lean or rich sides. That is because the burning velocity peaks near stoichiometric conditions, reducing combustion duration. This finding is consistent with general trends of burning velocity versus equivalence ratio, as shown in figure 38, where the maximum burning velocity for methane occurs approximately at an equivalence ratio of 1.1, decreasing for richer or leaner mixtures [13].

Table 14. Combustion duration versus equivalence ratio for a 0.6L, methane-fueled CFR engine.
Conditions: WOT, 600 RPM

Equivalence Ratio Measured	Equivalence Ratio (Calculated)	Standard Deviation (calculated Φ)	Combustion Duration (Degrees)	Standard deviation (combustion duration)
0.830	0.728	0.051	52.4	2.11
0.903	0.845	0.029	51.4	2.11
0.991	1.007	0.008	50.7	2.86
1.131	1.322	0.096	38.7	1.53
1.250	1.465	0.107	45.0	1.49
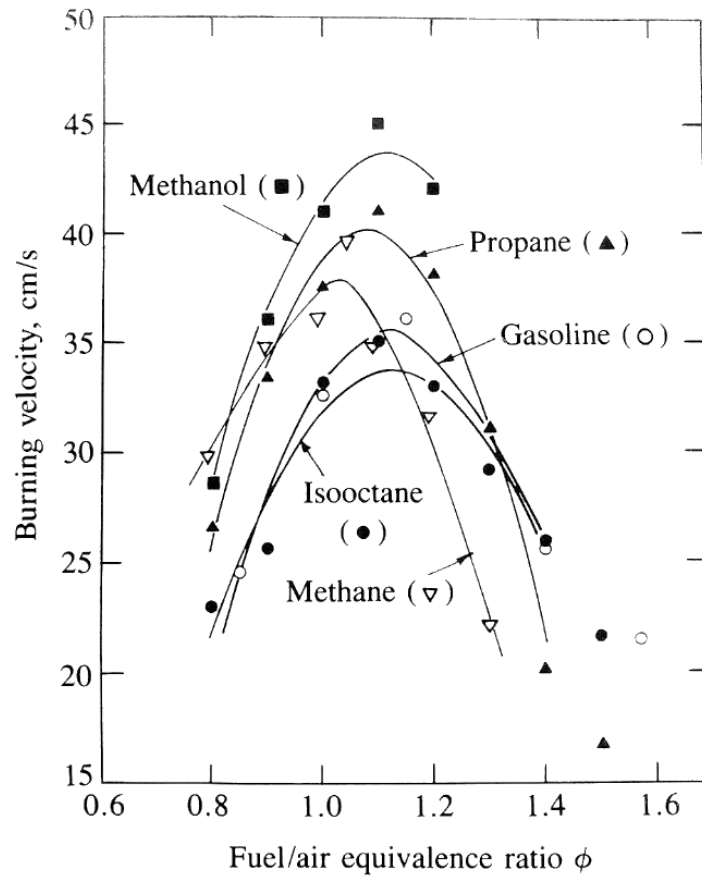
Figure 38. Burning speed versus equivalence ratio [13].

After evaluating the combustion duration, the polytropic exponents were needed to for the temperature analysis (equation 3.27). Equation 3.4 (repeated below), was

79

$$n = \frac{\log P2 - \log P1}{\log v2 - \log v1}$$

used to evaluate the exponent at each equivalence ratio. In the log P-log V graph, n represents the

slope, as shown in figure 39. This method was applied to all equivalence ratios, as summarized in

table 15.
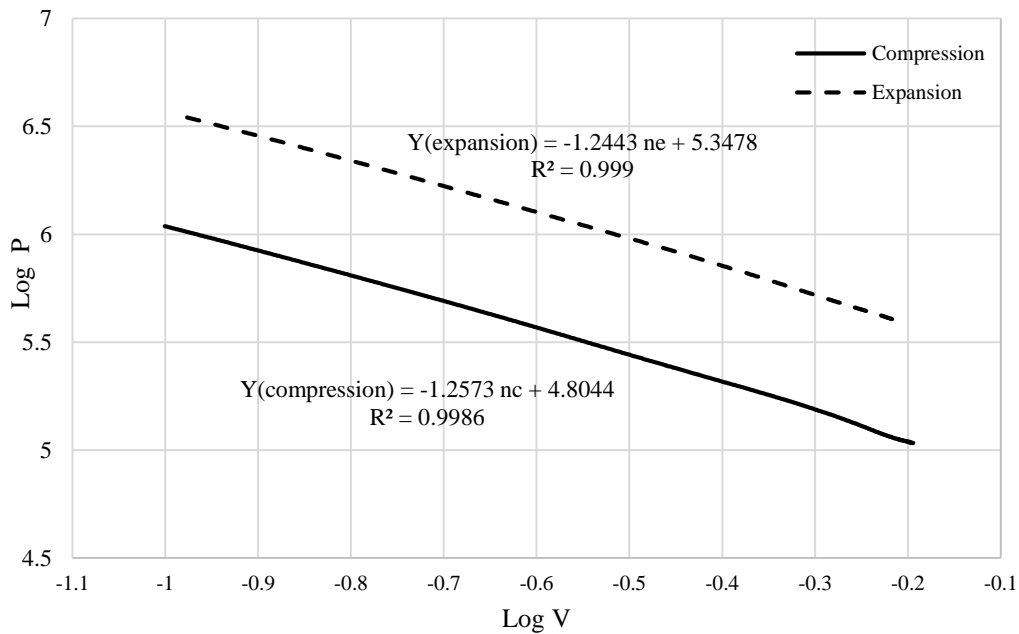
Figure 39. Logarithmic plot of in-cylinder pressure versus volume during the compression and expansion strokes for polytropic exponent prediction of a 0.6 L, methane-fueled CFR engine. Conditions: Φ =0.99, WOT, 600 RPM.

According to previous experimental studies [13], polytropic exponents are approximately

1.3 ± 0.05 for hydrocarbon fuels (including natural gas, of which methane is the main component).

Current results are consistent with these findings.

Table 15. Polytropic exponents for compression and expansion strokes of a 0.6 L, methane-fueled CFR engine as a function of equivalence ratio. Conditions: WOT, 600 RPM.

Equivalence ratio	n Compression	n Expansion
0.830	1.26	1.26
0.903	1.26	1.25
0.991	1.26	1.24
1.131	1.25	1.25
1.250	1.25	1.27

After evaluating the temperature, the specific heat at constant volume and specific heat ratio were analytically found. First, the specific heat at constant pressure was calculated by using the empirical correlation [1] defined by equation (3.2).

$$\overline{Cp} = a + bT + cT^2 + dT^3 \quad \text{(kJ/kmol. k)}$$

The fuel contribution to this parameter was neglected, due to the small mole fraction of fuel relative to that of the air. Also, we confirmed that the fuel fraction numerically has a very small effect when we add it to the specific heats calculations. Then, γ and Cv were be found as described in section 3.1.2. Finally, the terms q^* , and x_a were calculated as for the ideal Otto cycle.

4.3.1.2 Data Validation: Temperature Profiles, and Combustion Products

Previous studies have shown that the highest energy release for a spark ignition internal combustion engine happens at an equivalence ratio around of 1.1, and therefore, the maximum temperature should be expected at this point [14], [13]. The lean mixture has less energy content, and therefore lower combustion temperatures. Though rich mixtures have higher energy content, the absence of enough oxygen to burn the fuel results in lower combustion efficiencies, and hence lower temperatures. Figure 40 displays the experimentally obtained temperature profiles as a

function of equivalence ratio versus crank angle. Trends are consistent with previous studies. The maximum temperature occurs between equivalence ratios of 0.991 and 1.131, decreasing at leaner and richer conditions. The shift in the temperature profile peaks indicates variations in combustion speed with equivalence ratio.
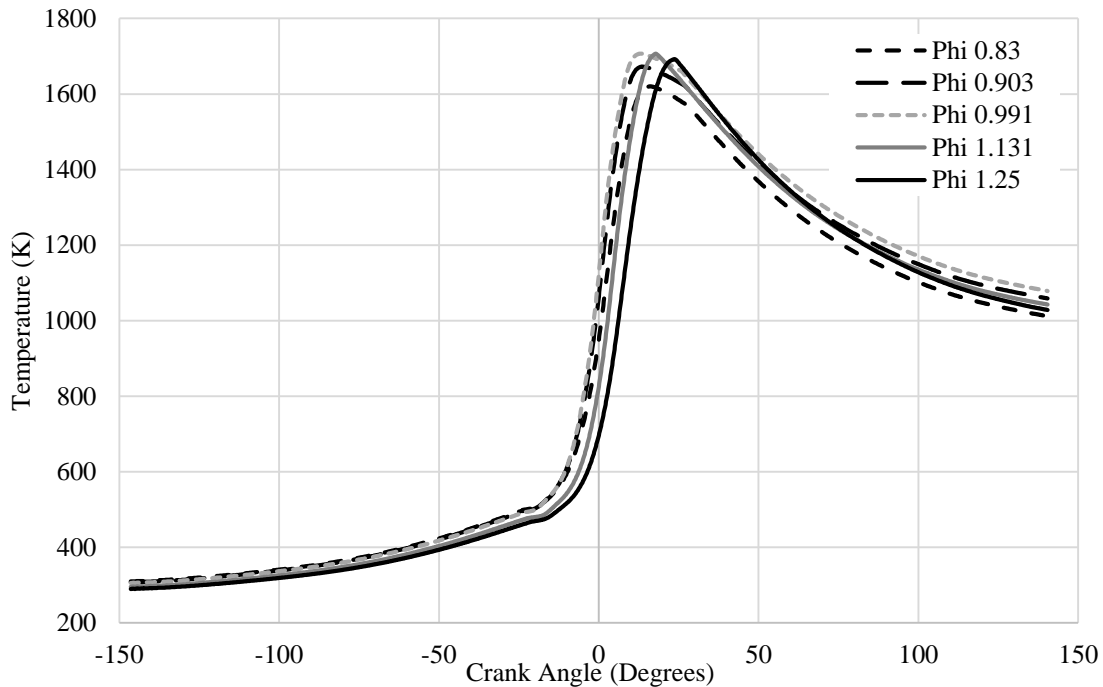
Figure 40. Temperature profiles at multiple equivalence ratios for a single- cylinder, 0.6L, spark-ignited, methane-fueled CFR engine. Conditions: WOT, 600 RPM.

Figure 41 illustrates the general pollutant emission trends as a function of equivalence ratio. Carbon dioxide (CO_2) concentrations reach a maximum at around stoichiometric conditions (complete combustion) and decreases on both sides of stoichiometry due to fuel shortage (lean mixtures) or incomplete combustion (rich mixtures), which yield carbon monoxide (CO). Carbon monoxide and unburned hydrocarbon (HC) concentrations increase as the equivalence ratio increases (from lean to rich) because of shortage in the oxygen level, which causes incomplete

combustion. Concentration of nitrogen oxides increase as the equivalence ratio decreases because of the high air content and relatively high combustion temperatures [14].
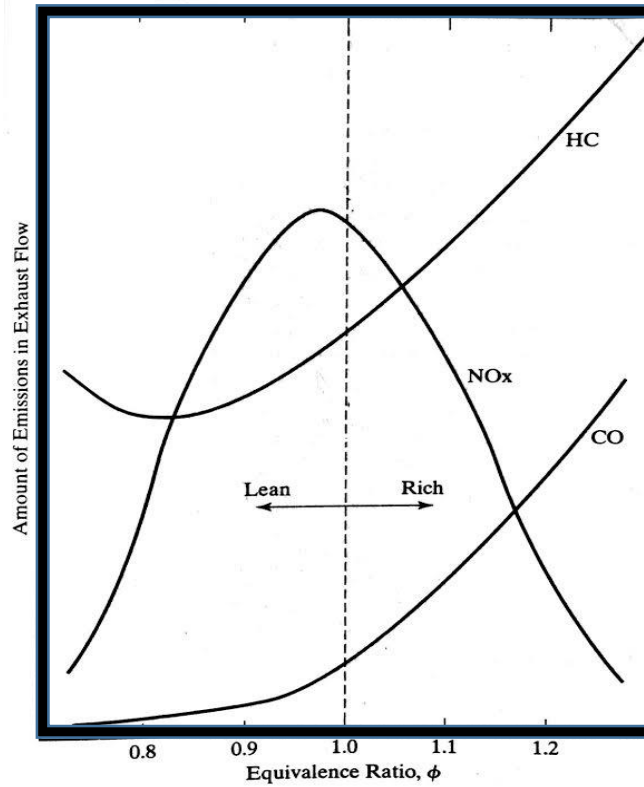
Figure 41. Exhaust emissions versus equivalence ratio [14].

Experimental results are shown in figures 42 and 43. Trends in volumetric concentrations of carbon dioxide (CO_2) carbon monoxide, (CO), nitric oxide (NO) and unburned hydrocarbons (HC) versus equivalence ratio are consistent with expectations.
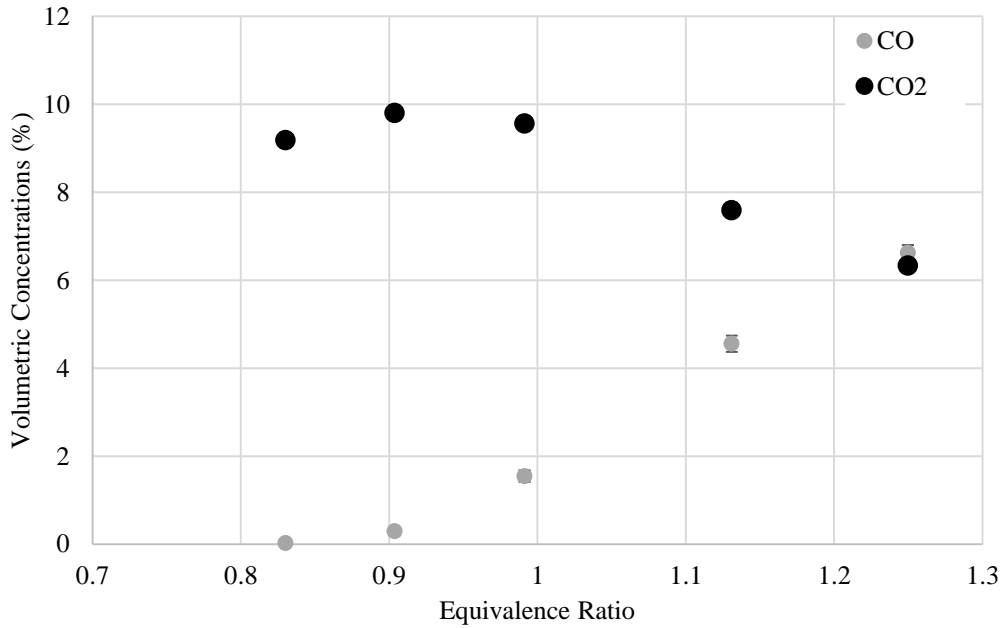
Figure 42. Volumetric concentrations of carbon dioxide (CO_2) and carbon monoxide (CO) versus equivalence ratio for the single-cylinder, 0.6 L, methane-fueled CFR engine, operated at wide-open-throttle and 600 RPM.
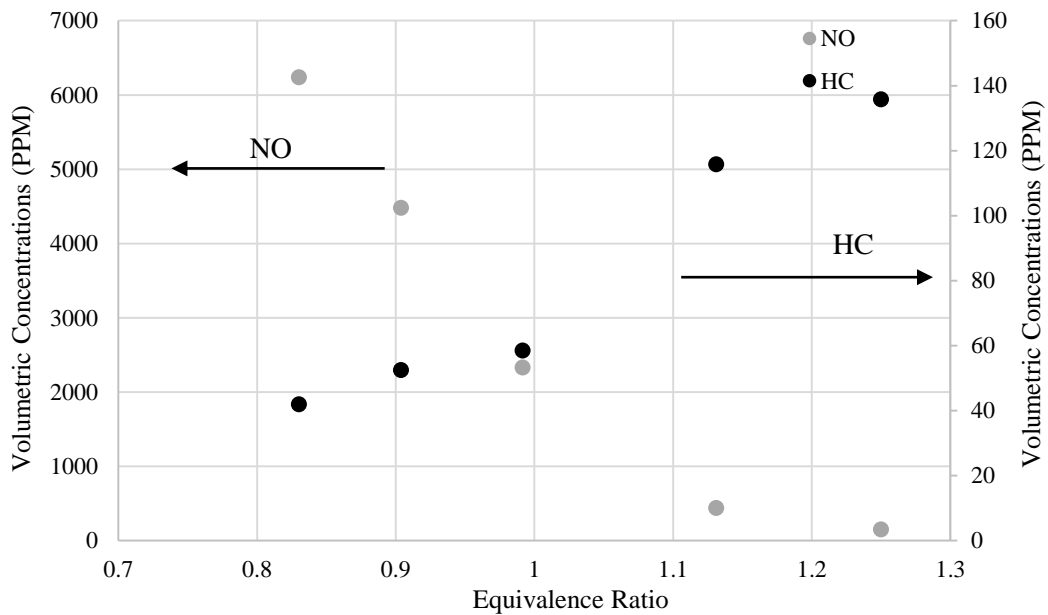
Figure 43. Volumetric concentrations of nitric oxide (NO) and unburned hydrocarbons (HC) versus equivalence ratio for a single cylinder, methane-fueled, 0.6 L CFR engine operated at wide-open-throttle and 600 RPM.

4.3.2 Availability Analysis of the SI Engine Cycle at Stoichiometric Conditions

Figure 44 displays the non-dimensional thermo-mechanical availability versus crank angle for the SI engine during compression, combustion and expansion processes. Part (A) in figure 44 represents the availability increase during the compression stroke because of piston compression. Part (B) is the availability change during combustion, which increases due to the rise in the internal energy of the mixture (i.e., the term $\left(c_v T_o \left(\frac{T_i}{T_o} - 1\right)\right)$ in equation 3.26) due heat release. Note that since combustion starts before the end of the compression stroke, the availability is also increasing due to piston compression in the later portion of the stroke. The availability increases after combustion even though some availability is destroyed as a result of entropy generation. Part (C) shows the decrease in availability due to expansion. The curve ends at exhaust-valve-opening. At this point, the in-cylinder charge temperature is 1078 K, much higher than that of the dead state, indicating substantial availability waste unless recovery systems are implemented.
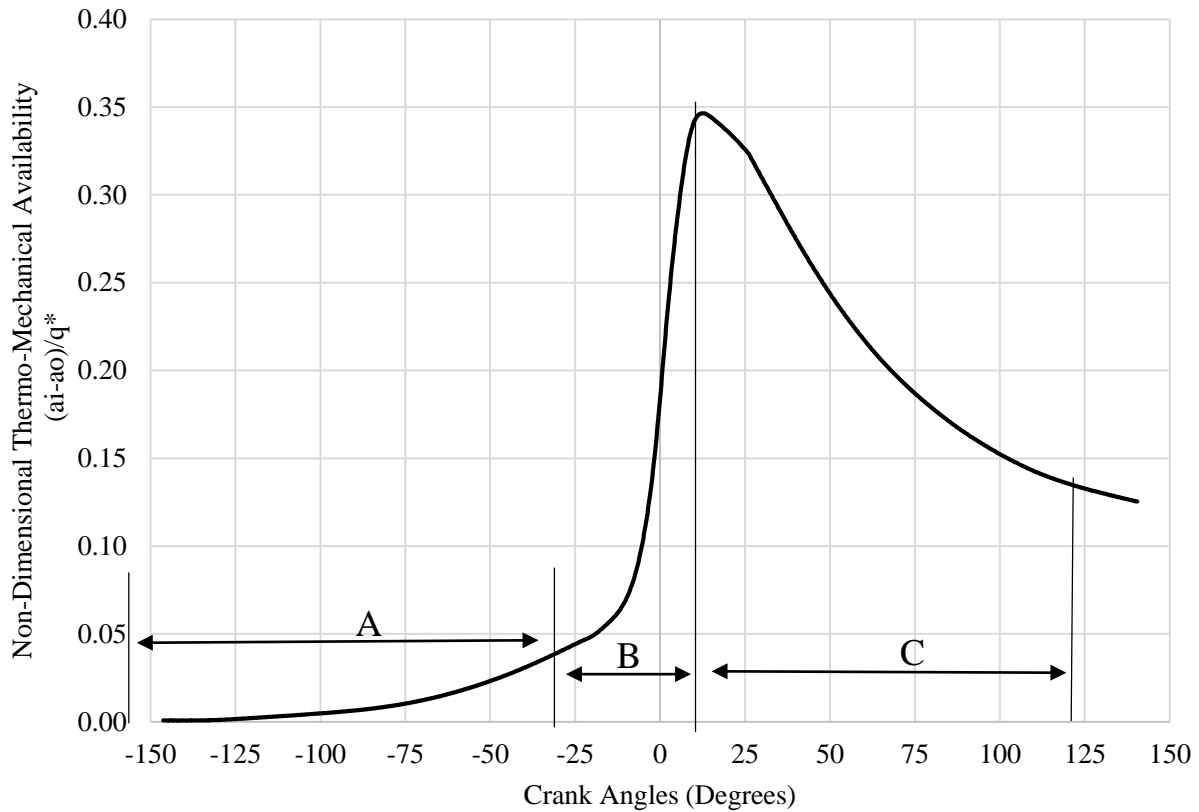
Figure 44. SI engine cycle non-dimensional thermo-mechanical availability versus crank angle for a single cylinder, 0.6 L, methane-fueled CFR engine operated at wide-open-throttle and 600 RPM at equivalence ratio of 0.991.

4.3.3 Availability Analysis of the SI engine Cycle at Multiple Equivalence Ratios

Figure 45 shows the non-dimensional thermo-mechanical availability versus crank angle at multiple equivalence ratios. Part (A), which represents the availability profile during the compression stroke, shows that the availability of the mixture is highest at $\Phi=0.83$ and decreases as the equivalence ratio increases. Since the availability is normalized, the trend indicates higher availability of lean mixtures relative to their energy content. This finding is consistent with ideal Otto cycle results.
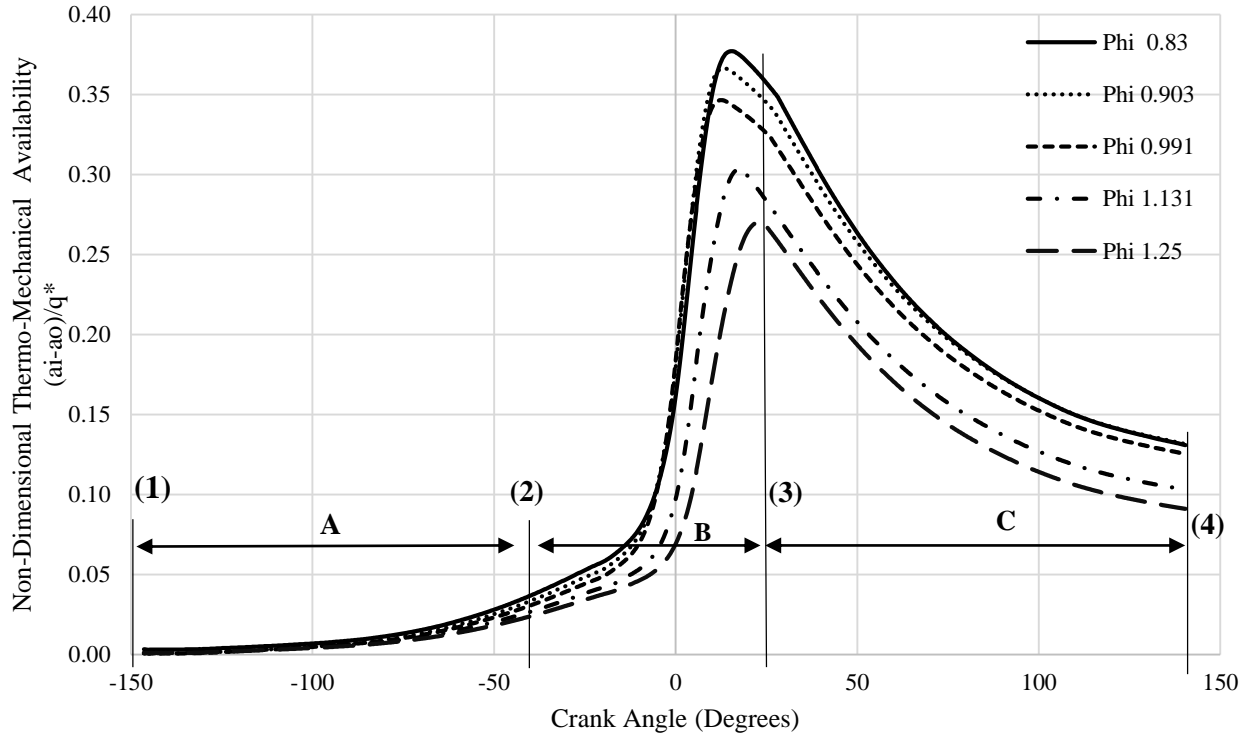
Figure 45. The non-dimensional availability versus crank angle for the SI engine cycle of a single cylinder, 0.6 L, methane-fueled, CFR engine operated at wide-open-throttle and 600 RPM at multiple equivalence ratios.

Also, the term $\left(\frac{T_i}{T_o} - 1\right)$ in equation 3.26 has a noticeable effect during the compression stroke. It increases the availability of the leaner mixtures due to the higher polytropic exponents and the initially higher temperature for leaner mixtures. Part (B) in figure 45 shows the availability profiles during combustion. At the end of combustion, the leaner methane-air mixture has the highest availability content relative to the initial energy content per unit mass of the mixture (q*) and, therefore, the highest potential to produce work. The decrease in end-of combustion availability as the equivalence ratio increases beyond one may be attributed to combustion efficiency degrading as the mixture becomes richer [13]. Part (C) in figure 45, shows the availability profile during the expansion stroke. During this process the trend is similar for all equivalence ratios, but at the end of expansion the thermo-mechanical availability is still higher

for leaner mixtures due to the gain during combustion. The non-normalized thermo-mechanical availability versus crank angle at different equivalence ratios is presented in figure 46. Trends are in agreement with those for the ideal Otto cycle (figure 33) trends, where the maximum thermo-mechanical availability was achieved around stoichiometric conditions. However, again the leaner mixture is preferable since it has a higher thermo-mechanical availability relative to its energy content. These results are consistent with a previous study at the lean operating conditions [19].
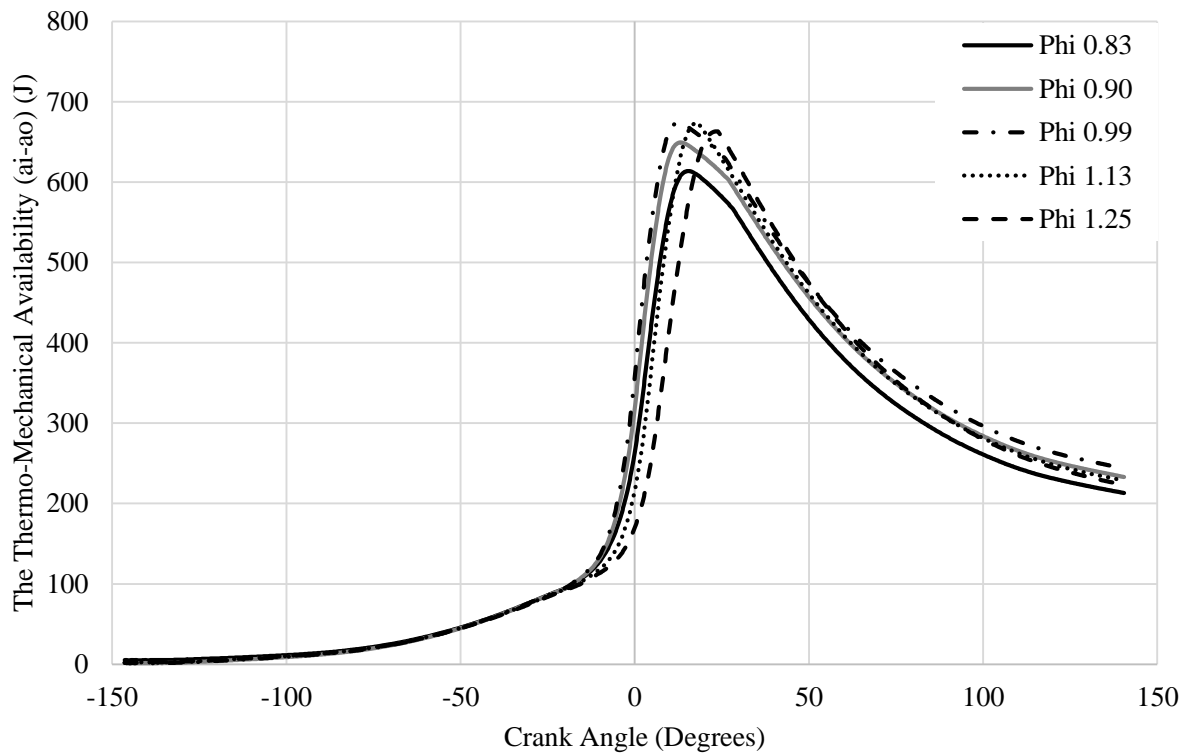
Figure 46. Non-normalized thermo-mechanical availability versus crank angle at different equivalence ratios for an SI engine cycle fueled with methane operated at WOT and 600 RPM.

Figure 47 shows first and second law efficiencies (equations 4.14 and 4.15) results as a function of equivalence ratio. Recall that $W_{g,i}$ is the gross indicated work, calculated from the experimentally obtained pressure-volume diagram at MBT timing. The SI cycle trends are consistent with those found for the ideal Otto cycle. The two efficiency curve have almost the same

values because the lower heating value and the energy of the reaction is approximately the same for methane, as described in section 3.1.5.
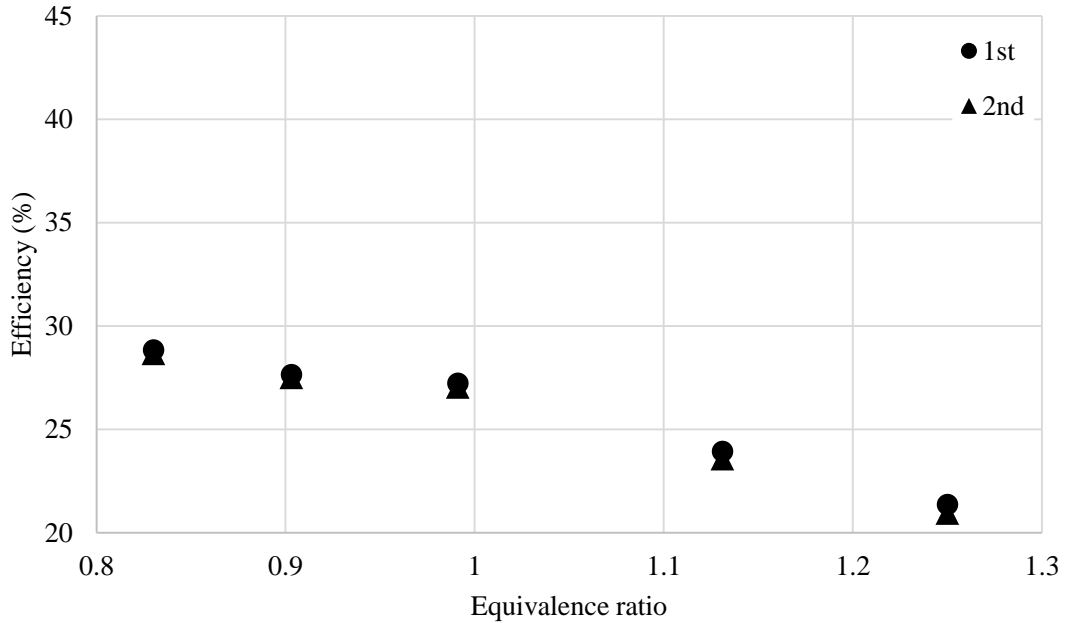
Figure 47. First and second law of Thermodynamics efficiencies as a function of equivalence ratio for the S.I engine cycle of a single cylinder, 0.6 L CFR engine operated at wide-open-throttle and 600 RPM.

The maximum non-dimensional thermo-mechanical availability values as a function of equivalence ratio for the SI engine cycle are shown in table 16. Consistent with figure 45, this parameter is highest at the leanest equivalence ratio ($\Phi=0.83$) and decreases as the equivalence ratio increases.

Table 16. Maximum non-dimensional thermo-mechanical availability of the SI cycle as a function equivalence ratio for a single cylinder, 0.6 L, methane-fueled, CFR engine operated at wide-open-throttle and 600 RPM.

Equivalence ratio	The maximum non-dimensional thermo-mechanical availability of the SI engine cycle
0.830	0.38
0.903	0.37
0.991	0.35
1.131	0.30
1.250	0.27

The non-dimensional thermo-mechanical availability ratio *during combustion* was also calculated. This parameter was computed as the ratio of the availability of products to the availability of reactants at each equivalence ratio. Results are shown in table 17. For the SI engine cycle, the availability ratio *during combustion* was found to decrease as the equivalence ratio increased (i.e., notice the lower ratio, hence highest availability loss, at $\Phi= 1.250$). This trend is consistent with the higher (non-dimensional) maximum available work for leaner mixtures of the SI engine cycle. This is because of the total availability gained during combustion for leaner mixtures *relative to the mixture energy content* is very high, offsetting the availability destruction due to entropy generation during combustion.

Table 17. The ratio of the non-dimensional thermo-mechanical availability of the combustion products to the availability of the reactants for the SI engine cycle as a function of equivalence ratio.

Equivalence ratio	The non-dimensional thermo-mechanical availability ratio during combustion
0.830	1.284
0.903	1.280
0.991	1.269
1.131	1.245
1.250	1.222

4.4 Comparison of Ideal and SI Engine Cycles

The motivation for this section is first, to clarify differences between availability analysis results between ideal and SI engine cycles and second, to investigate fuel effects on the Otto cycle availability. The latter was accomplished theoretically by using isooctane in place of methane in the ideal Otto cycle analysis, due to the absence of experimental data for isooctane.

Figure 48 shows thermo-mechanical availability trends at $\Phi= 0.991$ for the ideal and SI cycles. The profiles are similar during the compression stroke, except in the area near TDC, where the thermo-mechanical availability is higher for the ideal than for the SI cycle. Whereas isentropic compression was assumed for the ideal Otto cycle, polytropic compression was assumed for the SI cycle. The absence of heat loss increases the thermo-mechanical availability for the ideal Otto cycle. The thermo-mechanical availability for both cycles starts to increase dramatically directly after combustion due to the increase in internal energy that results from heat release.
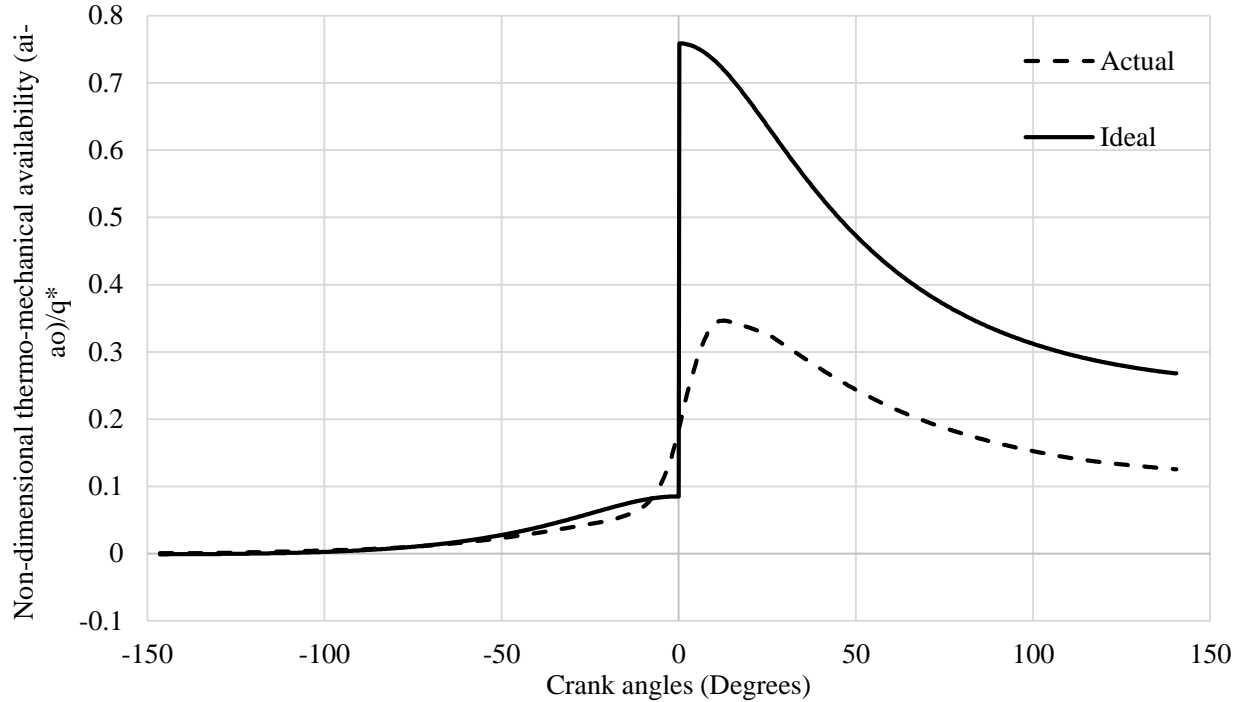
Figure 48. SI engine and ideal Otto cycle availability analyses for a 0.6L, methane-fueled, single cylinder internal combustion engine at WOT, 600 RPM, and 0.991 equivalence ratio.

Figure 48 shows higher availability associated with ideal Otto cycle during combustion due to the adiabatic combustion assumption. The start and duration of combustion are also different in each case. For the ideal Otto cycle, combustion starts at TDC and the process is instantaneous, whereas for the SI engine cycle combustion begins before TDC (consistent with the prescribed spark timing) and occurs over a finite amount of time with significant heat loss, which lowers the thermo-mechanical availability. After expansion, the mixture undergoing the ideal Otto cycle also exits the engine with higher availability.

Figure (49) shows the second law of Thermodynamics efficiency for the ideal and the SI engine cycles as a function of equivalence ratio. The trend is similar, with the efficiency decreasing as the equivalence ratio increases. Clearly, that the ideal Otto cycle efficiency is

higher than that of the SI cycle due to the assumptions built into the model (e.g., isentropic compression and expansion process, 100% combustion efficiency).
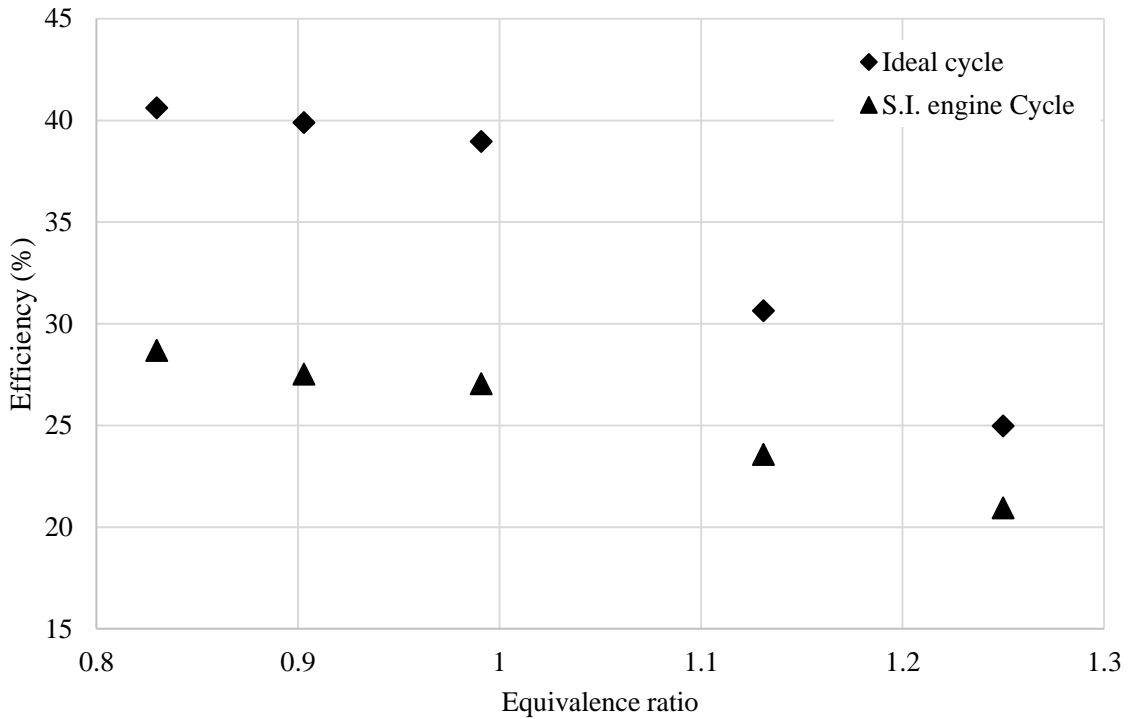
Figure 49. Second-law of efficiency as a function of equivalence ratio for the ideal and SI engine cycles

Figure 50 shows results of the ideal Otto cycle availability comparison for methane and isooctane as motivation for future work. Methane has less (albeit comparable) total thermo-mechanical availability, as a percentage of the initial energy content per unit mass of mixture (q*).
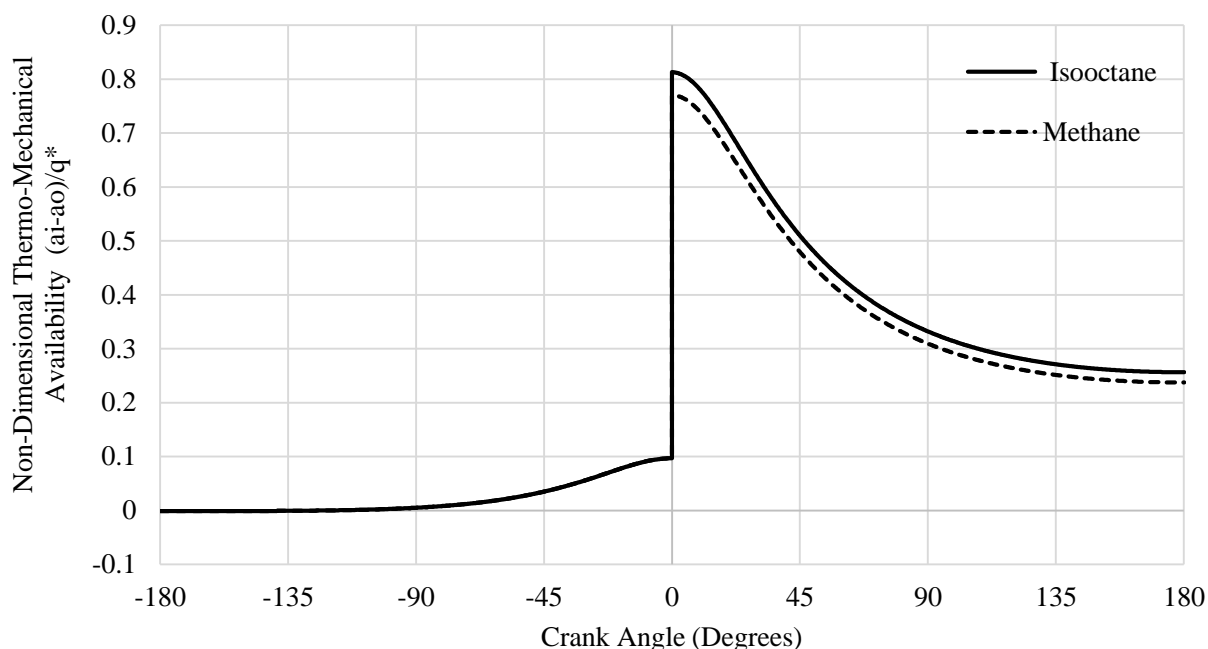
Figure 50. Ideal Otto cycle thermo-mechanical availability analysis for methane and isooctane at Φ=1 for a 0.6L, single cylinder internal combustion engine.

Table 18 summarizes the availability comparison between the two fuels. Shon are the non-dimensional maximum available work from the thermo-mechanical balance, calculated according to equation 4.16, and the adiabatic flame temperature, which has a direct effect on the internal energy content (see equation 3.26).

Table 18. Comparison between methane and isooctane thermo-mechanical availability for an ideal Otto cycle at Φ= 1 for a 0.6 L, single-cylinder internal combustion engine.

Fuel Type	$(\dfrac{a}{q^*})_w$	Adiabatic Flame Temp (K)
Methane	0.43	3082
Isooctane	0.46	3217

CHAPTER V

CONCLUSIONS AND FUTURE WORK

5.1 Conclusions

The second law of Thermodynamics was used to investigate the availability of a methane-fueled, spark-ignition engine during compression, combustion, and expansion processes. The availability analysis was conducted over a range of equivalence ratios (0.83-1.25) for both the ideal and SI engine cycles. The main findings are as follows:

- Whereas the total thermo-mechanical availability (in J) increases as the equivalence ratio increases, the trend reverses when the thermo-mechanical availability is normalized by the mixture energy. That is, the *non-dimensional* thermo-mechanical availability increases as the equivalence ratio decreases.

- Mixtures undergoing the ideal Otto cycle have higher thermo-mechanical availability at the end of the expansion stroke for all equivalence ratios.

- The *non-dimensional* thermo-mechanical availability ratio *during combustion* increases as the equivalence ratio decreases for both the ideal and SI cycles.

- First and second law of Thermodynamics efficiencies increase as the equivalence ratio decreases. For methane, these efficiencies remain within four percent of each other for both the ideal and the SI engine cycle as a function of equivalence ratio. This is because the ratio of the caloric heat value to the energy of the reaction is approximately equal to one for methane.

5.2 Future Work

      The current research can be extended to include the chemical availability component in practical SI engine cycles, and investigate total availability for methane and other fuels as a function of engine operating conditions (e.g., speed, load, EGR concentrations).

APPENDICES

Appendix I. Abbreviations and Key Symbols

A_{start} Availability at start of a process

A_{end} Availability at end of a process

A_W Availability transferred due to work

A_Q The availability transferred due to heat

A_{Dest} Availability destruction

A_R Availability of reaction

A Constant

a Specific availability

B Bore

B_1 Constant

B_2 Constant

C Critical flow factor

Cd Coefficient of discharge

C_P Specific heat at a constant pressure

C_v Specific heat at a constant volume

G Gibbs Function

h Enthalpy

h_o Specific Enthalpy at datum

k Specific heat ratio

$\dfrac{l}{a}$ Connecting rode to crank offset ratio

m Mass

m_t Total mass

m_f Fuel mass

$\dot{m}_{air}$ Air flow rate

$\dot{m}_{fuel}$ Fuel flow rate

N Engine speed

n Number of revolutions

Nc Number of cylinders

P Pressure

P_o Surrounding Pressure

Q Heat

$Qlhv$ Lower heating value

$Qhhv$ Higher heating value

$\dot{Q}_f$ The energy of the fuel losses

$\dot{Q}_a$ The energy of the intake air losses

$\dot{Q}_e$ Exhaust energy losses

$\dot{Q}_c$ Cooling energy losses

$\dot{Q}_u$ Unaccounted energy losses

q^* Energy of reaction

R Gases constant

r Compression ratio

S_P Entropy of combustion Products

S_R Entropy of combustion reactants

S Stroke

s Specific Entropy

s_o Specific Entropy at datum

T Temperature

T_o Surrounding Temperature

T_S Temperature at spark ignition

U_R Internal energy of combustion reactants

U_P Internal energy of combustion products

u Specific Internal Energy

u_o Specific Internal Energy at datum

$\forall_d$ Displacement volume

$\forall_c$ Clearance volume

v Specific volume

v_o Specific volume at datum

$\dot{W}_{sh}$ Shaft power output losses

W Work

A Availability

A_{fuel} Availability of the fuel

A_{in} Availability transfer through mass flowing through the intake

A_{ex} Availability transfer through mass flowing through the Exhaust

A_Q Availability transfer through heat exchange

A_W Availability transfer through Work

A_{dest} Availability Destroyed

λ Air/ Fuel equivalence ratio

Φ Fuel/Air equivalence ratio

ε Air/ fuel ratio

ξ_v Volumetric efficiency

θ Crank angles

$V(\theta)$ Instantaneous volume at any crank angle

σ Internal irreversibility of the system

η_{II} Second law of thermodynamics efficiency

η_{II} First law of thermodynamics efficiency

Appendix II. Air flow meter sensor calibration table

Table 19. Air flow meter calibration information

No.	The inlet pressure (Psia)	The inlet pressure (Psi) Gauge	The inlet pressure (kPa)	Air mass flow rate (LBMS)	Air mass flow rate (kg/s)
1	18.88	4.18	130.18	0.0025	0.0012
2	18.88	4.18	130.18	0.0025	0.0012
3	28.19	13.49	194.35	0.0038	0.0017
4	28.18	13.48	194.32	0.0038	0.0017
5	37.52	22.82	258.67	0.0051	0.0023
6	37.52	22.82	258.70	0.0051	0.0023
7	46.85	32.15	323.01	0.0063	0.0029
8	46.85	32.15	323.01	0.0063	0.0029
9	51.71	37.01	356.56	0.0070	0.0032
10	51.71	37.01	356.55	0.0070	0.0032
11	56.49	41.79	389.48	0.0077	0.0035
12	56.49	41.79	389.48	0.0077	0.0035
13	71.14	56.44	490.47	0.0097	0.0044
14	71.11	56.41	490.30	0.0097	0.0044
15	85.76	71.06	591.30	0.0117	0.0053
16	85.75	71.05	591.24	0.0117	0.0053
17	100.39	85.69	692.13	0.0137	0.0062
18	100.38	85.68	692.11	0.0137	0.0062
19	115.00	100.30	792.88	0.0156	0.0071

Appendix III. Piezoelectric Transducer (Kistler model 7061B) calibration table

Table 20. Piezoelectric transducer (Kistler model 7061B) calibration table

Calibrated range bar	Temperature (C)	Sensitivity pC/bar	Linearity ≤ ± % FSO	Uncertainty of measurement %
0-250	23	-80.59	0.03	0.42
0-50	23	-80.40	0.06	0.42
0-5	23	-80.31	0.05	0.42
0-250	50	-80.70	0.03	0.42
0-50	50	-80.61	0.04	0.42
0-5	50	-80.35	0.14	0.42

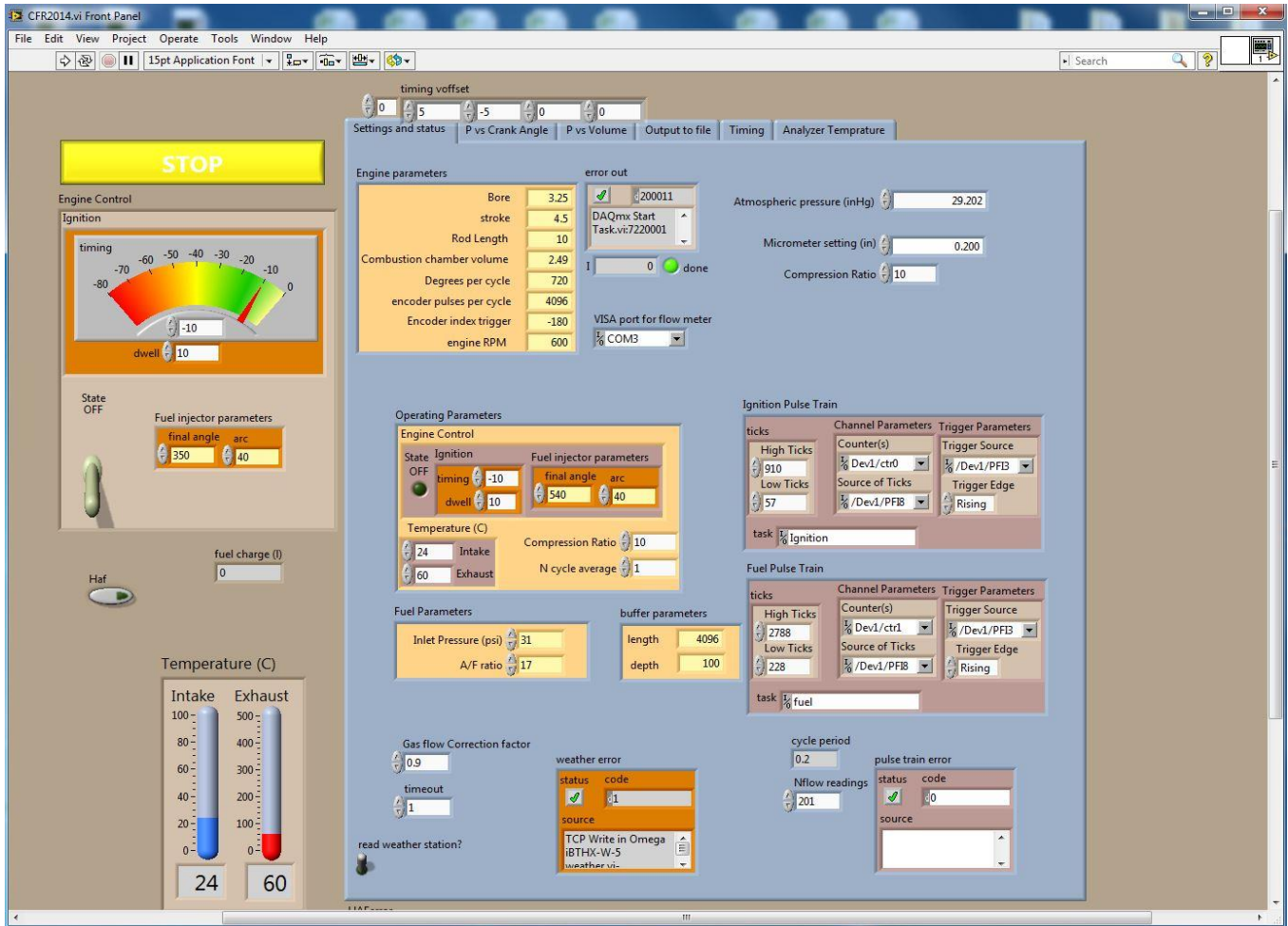Appendix IV. Graphical User Interface (GUI) by LabVIEW 15.0

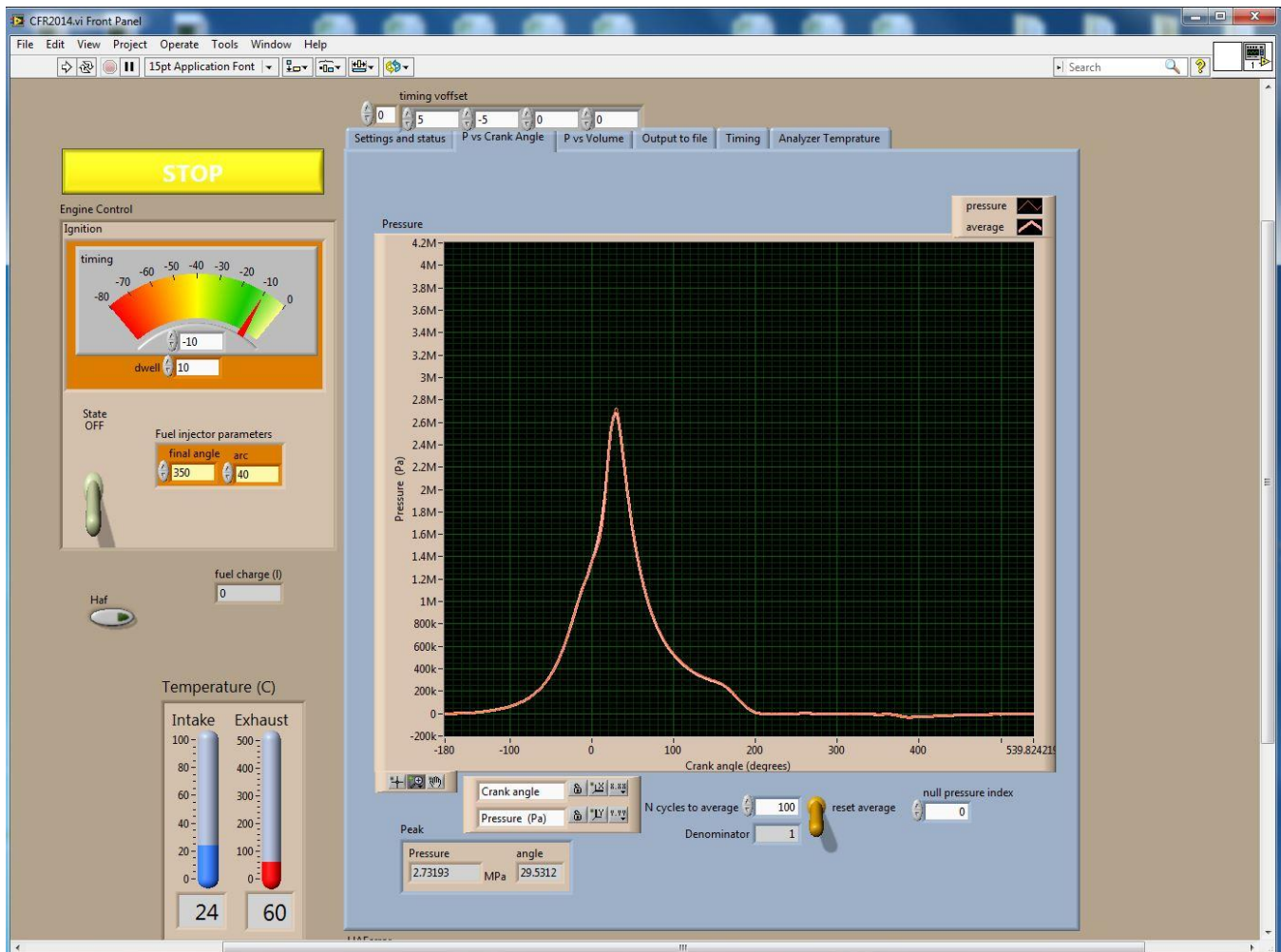Figure 51. Graphical User Interface LabVIEW 15.0 main screen.

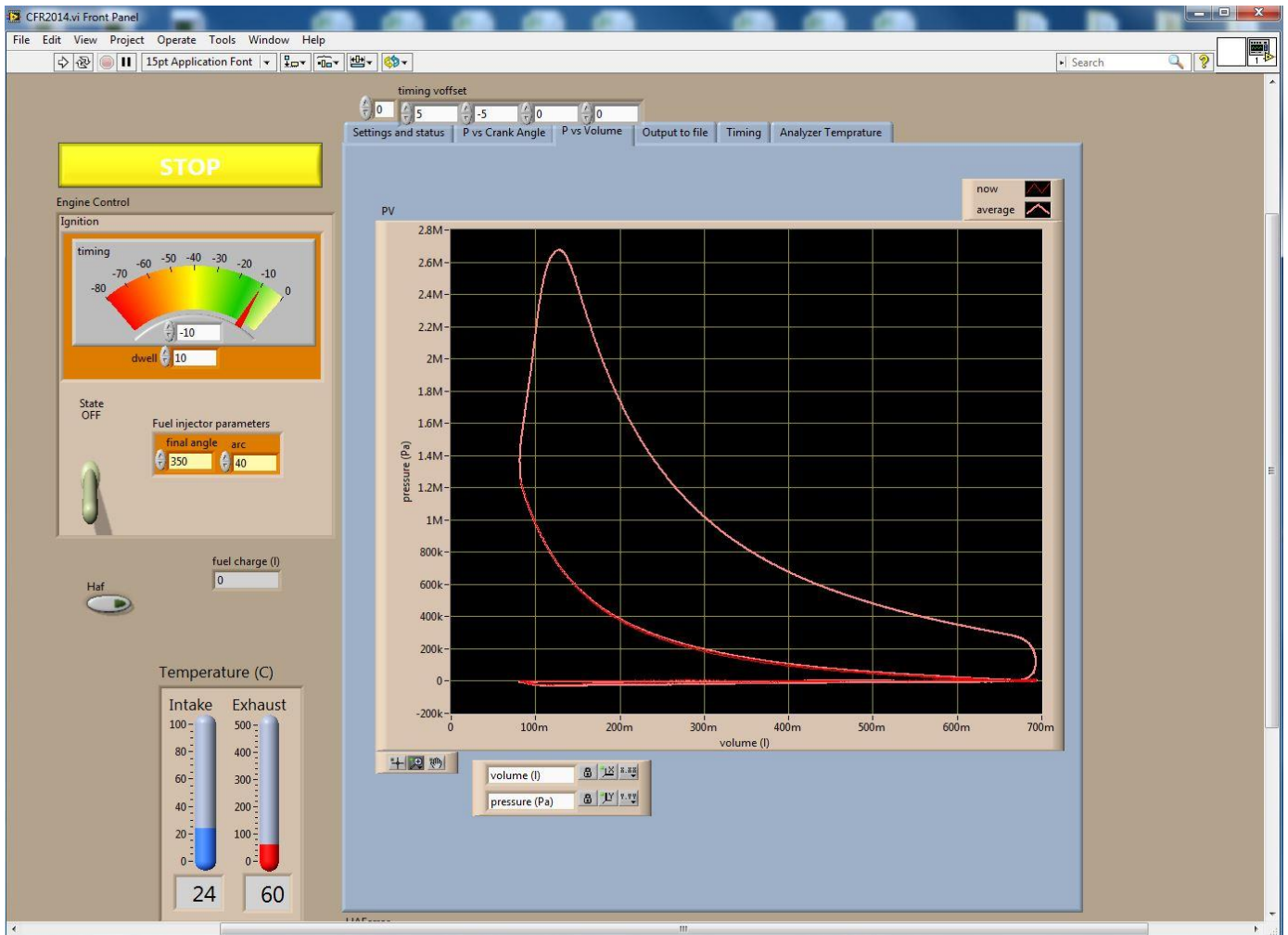Figure 52. Graphical User Interface LabVIEW 15.0 pressure-crank angle sub screen.

Figure 53. Graphical User Interface LabVIEW 15.0 Pressure-Volume sub screen.

REFERENCES

[1]   M. A. B. Yunus A. Cengel, Thermodynamics: An Engineering Approach, McGraw-Hill Science/Engineering/Math; 5 edition, 2005.

[2]   J. Caton, "A Review of Investigations Using the Second Law of Thermodynamics to Study Internal-Combustion Engines.," *SAE technical paper Series* , 2000.

[3]   F. Alasfour, "Butanol—A single-cylinder engine study: Availability analysis," *Elsevier,* 1997.

[4]   J. &. C. J. Zheng, " Second law analysis of a low temperature combustion diesel engine: Effect of injection timing and exhaust gas recirculation," *Elsevier,* 2012.

[5]   J. S. J. &. W. W. Farrell, "A Second Law Analysis of High Efficiency Low Emission Gasoline Engine Concepts.," *SAE Technical Paper Series,* 2006.

[6]   J. Caton, " A Thermodynamic Evaluation of the Use of Alcohol Fuels in a Spark-Ignition Engine," *SAE International Journal of Fuels and Lubricants,* 2009.

[7]   C. Sayin, "Energy and exergy analyses of a gasoline engine," *INTERNATIONAL JOURNAL OF ENERGY RESEARCH,* 2006.

[8]   A. &. Z. S. Sobiesiak, "The First and Second Law Analysis of Spark Ignition Engine Fuelled with Compressed Natural Gas," *SAE Technical Paper Series,* 2003.

[9]   A. H. R. M. M. &. Y. T. Gharehghani, "A comparative study on the first and second law analysis and performance characteristics of a spark ignition engine using either natural gas or gasoline," *Elsevier,* 2015.

[10]   I. &. B. Baxter, "An international historic mechanical engineering landmark: The Waukesha CFR fuel research engine," 1980.

[11]   S. N.-C. F. Nozzles, Flow systems Inc. , 2016. [Online]. Available: http://www.flowsystemsinc.com/sonic-nozzles-and-critical-flow-venturis.

[12]   Honeywell, "Honeywell zephyr analog airflow sensor: Haf series-high accuracy," Honeywell, 2016. [Online]. Available: www.sensing.Honeywell.com.

[13]   J. B. Heywood, Internal Combustion Engine Fundamentals, Mc-Graw Hill Inc., 1988.

[14]   W. W. Pulkrabek, Engineering fundementals of the internal combustion engines, Pearson, 2003.

[15]   A. T. K. Colin R. Ferguson, Internal Combustion Engines: Applied Thermosciences, Wiley; 2 edition, 2000.

[16] T. g.-w. C. Inc, "Small Gas Engines Workbook," The goodheart-willcox Co. Inc, [Online]. Available: http://bennettco.k12.sd.us/cms/lib/SD01001545/Centricity/Domain/223/SMALL%20ENGINE%20 IGNITION%20SYSTEMS%20CH10.pdf.

[17] D. winterbone, Advanced Thermodynamics for engineers, London, 1997.

[18] J. Caton, "On the destruction of availability (exergy) due to combustion processes — with specific application to internal-combustion engines," *Elsevier,* 2000.

[19] K. Rezapour, "AVAILABILITY ANALYSIS OF A BI-FUEL SI ENGINE MODEL FOR IMPROVEMENT ITS PERFORMANCE," 2012.

[20] S. Kasap, "Themoelectric Effects in metals:Thermocouples," 1990.

[21] A. Inc., "AFC-121 Lockoff Multi-Purpose Shut-Off Valve," [Online]. Available: http://www.centuryfuelproducts.com/afc-121-lockoff.html.

[22] M. H. ,. D. D. G. G.-B. ,. A. B. G. S. Mohsen Ghazikhani, "Exergy recovery from the exhaust cooling in a DI diesel engine for," *Elsevier,* 2014.

[23] J. H. V. G. &. H. N. Shapiro, "Second-Law Analysis of Diesel Engine Combustion," *Journal of Engineering for Gas,* 1990.

[24] D. N. A. ,. Z. S. F. Michael K. Anderson, "First and Second Law Analyses of a Naturally-Aspirated, Miller Cycle, SI Engine with Late Intake Valve Closure," *SAE Technical Paper ,* 1998.

[25] J. Caton, "Results from the second Law of thermodynaimcs For a spark ignition engine using an engine cycle simulation," *ASME,* 1999.

[26] G. Woschni, "A universally Applicable Equation For instantaneous Heat transfer coefficient in the Internal combustion engines," *SAE Technical Paper,* 1967.

[27] C. G. E. Rakopoulos, "Second-law analyses applied to internal combustion engines operation," *Elsevier ,* 2005.

[28] K. D. Som, "Thermodynamic irreversibilities and exergy balance in combustion processes," *Science Direct,* 2008.

[29] B.-Q. H. Haeng Muk Cho, "Spark ignition natural gas engines—A review," *Elsevier,* 2007.

[30] G. T. ,. H. X. ,. S. S. Ritchie Daniel, "Ignition timing sensitivities of oxygenated biofuels compared to gasoline in a direct-injection SI engine," *Elsevier,* 2012.

[31] K. Rezapour, "Availability analysis of A bio fuel SI engine model for improvment its performance," *IJTPE Journal,* 2012.

[32] S. Z. Andrzej Sobiesiak, "The First and Second Law Analysis of Spark Ignition Engine Fuelled with Compressed Natural Gas," *SAE TECHNICAL PAPER SERIES ,* 2003.

[33] A. O. Mohamed Djermouni, "Thermodynamic analysis of an HCCI engine based system running on natural gas," *ScienceDirect,* 2014.

[34] S. Turns, An Introduction to Combustion: Concepts and Applications, McGraw-Hill Education; 3 edition, 2011.

[35] K. Raznjevic, Handbook of Thermodynamic Tables and Charts, Hemisphere Publishing Corporation; 2 edition, 1976.